FAA-RD-76-219

Project Report
ATC-72

DABS Monopulse Summary

D. Karp
M. L. Wood

4 February 1977

Lincoln Laboratory
MASSACHUSETTS INSTITUTE OF TECHNOLOGY
LEXINGTON, MASSACHUSETTS

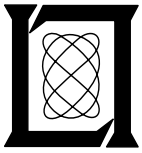

Prepared for the Federal Aviation Administration,
Washington, D.C. 20591

TECHNICAL REPORT STANDARD TITLE PAGE

1. Report No.	2. Government Accession No.	3. Recipient's Catalog No.
FAA-RD-76-219		

4. Title and Subtitle	5. Report Date
DABS Monopulse Summary	4 February 1977
	6. Performing Organization Code

7. Author(s)	8. Performing Organization Report No.
D. Karp and M.L. Wood	ATC-72

9. Performing Organization Name and Address	10. Work Unit No.
Massachusetts Institute of Technology Lincoln Laboratory P.O. Box 73 Lexington, Massachusetts 02173	11. Contract or Grant No. DOT-FA72-WAI-261
	13. Type of Report and Period Covered Summary Report
12. Sponsoring Agency Name and Address Department of Transportation Federal Aviation Administration Systems Research and Development Service Washington, D.C. 20591	14. Sponsoring Agency Code

15. Supplementary Notes

The work reported in this document was performed at Lincoln Laboratory, a center for research operated by Massachusetts Institute of Technology under Air Force Contract F19628-76-C-0002.

16. Abstract

Improved azimuthal resolution of proximate aircraft necessary to support ATC automation can be achieved by beacon surveillance systems employing monopulse angle estimation techniques described in this report.

Included in the report are the results of beacon surveillance monopulse system analyses relating to off-boresight angle estimation using short (1/2 μsec) pulses; the effects of specular and diffuse multipath signal return; the effects of overlapping ATCRBS fruit replies, and the problems of antenna pattern design. These topics have been studied in detail as part of the Lincoln Laboratory design of the Discrete Address Beacon System (DABS).

This report summarizes significant analytical results obtained. In general, it has been concluded that the ATC environment does not pose a serious problem to the use of the monopulse concept for beacon system direction finding and that sufficient direction finding accuracy can be obtained using a small number of narrow pulses for each scan.

17. Key Words	18. Distribution Statement
Air Traffic Control Beacon System Monopulse Azimuth Estimation Aircraft Position Measurement	Document is available to the public through the National Technical Information Service, Springfield, Virginia 22151.

19. Security Classif. (of this report)	20. Security Classif. (of this page)	21. No. of Pages	22. Price
Unclassified	Unclassified	104	

Form DOT F 1700.7 (8-69)

DABS MONOPULSE SUMMARY

TABLE OF CONTENTS

LIST OF ILLUSTRATIONS

LIST OF ILLUSTRATIONS (continued)

LIST OF ILLUSTRATIONS (continued)

DABS MONOPULSE SUMMARY REPORT

1.0 INTRODUCTION

Studies have shown [1] that beacon surveillance performance required to support ATC automation can be achieved by minimizing self interference and by improving resolution of proximate aircraft. Interference can be reduced by lowering the interrogation rate. Proximate targets can be resolved by interrogating each target separately (by an addressed interrogation) so as to separate their replies in time. There is sufficient time on the up and down links to discretely address all targets, even in high traffic densities, if position and identity can be derived from about two replies per scan.

Azimuth estimation in the current ATCRBS is based upon a beam-splitting or sliding window process. The estimate accuracy for these techniques is related to the beamwidth/runlength ratio using runlengths of 16 to 20 per scan. A method that measures azimuth accurately on the basis of a few replies per scan is required.

This capability can be achieved using a monopulse angle estimation system. Important monopulse considerations are: off-boresight angle estimation using short (1/2 μsec) pulses; the effects of specular and diffuse multipath signal return; the effects of overlapping ATCRBS fruit replies, and the problems of antenna pattern design. These topics have been studied in detail as part of the Lincoln Laboratory design of the Discrete Address Beacon System (DABS). This report summarizes the significant analytical results obtained. In general, it has been concluded that the ATC environment does not pose a serious problem to the use of the monopulse concept for beacon system direction finding and that sufficient direction finding accuracy can be obtained using a small number of narrow pulses for each scan.

Sections 2., 3., and 4. of the report describe antenna characteristics required to support monopulse, and summarize the features of several possible hardware realizations of the monopulse processor. The realization selected is the so-called half-angle phase comparator which utilizes phase detectors to produce an unambiguous off-boresight indication over a large fraction of the beamwidth. Sections 3. and 4. discuss the effects on monopulse performance of interference from various sources and of various antenna design parameters. The impact of diffraction of the incoming wavefront around obstructions such as nearby buildings is also briefly discussed.

Sections 5. through 7. describe the performance actually obtained using the monopulse processor employed at DABSEF, an implementation of the processor specified in the DABS sensor engineering requirement. Section 5. focuses on the stability of the processor and its sensitivity to the frequency and amplitude of the received signal. Section 6. describes the method used to evaluate reply accuracy as a function of off-boresight angle, and gives results for a large number of ATCRBS targets of opportunity. In Section 7. target report accuracy is evaluated using smoothing techniques to estimate aircraft position.

Section 8. describes analytical and experimental work done at Lincoln Laboratory to quantify and confirm the effects of obstacle shadowing upon DABSEF monopulse direction finding accuracy. Conclusions are drawn in Section 9.

Appendix A describes the system used to evaluate DABS monopulse performance (DABSEF). An error analysis is included to estimate the effect on performance of variations in half-angle processor hardware elements.

Appendix B is a summary of a curve fitting technique using look-back and look-ahead data to accurately develop aircraft trajectory. This technique is the basis for calculating the DABSEF monopulse angle estimator's accuracy.

2.0 MONOPULSE PROCESSING

2.1 Introduction

The ability of monopulse techniques to estimate target azimuth from a single received pulse is based on:

a. An antenna that can provide outputs related to the angle of incidence of the incoming plane wave (offboresight angle),

b. A processor that can convert the antenna outputs to a signal related to offboresight angle, and

c. A calibration method which can establish the exact relation between processor output and actual offboresight angle.

Section 2.2 introduces the subject of monpulse antennas, and notes their principal parameters and requirements. Detailed discussion of monopulse antennas, their influence on overall monopulse angle estimation accuracy, and characteristics which minimize their vulnerability to interference is, however, deferred to Section 4. Section 2.3 proceeds with a detailed discusion of the monopulse processor, noting differences between amplitude and phase comparison processing and explaining why the so-called half-angle phase comparator has been selected for the DABS application. For purposes of this discussion, the monopulse antenna is treated as a simple "three-port network" providing sum (Σ), difference (Δ) and omnidirectional (Ω) control outputs.

2.2 Monopulse Antennas

A monopulse antenna requires:

- A "Sum" pattern (Σ) corresponding to a symmetric directional mainlobe, typically a few degrees wide.

- An asymmetric "Monopulse Difference" pattern (Δ) with a directional pattern commensurate in width with the Σ pattern and accurately centered with respect to it. Its signals are used, in conjunction with those from Σ, to determine the bearing angle of targets known to be in the main beam (sometimes referred to as "monopulse window").

- A "Control" pattern (Ω, often implemented as an omnidirection pattern). This pattern is used in conjunction with the Σ pattern to provide the various transmit sidelobe suppression functions (SLS) and the receive sidelobe flagging functions (RSLS).

Fig. 2-1 is a simple representation of a monopulse antenna in which the antenna outputs correspond to these three essential patterns.

The types of antennas under discussion when operating in conjunction with the monopulse processors discussed in the following section introduce system angle errors which are dependent on the beamwidth and on the difference pattern

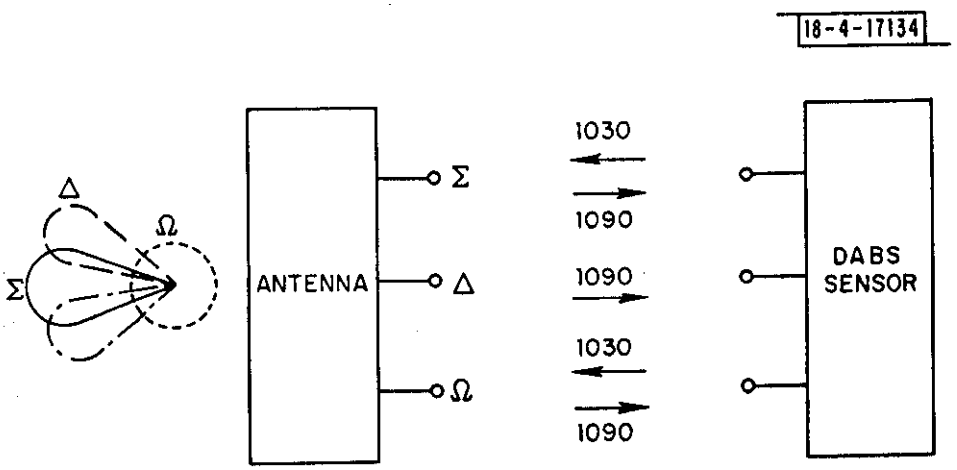

Fig. 2-1. Monopulse antenna (simplified representation).

shape. It is common practice to characterize the slope of the difference pattern by the location of the sum-to-difference cross-over point ($\Delta/\Sigma = 1$); this essentially specifies the difference pattern beamwidth relative to that of the sum. The desirable location of the cross-over point varies between -3 dB on the sum pattern (this makes the aperture width required for the difference compatible with that required for the sum) and -4 dB (anything less implies that the aperture is inefficiently utilized). This desirable range of cross-over values results in a small variation in accuracy; the sum beamwidth emerges, therefore, as the dominant antenna determinant of inherent accuracy. Lincoln Laboratory's experience with the monopulse receiver and antenna at DABSEF indicates that it is reasonable to expect field deployable equipment to achieve a beamsplit factor of 40:1. Thus, a 4^{o} sum azimuth beamwidth is about the upper limit if inherent direction finding accuracy of 0.1^{o} rms is desired.

The relative importance of monopulse antenna design parameters upon monopulse processing performance and upon overall monopulse angle estimation system performance is discussed in detail in Section 4.

2.3 Monopulse Processors

The monopulse processor provides a signal indicative of the azimuth angle between the target and the antenna pointing direction for each received pulse. Two basic receiver configurations can be used to generate "monopulse" signals: amplitude comparison and phase comparison [3].

In the amplitude comparison scheme, shown in Fig. 2-2a (sometimes referred to as the Chubb approach) RF antenna outputs corresponding to two angle-squinted beams are logarithmically amplified and detected, and then subtracted, yielding a bi-polar video from which off-boresight angle can be deduced. The angular region over which this scheme generates an unambiguous output is more limited than desired. This is true since when the squinted beams are generated:

(i) directly by the antenna, the angular limit is determined by the first nulls of the individual patterns.

(ii) from linear combinations of independent sum and difference beams ($\Sigma + \Delta$, and $\Sigma - \Delta$), the limit corresponds to the sum difference crossover or about the 3 dB beamwidth.

This limitation reduces the desired flexibility for DABS interrogation scheduling. Specifically, it may preclude direction finding in situations when there is sufficient signal strength to perform detection and communication, for example, for near-in targets outside the 3 dB beamwidth.

The phase comparison scheme shown in Fig. 2-2b, (sometimes referred to as the Bell Labs approach), had its origin in the simple direction finding scheme in which the bearing angle is obtained by measuring the relative phase between two displaced antennas. This scheme is refined in optimized monopulse systems by first generating independent sum and difference patterns, each having low sidelobes,

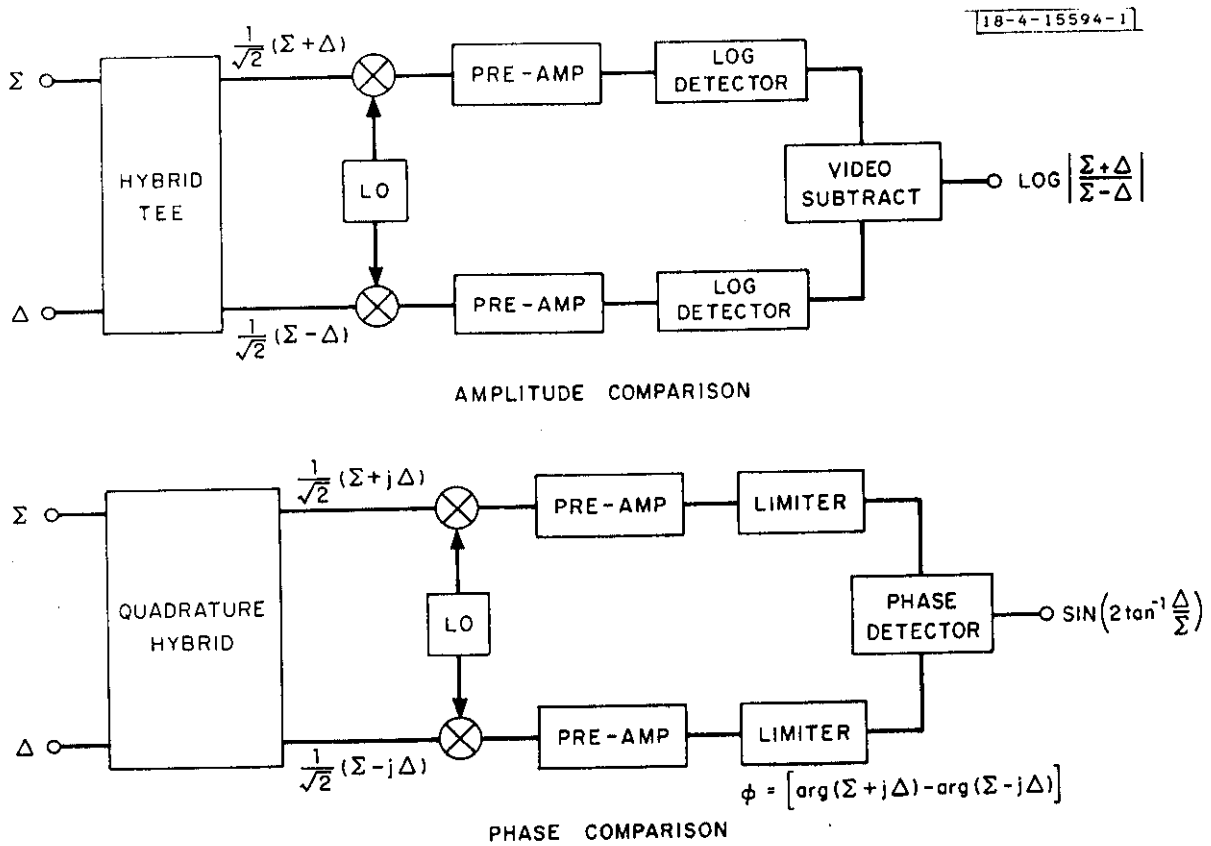

Fig. 2-2. Block diagrams of monopulse processors.

and making maximum use of the available aperture, then combining the sum and difference outputs in a hybrid to yield outputs $\Sigma + j\Delta$ and $\Sigma - j\Delta$. It can be verified that the aperture illuminations associated with these new patterns tend to look like overlapping antennas with displaced phase centers. The normalization of the two signals is accomplished by phase-matched limiters. The bi-polar video output of the phase detector contains all the angle information.

It has been shown in [4] that the optimum azimuth estimate in a receiver noise background can be obtained by solving

$$\frac{G_\Delta(\hat{\theta})}{G_\Sigma(\hat{\theta})} = \tan\frac{\phi}{2} = \frac{\sin\phi}{1+\cos\phi} \qquad (2\text{-}1)$$

where

$$\phi = \arg(\Sigma + j\Delta) - \arg(\Sigma - j\Delta) \qquad (2\text{-}2a)$$

$$\hat{\theta} = \text{offboresight angle estimate} \qquad (2\text{-}2b)$$

and where $G_\Sigma(\theta)$, $G_\Delta(\theta)$ represent the amplitudes of the sum (Σ) and difference (Δ) radiation patterns. The ratio $G_\Delta(\theta)/G_\Sigma(\theta)$ is often referred to as the monopulse function. For large signal-to-noise ratio (SNR) and targets near boresight, it turns out that $|\Delta/\Sigma| \ll 1$ and ϕ is a small angle. In this case $\cos\phi \approx 1$ so that

$$\frac{G_\Delta(\hat{\theta})}{G_\Sigma(\hat{\theta})} \approx 1/2 \sin\phi \qquad (2\text{-}3)$$

Therefore the detector shown in Figure 2-2b with output represented by a simple sine function, represents an optimum configuration under the above conditions. Its output can be fed into a table look-up to invert the monopulse function and hence provide an implementation of (2-3). Unfortunately as $|\Delta/\Sigma| \to 1$ serious noise errors begin to occur and then for $|\Delta/\Sigma| > 1$ the sinusoidal phase detector output becomes ambiguous. This results in the same restriction in the unambiguous monopulse "field of view" as the previous amplitude comparison system.

Fortunately, unlike the amplitude system, the phase comparison system can be made to work over the full width of the beam (where $|\Delta/\Sigma|$ is monotonically increasing). Two classes of design options are available. In the first, a quadrature channel is provided to measure $\cos[\arg(\Sigma + j\Delta) - \arg(\Sigma - j\Delta)]$. This can be used by

(1) taking the sine output as the primary estimate and use using the polarity of the cosine output to resolve the sine ambiguity.

(2) taking the output of the phase detector that has the more favorable characteristics for the specific measurement, e.g., use the sine output for $|\sin \phi| \leq 0.707$, $\cos \phi < 0$, and use the cosine output for $|\cos \phi| < 0.707$.

(3) using both outputs together to compute, or look up in a table, the estimate of off-boresight angle using the optimum estimation equation (2-1).

None of the above alternatives is entirely satisfactory. The first is subject to large errors in the estimate near $|\Delta/\Sigma| = 1$, while the other two lead to rather complex implementations.

The second class of design options to overcome the ambiguity problem uses a "half-angle processor". If angles

$$\alpha,\beta = \arg (\Sigma \pm j\Delta) - \arg \Sigma \tag{2-4}$$

are defined and it is noted from (2-2) that $\phi = (\alpha - \beta)$, (2-1) becomes

$$\frac{G_\Delta(\hat{\theta})}{G_\Sigma(\hat{\theta})} = \tan \frac{(\alpha - \beta)}{2} \tag{2-5}$$

Since the angles α,β are always less than 90°, phase detectors are available that will linearly and unambiguously measure the phase difference between the signals $\Sigma \pm j\Delta$ and Σ. Therefore summing the outputs of the two half-angle phase detectors yields an azimuth estimate that is identical to the optimum Bell Labs processor without any inherent ambiguity.

A realization of the half-angle processor is shown in Figure 2-3. Although the two pairs of limiter channels do not carry equal level signals, the amplitude difference will not be large because of the quadrature relationship between Σ and $j\Delta$ and the fact that since detectability must always be maintained, the Σ signal cannot vanish. It is desirable to use two redundant half-angle processors, rather than one, because the sensitivity to phase errors between the channels $\Sigma + j\Delta$ and $\Delta + j\Sigma$ is half as great for the configurations shown as it would be for the corresponding channels $\Sigma + j\Delta$ and Σ. Furthermore, the additional phase detector yields a 3 dB improvement in SNR.

As suggested by (2-5) it remains to take the processor output $(\alpha - \beta)$ and calculate $\tan [(\alpha - \beta)/2]$, which is used with an inversion of the monopulse curve to obtain the azimuth estimate. This procedure requires separate calibration of the monopulse function and the phase detector characteristics.

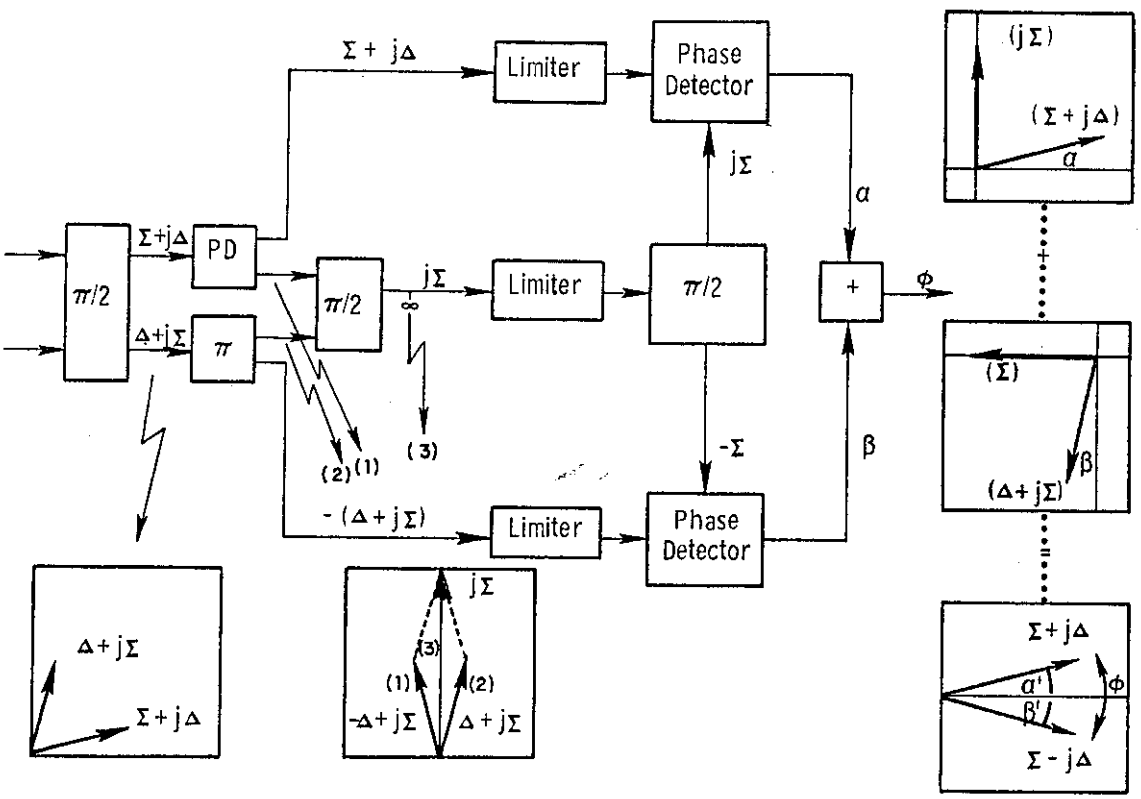

Fig. 2-3. The half-angle monopulse processor.

In practice it is easier to obtain a calibration curve that relates the azimuth estimate directly to the phase detector output $(\alpha - \beta)$ since this also accounts for receiver nonlinearities. Hence, the final form for the azimuth estimator is

$$\hat{\theta} = f(\alpha - \beta) \tag{2-6}$$

where the function table f(.) is generated from the quantized version of $(\alpha - \beta)$.

To complete the description, Figure 2-4 shows the output of the half-angle processor vs. Δ/Σ for two types of phase detectors. The relation $2 \tan^{-1} \Delta/\Sigma$ pertains to an ideal triangular or sawtooth phase detector, and

$$\frac{2\text{Real } \Delta/\Sigma}{\sqrt{1 + \left|\frac{\Delta}{\Sigma}\right|^2}}$$

applies to a sinusoidal device. Practical phase detector characteristics would lie between the two curves. The actual behavior of the processor output vs. target position off-boresight is also a function of the antenna monopulse characteristic, i.e., Δ/Σ vs. azimuth.

In summary, an azimuth estimate is obtained by processing the Δ and Σ signals with the monopulse-processor circuit.[+] The output of this device, referred to as monopulse video, MV, is a monotonic function of the complex ratio $\frac{\Delta}{\Sigma}$

$$MV = f(\Delta/\Sigma) \tag{2-7}$$

For the case when there is no noise and no interference,

$$\frac{\Delta}{\Sigma} = E(\theta) \tag{2-8}$$

where $E(\theta)$ is the normalized difference pattern as a function of offboresight angle θ

$$E(\theta) = \frac{G_\Delta(\theta)}{G_\Sigma(\theta)} \tag{2-9}$$

[+] Δ and Σ are the difference and sum beam outputs.

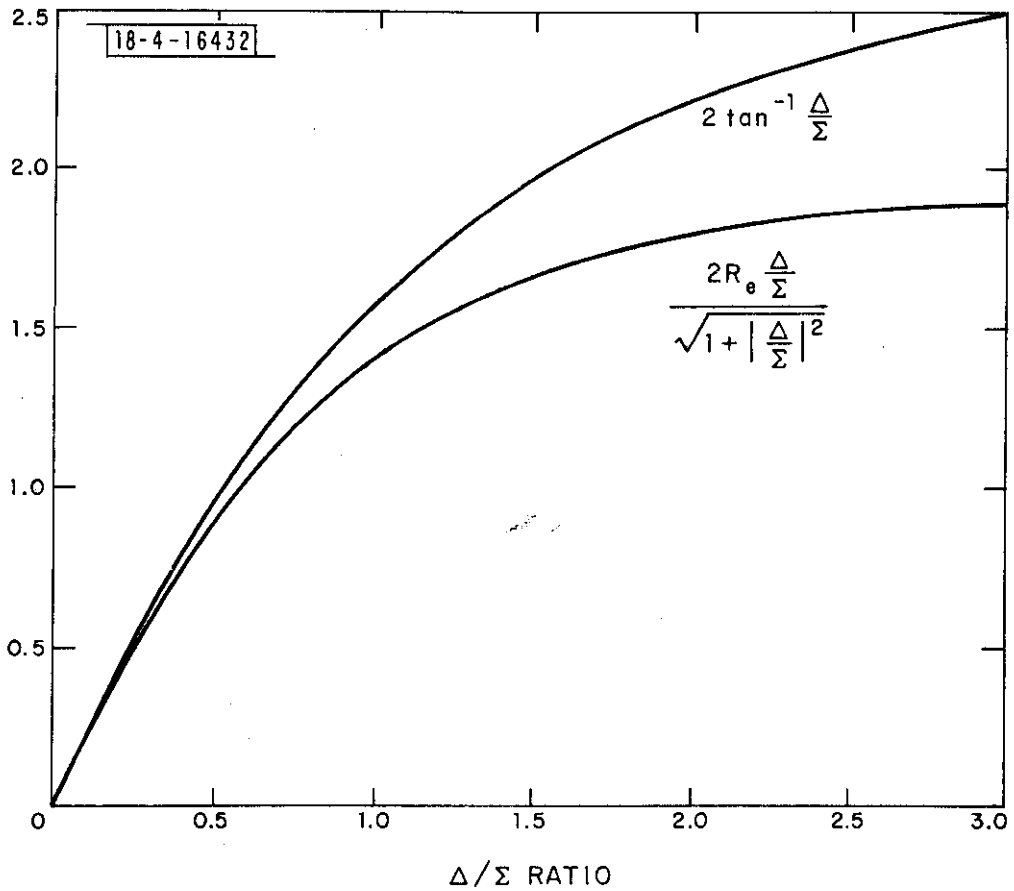

Fig. 2-4. Monopulse processor output vs Δ/Σ.

Typical $G_\Sigma(\theta)$ and $G_\Delta(\theta)$ characteristics are shown in Figure 2-5. The magnitude of the normalized difference pattern of the DABSEF array antenna system is shown in Figure 2-6. Note (from Figure 2-5) that $E(\theta)$ is $\approx$ real for $|\theta| < 3.0^o$ and is monotonically increasing for this range of θ. Thus, there is an unambiguous relationship between MV and θ; i.e.,

$$MV = f[E(\theta)] = h(\theta) \tag{2-10}$$

This function $h(\theta)$ is referred to as the monopulse calibration curve+. Because $h(\theta)$ increases monotonically, it possesses an inverse, defined as

$$\theta = h^{-1}(MV) = g(MV) \tag{2-11}$$

Thus, the azimuth estimator is given by the relation

$$\theta = g(MV) = g[f(\Delta/\Sigma)] \tag{2-12}$$

Equations 2.7-2.12 are shown graphically in Figure 2-7. The operational procedure for obtaining g(MV), the monopulse calibration table, is described in Section 3.3 of Appendix A.

2.4 Monopulse Direction Finding Accuracy

The accuracy with which the azimuth angle of a target can be estimated using the processors described in Section 2.3 in the absence of multipath and interference, has been called "inherent" accuracy. The approach that has been used is to evaluate, for various sources, the error in reported azimuth when only a single reply is available. This will be taken as the "baseline performance." Rather than following the convention of resolving overall errors into contributions by subsystems, the errors will be ordered according to their statistical nature.

2.4.1 Totally Random Errors

In practice, receiver noise is the only source of error which is random on a pulse-to-pulse basis. The standard deviation of the error (σ) is given by the following formula [5]

$$\sigma = \frac{1}{\sqrt{2 \cdot N \cdot SNR}} \frac{\sqrt{1 + E^2(\theta)}}{E'(\theta)} \tag{2-13}$$

+This relationship may be determined by interrogating a fixed transponder at an accurately surveyed position. See Appendix A, Section 3.3.

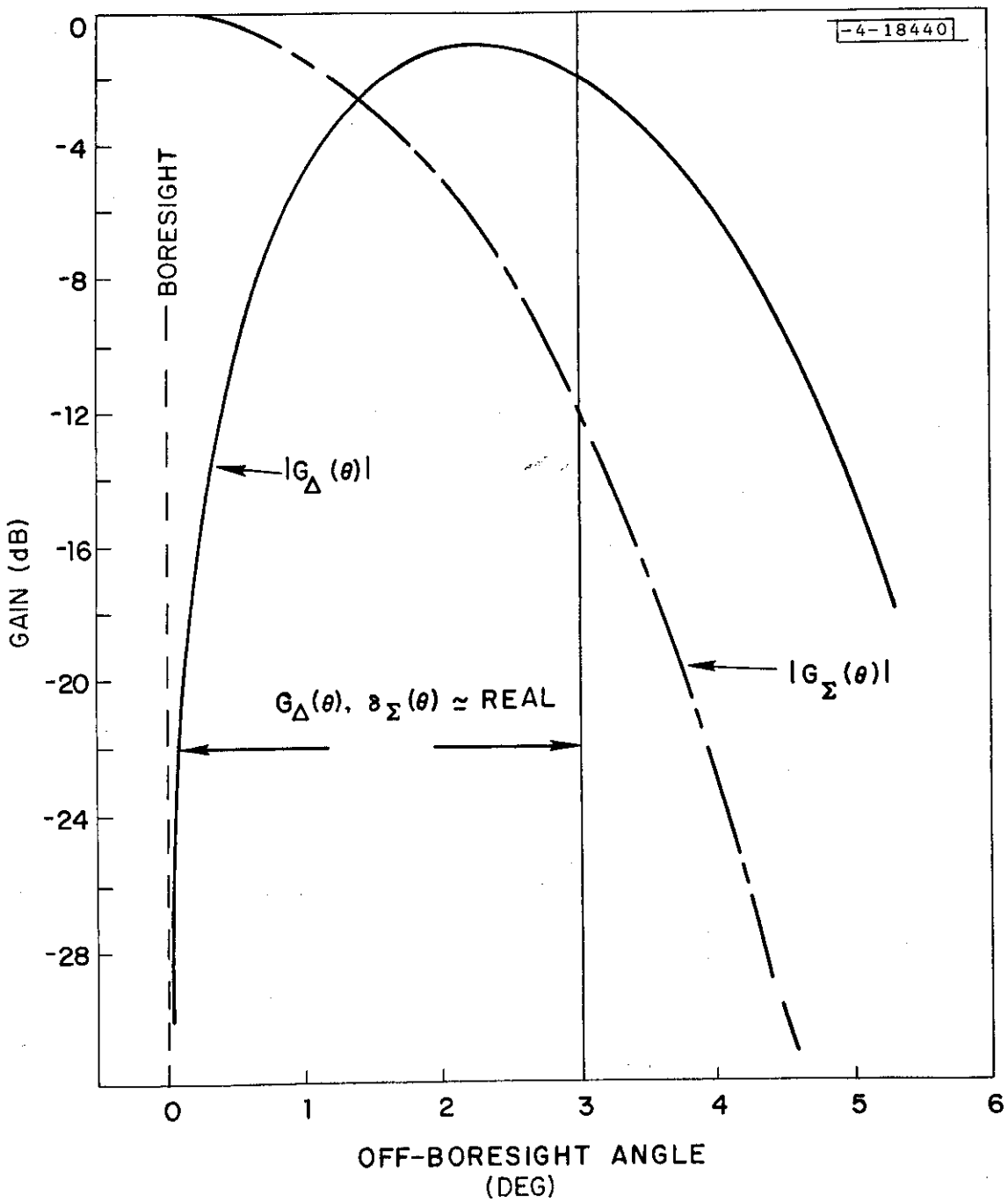

Fig. 2-5. DABSEF antenna patterns near boresight.

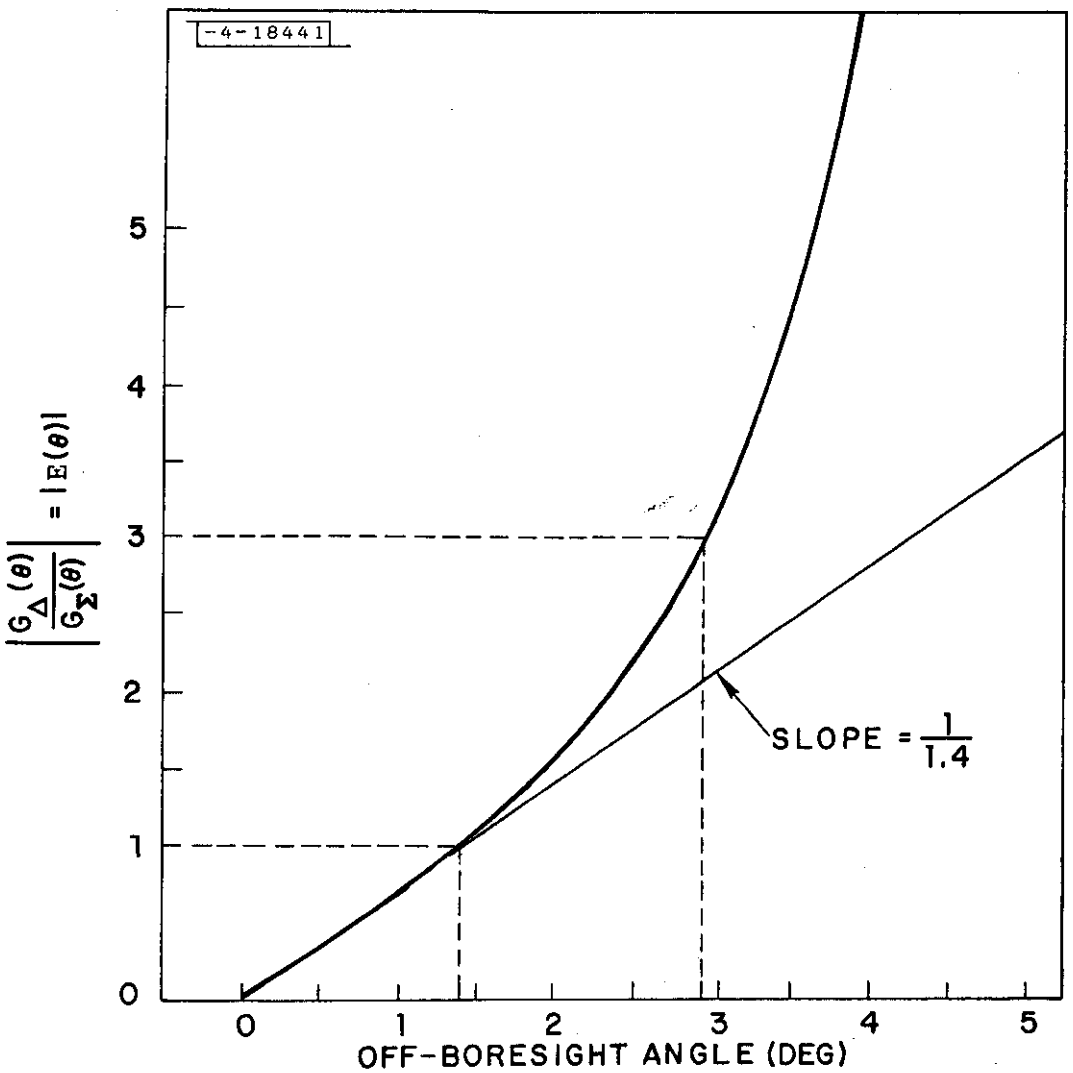

Fig. 2-6. DABSEF normalized antenna pattern.

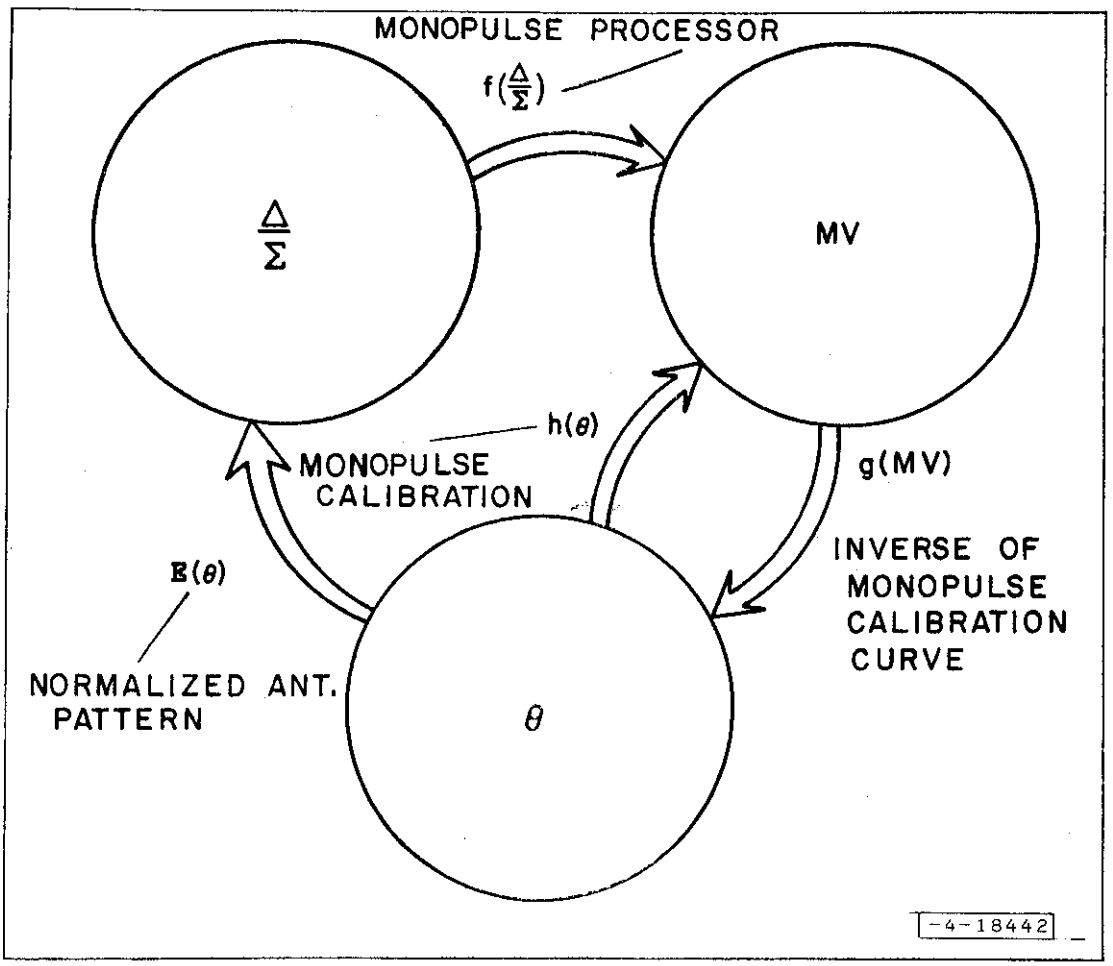

Fig. 2-7. Monopulse functional relations.

PAGE PURPOSELY
LEFT BLANK

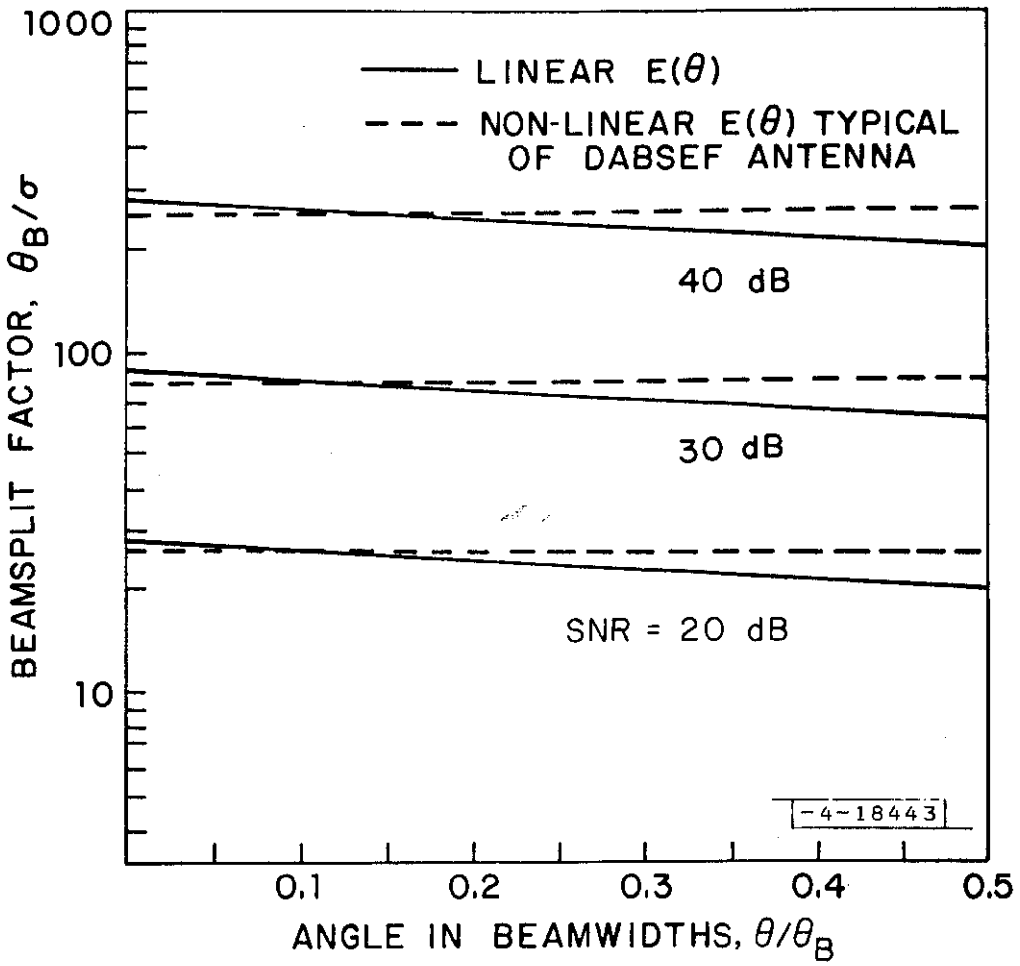

Fig. 2-8. Noise-limited beam-splitting ratio.

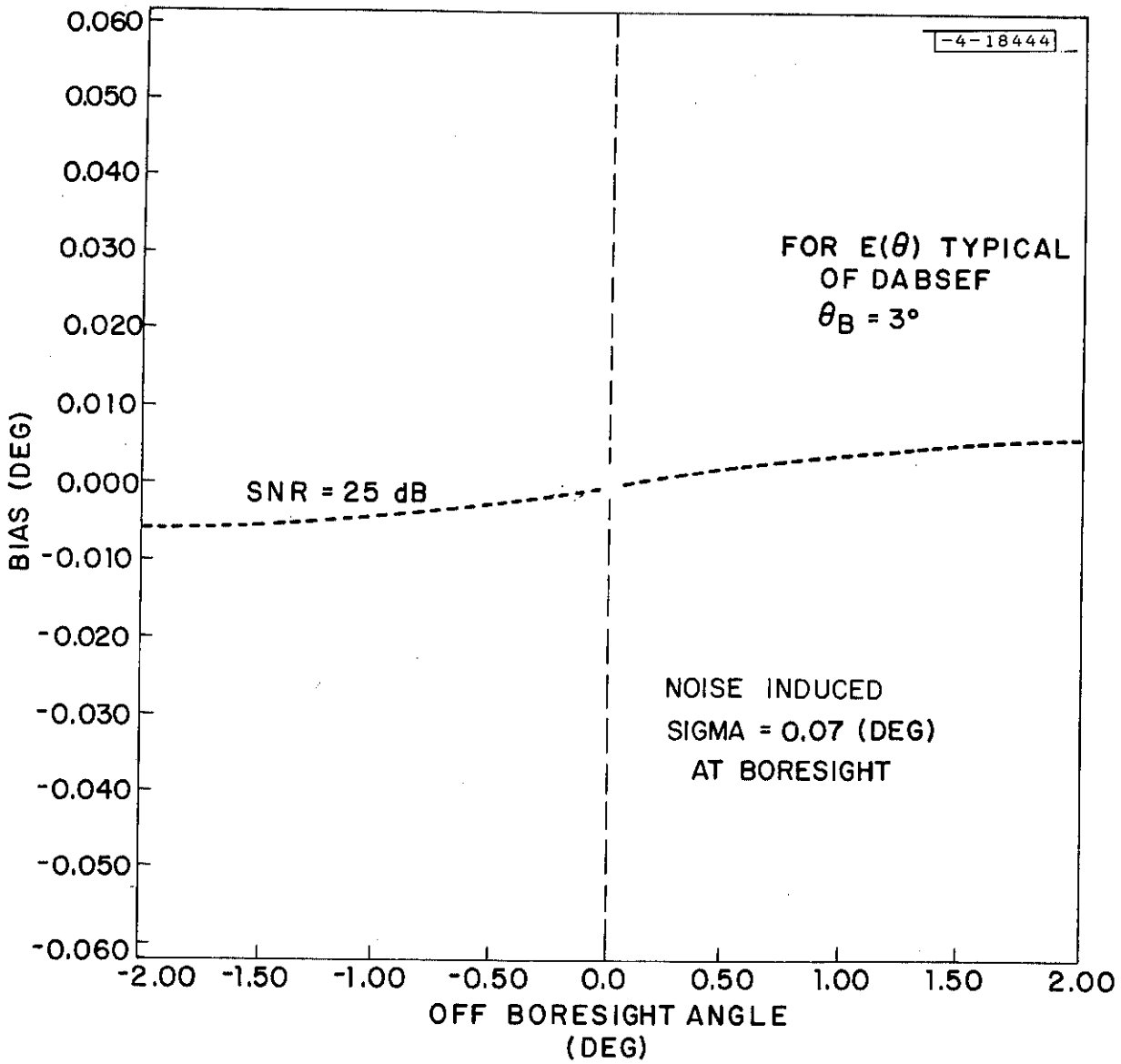

Fig. 2-9. Azimuth bias due to noise.

Insight into this behavior can be gained by assuming linear C(.) and $C_T(.)$.

Let

$$C_T(\gamma) = a\gamma$$

$$C(\gamma) = a'\ \gamma + b$$

Then

$$\varepsilon = a'\frac{\Delta\theta_{true}}{a} + b = \Delta\theta_{true}$$

$$\varepsilon = \Delta\theta_{true}\left(\frac{a'}{a} - 1\right) + b$$

Typical upper bounds on $\left(\frac{a'}{a} - 1\right)$ due to variations in signal characteristics are a few percent and 0.1°, respectively. Experimental measurements of $\left(\frac{a'}{a} - 1\right)$ for many beacon targets of opportunity appear in Appendix A.

The effect of a difference in target elevation angle (α), compared to calibration source elevation angle (α_c) can be derived for the linear region of the processor from geometric considerations with the result that:

$$\frac{a'}{a} \simeq \frac{\cos\ \alpha}{\cos\ \alpha_c}$$

Figure 2-10 shows $\left(\frac{a'}{a} - 1\right)$ vs α for various values of α_c.

Three significant observations may be made with respect to elevation induced errors. First, the "reply bias" errors tend to be of opposite polarity on either side of boresight; this provides a rapid reduction of the net error when two or more replies, sufficiently separated, are available. Secondly, the errors are essentially independent of beamwidth; the driving parameter is off-boresight angle. Thirdly, although azimuth accuracy is usually used to characterize position measurement, the associated cross-range accuracy is for most purposes more directly pertinent. Figure 2-11 shows the cross-range error as a function of ground range for various aircraft altitudes. The curves shown extend inward only to a ground range corresponding to about 40° in elevation and indicate that the cross-range errors vary from tens to a few hundreds of feet.

Other contributions to the reply-dependent errors are:

A/D quantization of the monopulse signal: for an 8-bit (7 plus sign) converter, the rms error is about 1/4% of the maximum off-boresight angle. Azimuth shaft encoder: typical azimuth shaft encoder errors of less than .02 degrees rms are achieved.

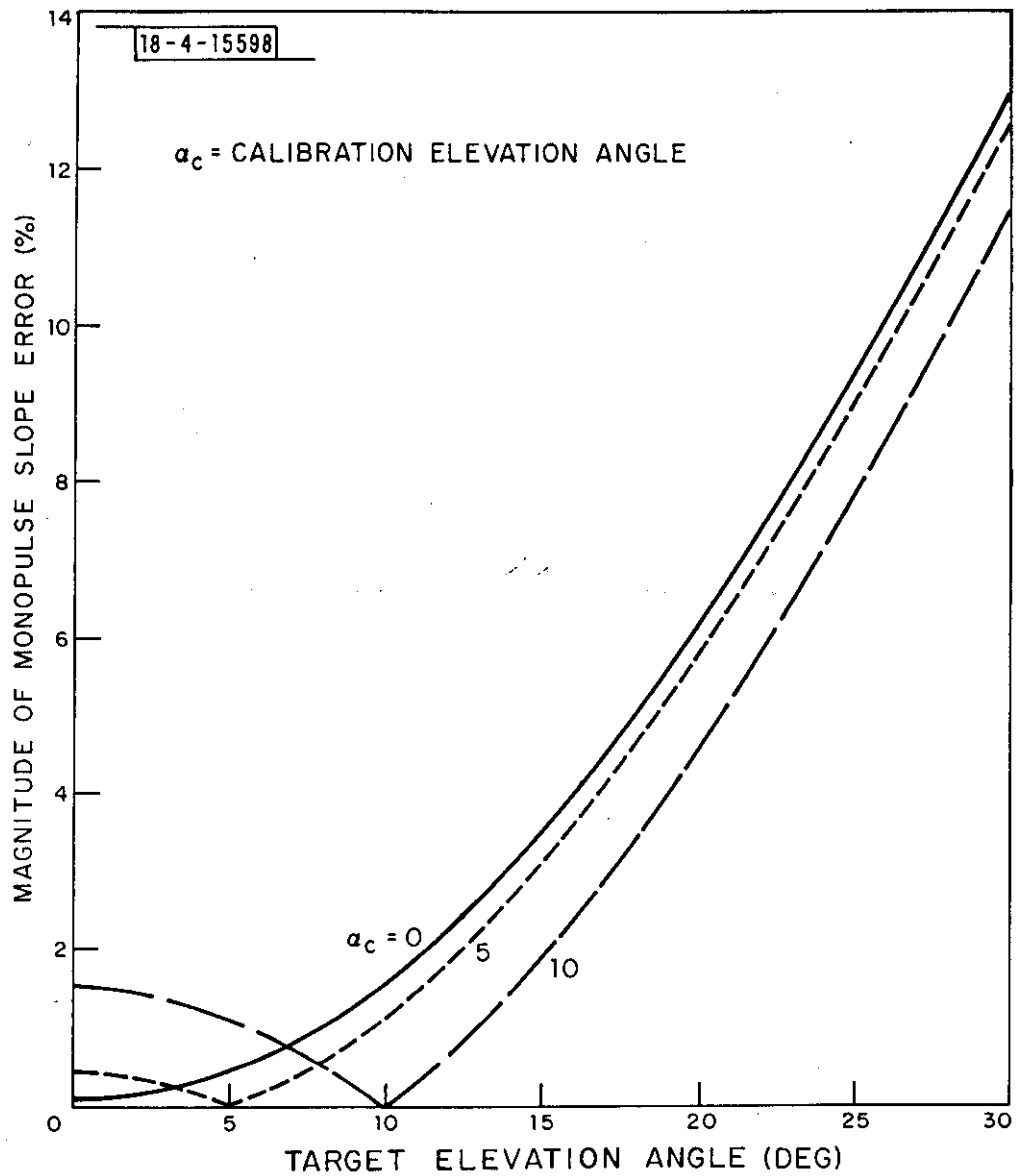

Fig. 2-10. Calibration slope error vs target elevation angle.

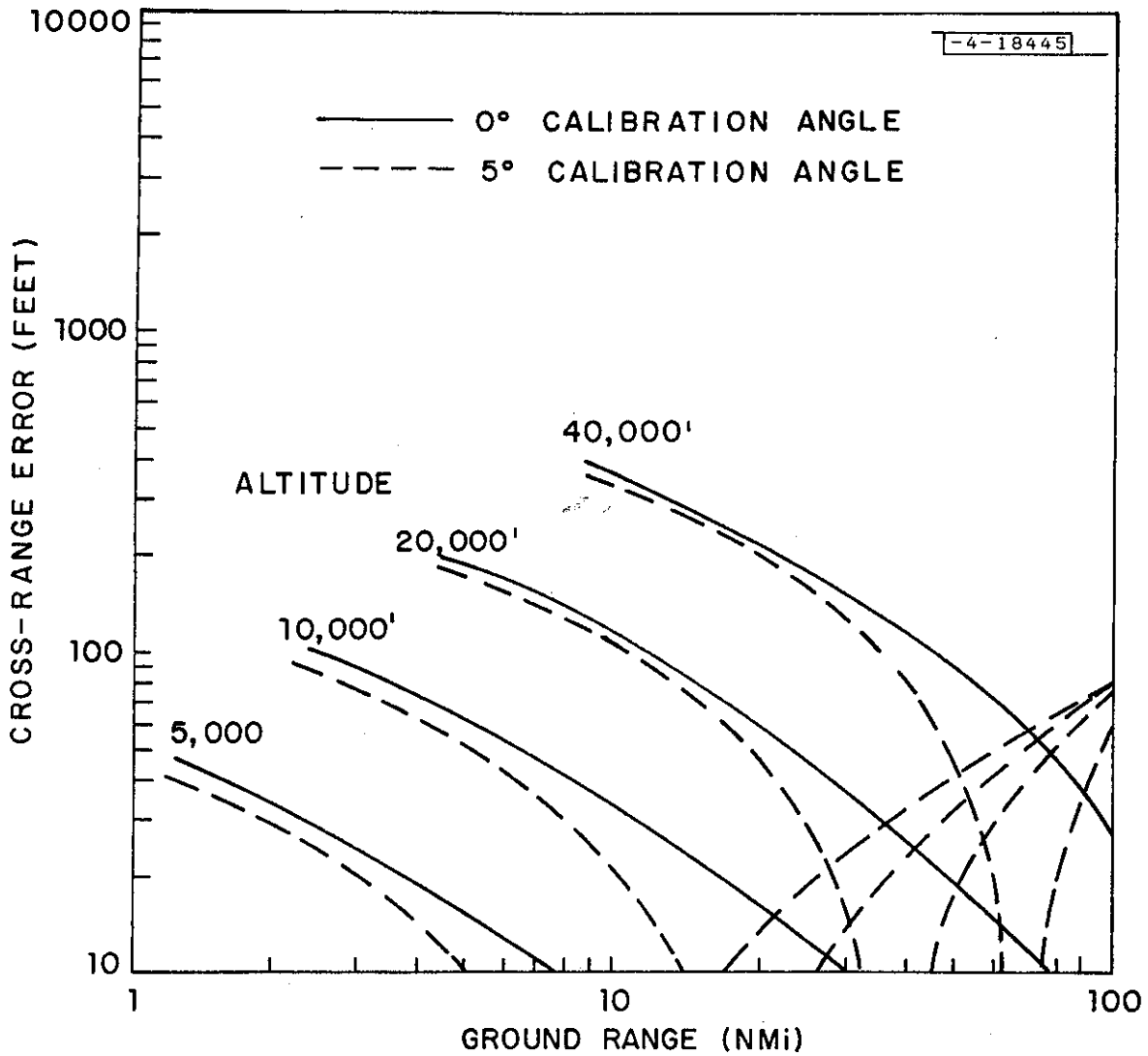

Fig. 2-11. Calibration induced cross-range error.

2.4.3 Scan-Dependent Errors

There are errors which vary only from scan to scan and therefore cannot be eliminated by any form of processing. Wind-induced deflections of the antenna aperture causing an electrical boresight shift is one example. It has been estimated from past experience that the maximum shift for a 40 ft. aperture can be kept to less than 0.05^{o} within the usual range of FAA environmental conditions. Another such error can be caused by drive gear backlash in the presence of wind. For typical drive mechanisms, this error has been estimated at 0.02^{o} maximum.

Whereas the above errors are related to time-varying factors, there are scan dependent errors which are also azimuth-dependent. For example, a radome can, in principle, be a source of such an error; however, the use of a foam radome has been found to virtually eliminate this problem. The rotary joint can also introduce an error if the Σ and Δ channels do not track in amplitude. A 0.05 dB differential error appears to be a reasonable design specification and leads to an error which is at most 1/2% of the off-boresight angle.

2.4.4 Scan-Independent Errors

The errors considered here are system biases. Sources of such errors include errors in the initial system boresight alignment during calibration. None of these appear sufficiently large to be taken into account in the total error budget. Also, since there are variations in the antenna boresight as a function of elevation which cannot be taken into account in the calibration or alignment, this causes an additional bias error for a target which does not change altitude rapidly from scan-to-scan. This error is primarily attributed to aperture errors, and is proportional to beamwidth. The nominal figure is ± 0.01 per degree of beamwidth, maximum.

2.4.5 Direction Finding Summary

An overall summary of monopulse direction finding accuracy is given in Table 2-1 for beamwidths of 4^{o} and 2^{o}. The numbers tabulated are to be interpreted as achievable performance. Contributions which are negligible have been omitted.

TABLE 2-1

DIRECTION FINDING ACCURACY SUMMARY FOR ROTATORS

Type	Origin	Basis	Error, 2^{o}BW	Error, 4^{o}BW
Bias	Calibration of DABS	Aircraft population	$.02^{o}$ rms	$.04^{o}$ rms
	Processor Drift	Long-term corrected	$.025^{o}$rms	$.025^{o}$rms
	Note: Skew, elevation dependent slope error, noise, interference, and azimuth dependent rotary joint errors, introduce negligible bias errors combined $\leq \longrightarrow$		$.01^{o}$	$.01^{o}$
Random	Noise	Median signal/ [N·SNR=Hz dB]	$.007^{o}$	$.013^{o}$
	Scheduler Variation		$.01^{o}$	$.02^{o}$
	Wind	Worst Case Electromechanical	$.03^{o}$	$.03^{o}$
	Shaft encoder quantization		$.001^{o}$	$.001^{o}$
	A/D quantization		$.003^{o}$	$.006^{o}$
	Interference	24K fruit environment within $\pm$ 0.4 BW	$.025^{o}$	$.05^{o}$
Structured	Note: Multi-path and diffraction effects are site/antenna dependent and are not accounted for.			
Total (rss)			$.05^{o}$ rms	$.08^{o}$ rms

3.0 EFFECTS OF INTERFERENCE ON MONOPULSE PERFORMANCE

3.1 Introduction

In addition to the hardware and receiver noise errors discussed in the preceding section, the performance of the monopulse processor is affected by the presence of other time coincident signals such as ATCRBS fruit and ground reflection multipath. Detailed studies of these effects have shown that, in addition to causing an increase in the estimate variance, the presence of interference can cause an estimator bias. For mainbeam interference [6] it has been shown in that this bias is

$$\overline{(\hat{\theta} - \tilde{\theta}_S)} \cong (\theta_I - \theta_S) \frac{\rho_o(\rho_o + \cos\phi)}{1 + 2\rho_o\cos\phi + \rho_o^2} \tag{3-1}$$

where

$$\rho_o = \frac{A_I}{A_S} \frac{G_\Sigma(\theta_I)}{G_\Sigma(\theta_S)} = \frac{1}{SIR} \tag{3-2}$$

where A_S, θ_S are the amplitude and azimuth of the signal, A_I, θ_I, the amplitude and azimuth of the interferer and ϕ is the relative phase between the DABS and the interference, and SIR is the signal to interference ratio. Eqn. 3.1 assumes the half-angle processor (Eqn. 2.13) is linear and modelled by

$$f(\tfrac{\Delta}{\Sigma}) = \mathrm{Re}(\tfrac{\Delta}{\Sigma}) \tag{3-3}$$

and the normalized ratio pattern and calibration curves are also linear.

The bias error is plotted in Fig. 3-1 for a target on boresight, and an interferer at the 3 dB beam edge. In general, the curve demonstrates the large bias that can occur, especially at the out-of-phase condition.

One can more accurately model the half-angle processor as non-linear by Eqn. 2.13,

$$f(\tfrac{\Delta}{\Sigma}) = \mathrm{Re}(\tfrac{\Delta}{\Sigma}) \left[\frac{1}{\sqrt{1 + |\frac{\Delta}{\Sigma}|^2 - 2\ \mathrm{Im}\ (\frac{\Delta}{\Sigma})}} + \frac{1}{\sqrt{1 + |\frac{\Delta}{\Sigma}|^2 + 2\ \mathrm{Im}\ (\frac{\Delta}{\Sigma})}} \right] \tag{3.4}$$

and the normalized ratio pattern, $E(\theta)$, and calibration curve as non-linear.

Figure 3-2 shows the difference between the linear and the non-linear approximations for $\rho_o = -3$ dB, $\theta_I = -2°$ and $\theta_S = 0°$. This variation in estimate error can be extended by averaging over ϕ and θ_I to yield the average interference - induced estimate error (given the presence of interference) vs off-boresight angle. Figure 3-3 shows this result for a cubic approximation to $E(\theta)$ (typical of DABSEF) and a linear approximation for $E(\theta)$ assuming the non-linear half-angle processor of Eqn. 3.4 when the signal to interference ratio (SIR) is 10 dB, and SNR = ∞.

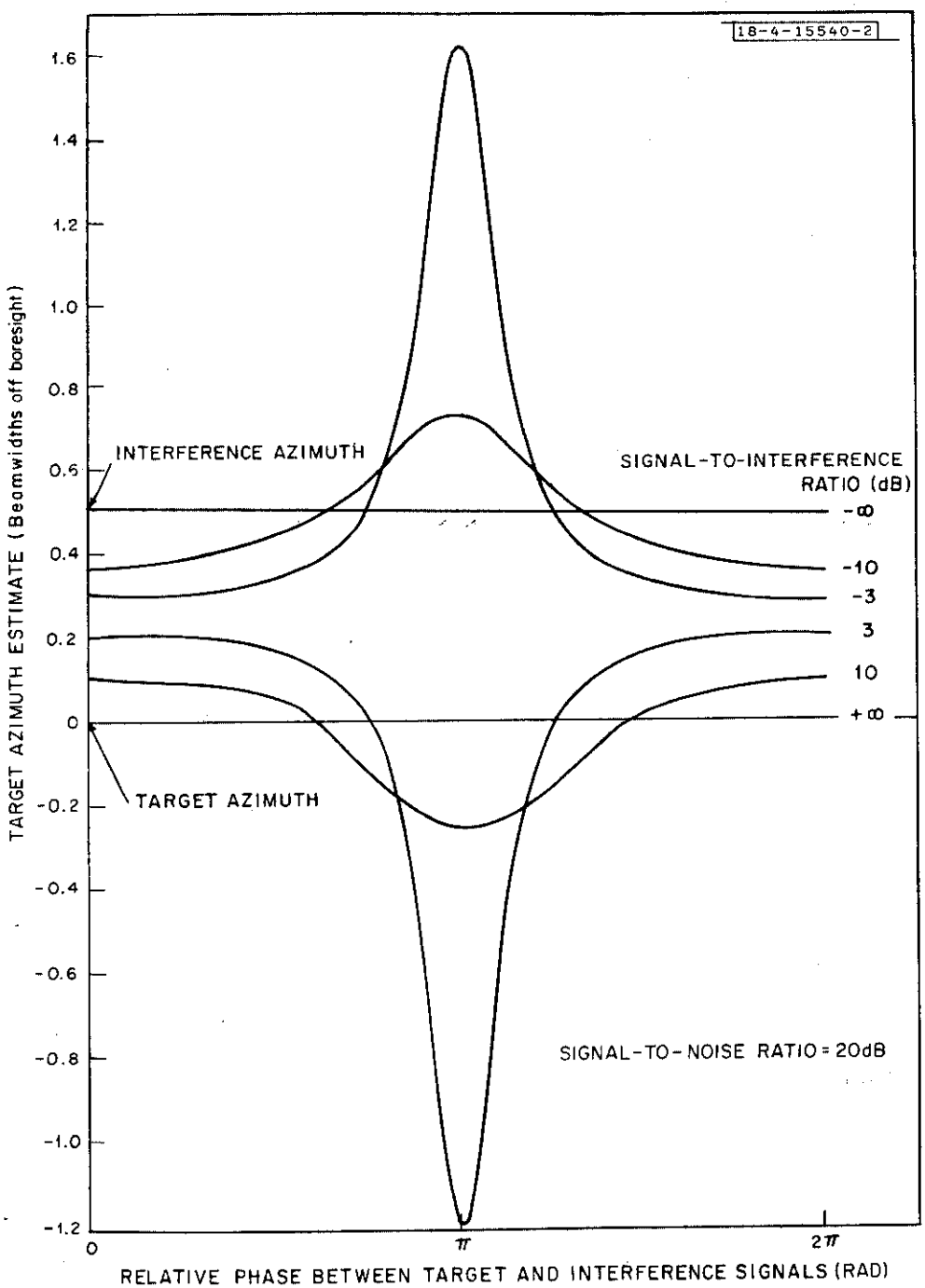

Fig. 3-1. Azimuth estimate in the presence of interference.

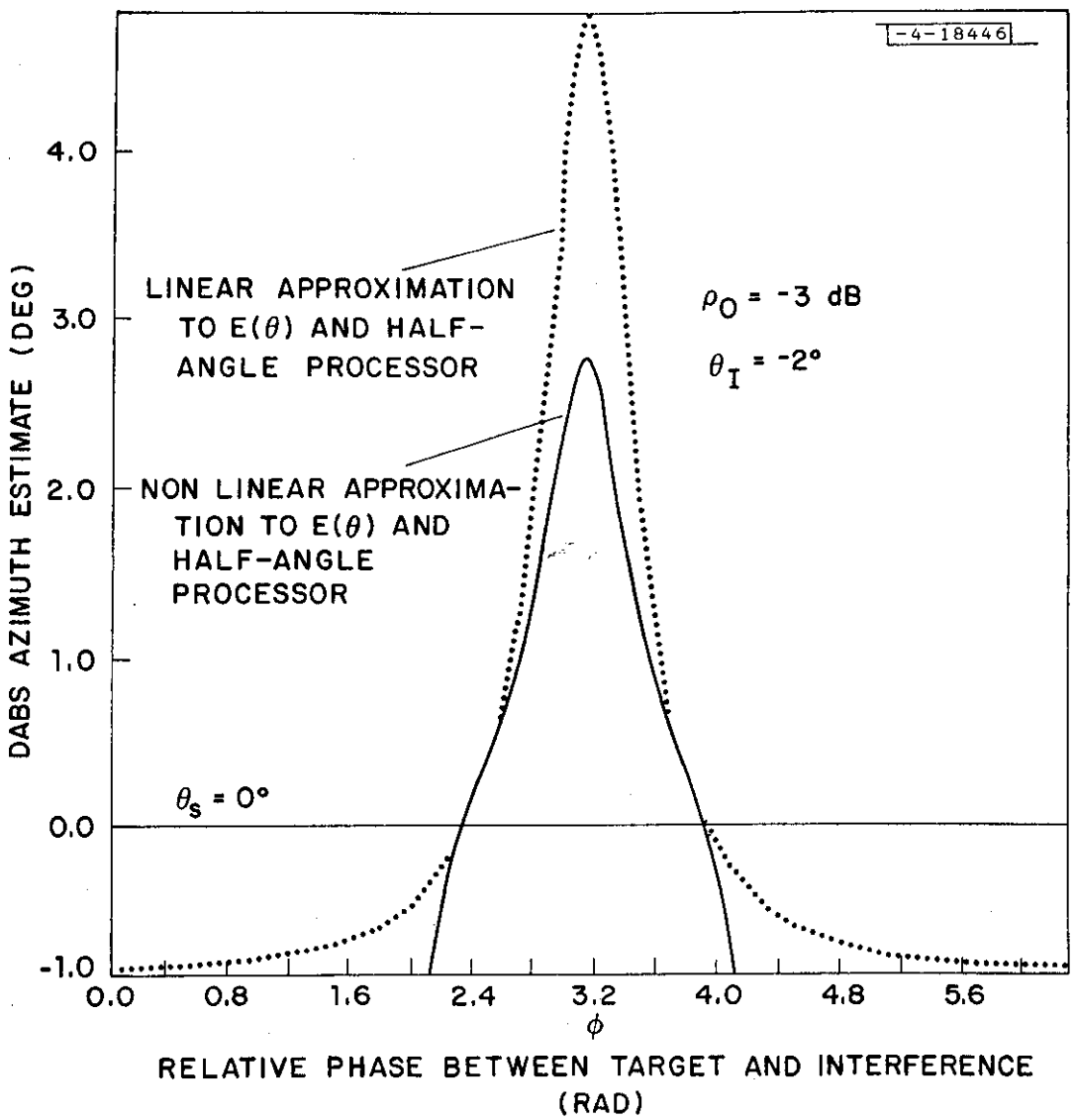

Fig. 3-2. Azimuth estimates vs ϕ.

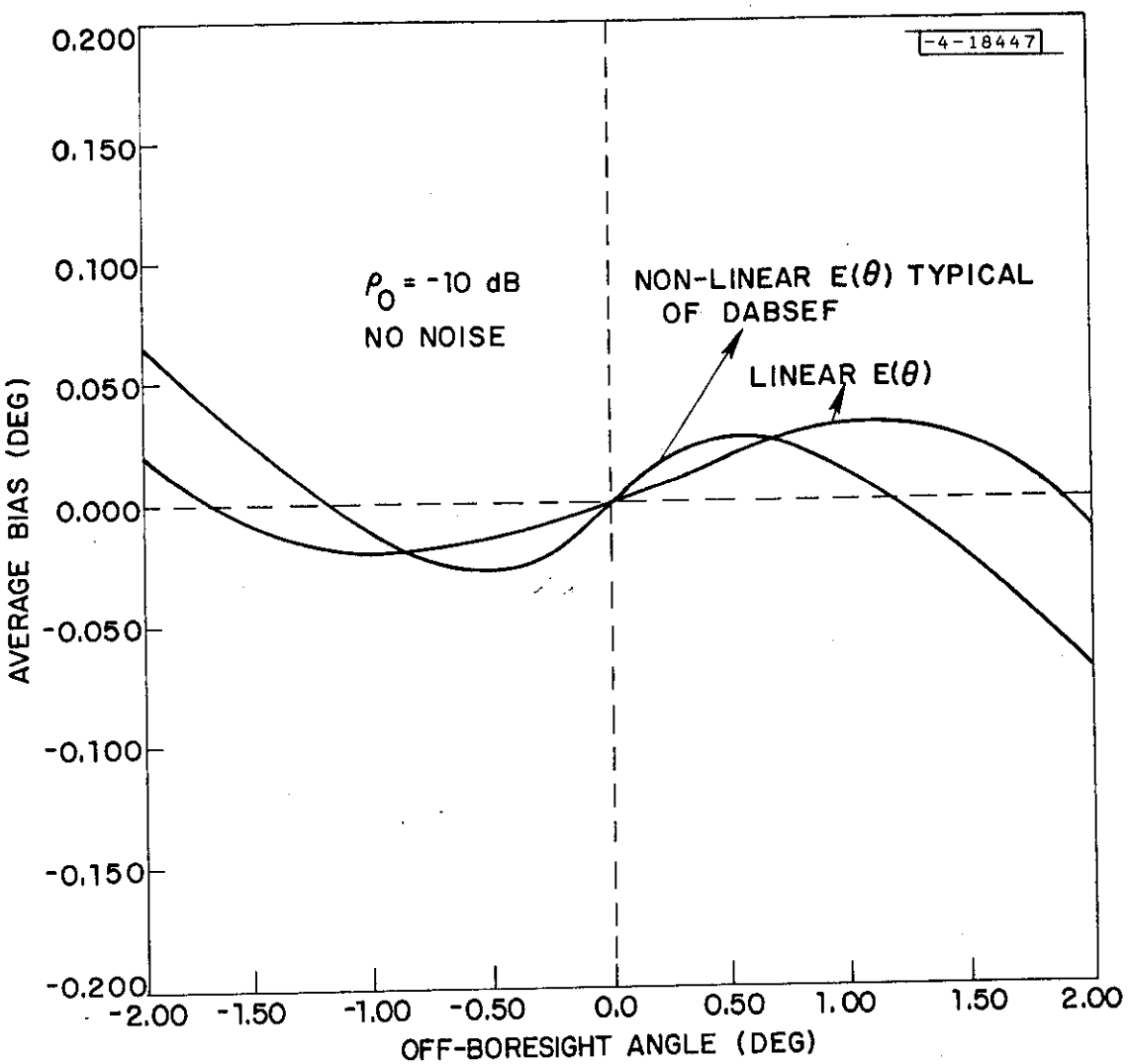

Fig. 3-3. Monopulse bias average.

The effects of interference can be reduced somewhat by attempting to recognize pulses that were possibly interfered with and discarding them from the angle estimation process. The method employed for this purpose by the DABS system is to base the reply azimuth estimate only on those pulses which have a consistent monopulse value; more detail is provided in Appendix A.

3.2 ATCRBS Fruit Interference

In this case the signal-to-interference ratio (SIR), ρ_o^{-1}, can vary over the entire dynamic range of the receiver. From Figures like 3-1 and 3-2 one can show that the interference will have a negligible effect on the bias error if the SIR is greater than +20 dB. As the power of interference increases, the bias increases, with a local maximum occurring at the out-of-phase condition. For SIR's greater than 0 dB, integrating over the phase difference leads to a zero average value for the monopulse error. Since the phases of the DABS and ATCRBS transponders are random from pulse-to-pulse, it is therefore reasonable to assume that the greatest percentage of the sidelobe fruit will result in monopulse bias errors that will tend to average to small errors. For strong mainbeam fruit or for those few sidelobe fruit whose power exeeds that of the DABS transponder, such that the SIR is less than 0 dB, the monopulse bias increases considerably when averaged over all phases, which indicates the fact that the stronger interferer is starting to capture the azimuth estimator. When the interferer completely overpowers the DABS signal, then of course, the monopulse processor simply estimates the fruit azimuth. Simulation and analytical studies have been conducted [7] which indicate that this situation will occur in only a small percentage of the cases to be encountered in the NAFEC area in 1980.

The most important aspects of ATCRBS interference, therefore are the facts that when a fruit overlap occurs, only a relatively small number of the DABS bits will be overlapped, and of those that are, since the DABS and ATCRBS transponders are incoherent from pulse to pulse, the bias error for low level interference, (SIR > 0 dB) will scintillate, and tend to average out to a small value.

3.3 Specular Multipath

In DABS, specular reflections from large flat surfaces typically overlap the direct received signal by a few tens of wavelengths, giving rise to errors of the form described by (3-1). The errors are constant for each pulse in a reply since the reflected signal is coherent with the direct signal.

For reflectors normal to the beam, the reflection azimuth is the same as that of the direct path and leads to changes in signal to noise ratio, but introduces no azimuth error, since $\theta_I = \theta_S$ (in 3-1).

When the surface is tilted slightly the effects of differences between θ_I and θ_S are mitigated somewhat by the reduced amplitude of the reflected signal

resulting from reflection coefficients less than unity and the cutoff in the antenna elevation pattern. Only very large and nearby structures will be sources of significant specular reflection multipath entering the mainbeam. Offboresight reflectors producing sidelobe multipath signals will have little effect since the relatively low sidelobe gain helps to reduce errors.

3.4 Diffuse Multipath

The antithesis of specular multipath is completely diffuse reflections in which each elemental area of the reflecting surface scatters the incident wave independently. Viewed from the interrogator the diffuse reflecting surface consists of a large number of point sources having random amplitudes and phases. The diffuse reflections combine randomly at the interrogator to produce a resultant that is coherent for the duration of a transponder reply because the change in path length due to a/c motion is insignificant during the reply. However, over an ensemble of transponder replies separated sufficiently in time or space, the resultant of the diffuse reflections has a Rayleigh amplitude distribution and a random phase. Analytical and simulation studies of the effects of diffuse multipath on monopulse performance have led to the following observations: (i) Time dispersion effects are not important for MHz data rate transmission; (ii) The errors in azimuth estimation are negligible and orders of magnitude smaller than those that might be observed for specular multipath [8]. Therefore, diffuse multipath should present no serious limitations in direction finding capabilities in DABS direction finding, a conclusion which has also been supported by analysis of the DABSEF experimental data.

3.5 Diffraction Effects

Beacon or radar surveillance systems measure target azimuth by estimating the orientation of the wavefront arriving at the antenna. DABS utilizes monopulse processing to directly estimate the orientation of the wavefront relative to antenna pointing direction, while present day ATCRBS essentially computes the centroid of the pointing directions from which the directional beam receives signal energy greater than some threshold.

Phenomena which perturb the wavefront orientation must necessarily result in errors in target azimuth estimate. One such phenomena occurs when portions of the wavefront are intercepted or blocked by obstructions such as buildings. The resulting field at the ground receiving antenna can be shown to be the unperturbed field less the field through a rectangular opening (with dimensions of the blocking obstacle) in an opaque screen.

Recent investigations at Lincoln Laboratory (Refs. 10 and 11) have shown that in many cases the dimensions of the obstacle are such that the received field can be satisfactorily appoximated as the sum of several rays; one is from the target, and the other(s) from appropriate points on the obstacle* and having appropriate amplitude and phases relative to the direct ray.

The effect of diffraction on present day ATCRBS beamsplitting can be evaluated by modelling the azimuth estimator as the average of the antenna pointing directions at which the first and last replies having a power greater than some threshold are received. This involves computing the received power as the antenna sweeps past the target. The azimuth estimate error arises when the received power of replies near the beam edge in the absence of the obstacle is modified by diffraction rays such that the threshold crossing azimuths change, leading to an erroneous azimuth estimate.

The effect on DABS can be evaluated by superposing the various rays to obtain the sum and difference signals and then computing the monopulse processor output. This need only be done when the antenna is pointing at the target since DABS makes angle estimates only near boresight.

In both DABS and ATCRBS the azimuth estimate error is found to vary as a function of obstacle size and the azimuthal separation between the target and obstacle. When the separation is zero, there is no error, as would be suggested by symmetry arguments. As the separation increases the error oscillates. The oscillation reflects the phase changes in the obstacle ray implied by the differences between the direct path to the target and the path through the obstacle. The errors are zero when the direct and diffraction rays are nearly in quadrature.

---

*Consequently, one can use simple interferer analysis to analyze diffraction phenomena.

4.0 EFFECTS OF ANTENNA DESIGN

4.1 Introduction

The antenna design parameters that have an impact on monopulse processing performance are the sidelobe levels of the sum and difference patterns, the vertical cutoff of the lower edge of the elevation pattern, and the slope of the Δ/Σ ratio $[E'(\theta)]$. Since the sum pattern sidelobes also have an impact on the DABS message decoding performance, it is assumed that this is not a variable parameter. Therefore, we shall assume a sum pattern which is typified by the standard 28-foot hogtrough antenna, as shown in Fig. 4-1, and confine our attention to an examination of the effects of difference pattern sidelobe levels and the elevation pattern cutoff. As discussed in the preceding section, the most significant effect that interference has on the monopulse performance is the introduction of the bias term approximately given by (3-1).

$$\overline{(\hat{\theta} - \tilde{\theta}_S)} \cong (\theta_I - \theta_S) \frac{\rho_o(\rho_o + \cos\phi)}{1 + 2\rho_o\cos\phi + \rho_o^2} \tag{4-1}$$

where

$$\rho_o = \frac{A_I}{A_S} \cdot \frac{G_\Sigma(\theta_I)}{G_\Sigma(\theta_S)} = \frac{1}{SIR} \tag{4-2}$$

$$\tilde{\theta}_I = \frac{1}{K} \frac{G_A(\theta_I)}{G_\Sigma(\theta_I)} \tag{4-3}$$

(K, proportionality factor)

The maximum error occurs at the out-of-phase condition, $\phi = \pi$, hence

$$\overline{|\hat{\theta} - \theta_S|} \leq \frac{\rho_o}{1 - \rho_o} |\theta_I - \theta_S| \tag{4-4}$$

For a DABS target near boresight, $G_\Sigma(\theta_S) = G_\Sigma(0)$ and if the sum and difference patterns are normalized to $G_\Sigma(0)$, the error expression can be written

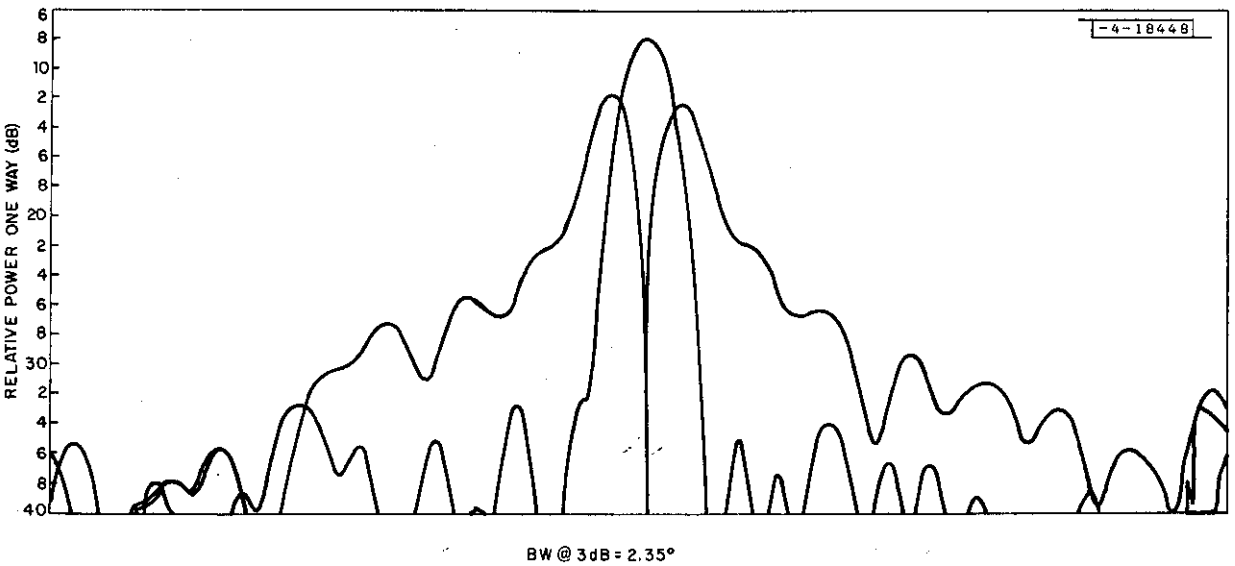

Fig. 4-1. RSi (hogtrough) Σ and Δ patterns.

$$\overline{|(\hat{\theta} - \theta_S)|} \leq \left\{ \frac{\rho' G_\Sigma(\theta_I)}{1 - \rho' G_\Sigma(\theta_I)} \right\} \left| \theta_s - \frac{1}{k} \frac{G_\Delta(\theta_I)}{G_\Sigma(\theta_I)} \right| \tag{4-5}$$

where $\rho' = \rho G_\Sigma(\theta_I)/G_\Sigma(\theta_S)$ is the reflection coefficient after the elevation pattern effects have been taken into account.

4.2 Mainbeam Multipath

For the mainbeam multipath, θ_I is near boresight so $G_\Delta(\theta_I)/G_\Sigma(\theta_I) \approx k\theta_I$ and $G_\Sigma(\theta_I) \approx 1$, so

$$\overline{|(\hat{\theta} - \theta_S)|} \leq \frac{\rho'}{1 - \rho'} |\theta_S - \theta_I| \tag{4-6}$$

As mentioned in a previous section, the interference azimuth is related to the surface tilt and elevation angle. The relationship is approximately

$$\theta_I = \theta_S + 2\beta\alpha_s \tag{4-7}$$

where β is the surface tilt and α_S the beacon elevation, both in radians. Therefore, the peak error is

$$\overline{|(\hat{\theta} - \theta_S)|} \leq \frac{\rho G_\Sigma(\alpha_I)/G_\Sigma(\alpha_S)}{1 - \rho G_\Sigma(\alpha_I)/G_\Sigma(\alpha_S)} \tag{4-8}$$

Therefore only the elevation pattern affects the monopulse performance in the presence of mainbeam multipath. However, its significance is negligible since even if we neglect the attenuation by this pattern and conservatively assume a reflection coefficient of 0.5, then the peak bias error will be $.003^o$ for a surface tilted at 2^o and a transponder equipped aircraft at 3^o elevation. Since this error is inconsequential, we conclude that antenna pattern design is of little importance in reducing the error due to mainbeam multipath.

4.2.1 Experiment Results

Experiments were conducted at DABSEF to verify the above analytical model. In these experiments the monopulse azimuth error was measured for a number of radial test flights around the DABSEF facility. The standard deviation of the monopulse error for a number of test flights is summarized in Figure 4-2. The data shown are for two conditions of antenna elevation pointing, 0° elevation and -5° elevation. The increase in monopulse estimation error, when the antenna was tilted down (-5°) is likely due to increased "in-beam" multipath.

4.3 Sidelobe Multipath

When the specular multipath enters through the antenna pattern sidelobes, then $\rho' G_{\Sigma}(\theta_I) << 1$ and

$$\overline{|(\hat{\theta} - \theta_S)|} \leq \rho' \left| G_{\Sigma}(\theta_I)\ \theta_s - \frac{1}{k} G_{\Delta}(\theta_I) \right| \qquad (4\text{-}9)$$

It is clear that for this case, the error is smallest when the sum and difference beam sidelobes are smallest. When in addition the target is near boresight, the expression reduces to

$$\overline{|(\hat{\theta} - \theta_S)|} \leq \rho [G_{\Sigma}(\alpha_I)/G_{\Sigma}(\alpha_s)]\ [G_{\Delta}(\theta_I)/k] \qquad (4\text{-}10)$$

which shows that the error can be reduced by lowering the difference beam sidelobes, increasing the slope of normalized difference pattern and increasing the cutoff of the vertical elevation pattern.

The direction finding (DF) error for a specific multipath signal has been compared for two antennas of interest, namely the DABSEF antenna, which has independent Σ and Δ distribution networks giving low Δ pattern sidelobes as shown in Figure 4-3, a, b, and the RSi split hogtrough shown in Figure 4-1. The DF error as a function of multipath signal azimuth is plotted in Figure 4-4 for a DABS target on boresight and a reflection coefficient of 0.5 where the elevation pattern attenuation effects have been ignored. Figure 4-4 shows the reduction in peak error resulting from the narrower mainbeam of the

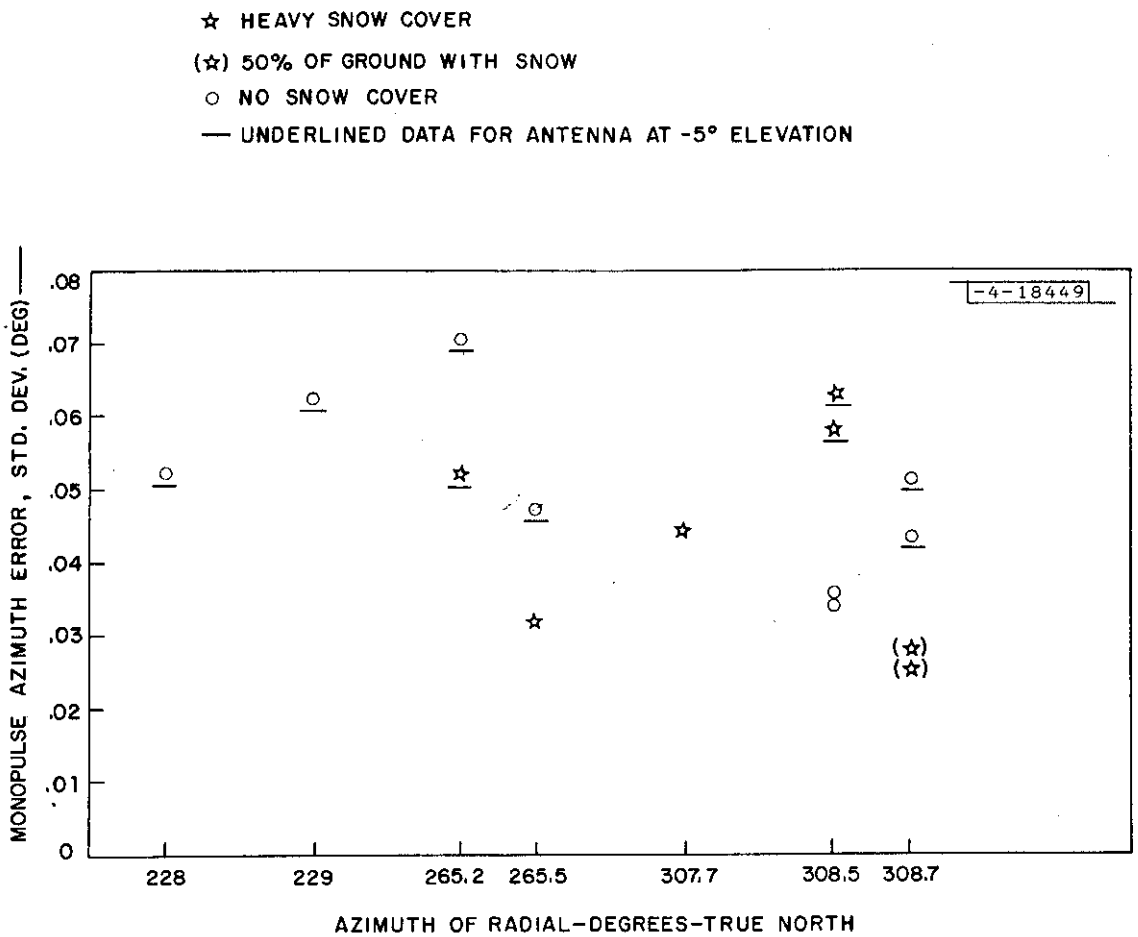

Fig. 4-2. Monopulse errors for antenna elevation angles of 0 and -5 degrees.

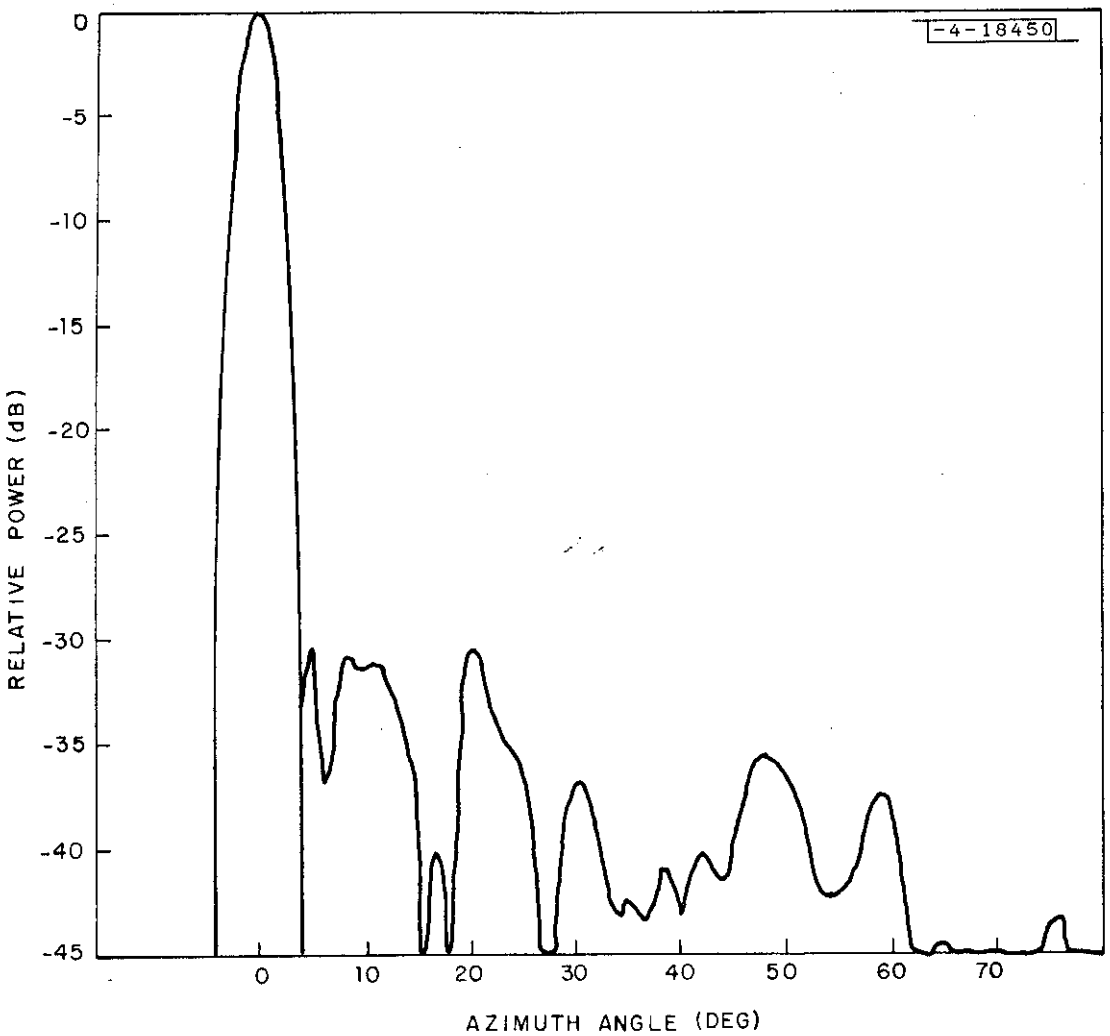

Fig. 4-3a. DABSEF sum pattern at 5° elevation (1090 MHz).

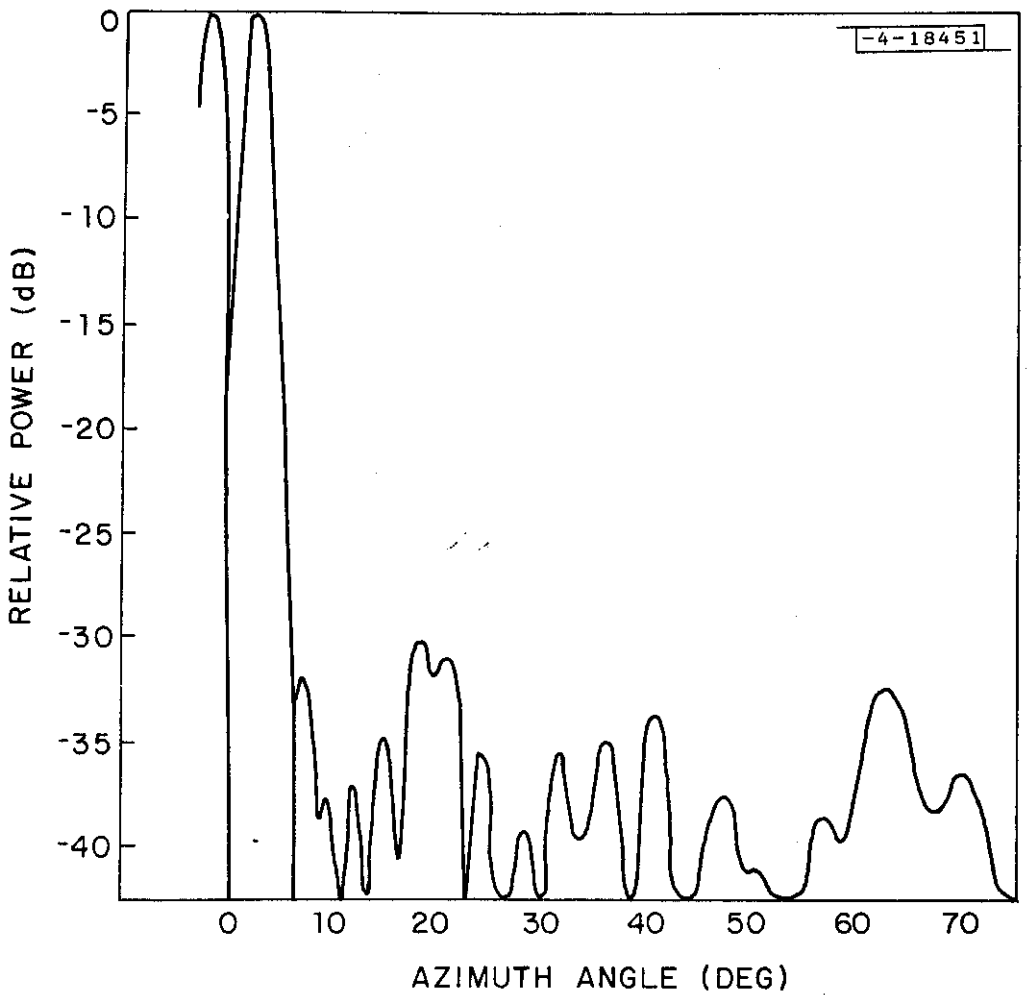

Fig. 4-3b. DABSEF difference pattern at 5° elevation (1090 MHz).

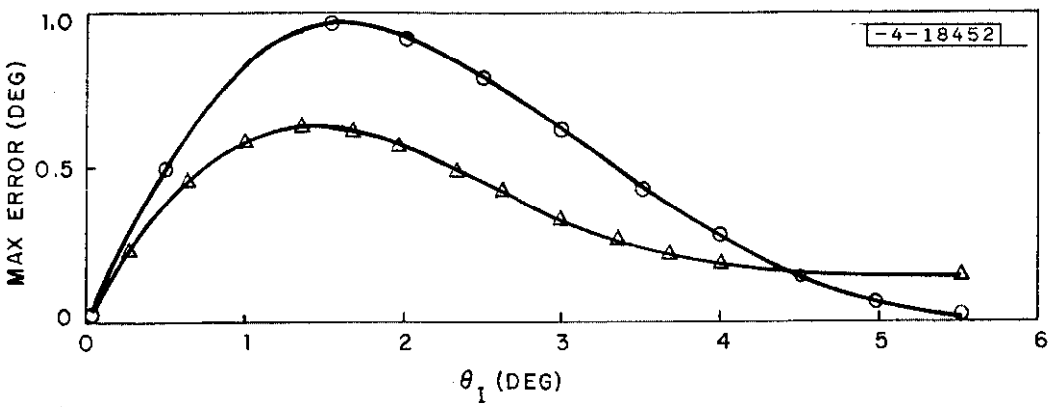

$\rho = 0.5$

⊖—⊖ = DABSEF ANTENNA (22 ft)

△—△ = RSi HOGTROUGH (28ft)

Fig. 4-4. Maximum direction finding error vs multipath azimuth.

hogtrough. (The DABSEF 3 dB beamwidth is 3.2° while for the RSi hogtrough it is 2.35°.) For larger multipath azimuths, the peak error for the hogtrough is larger because of the higher difference pattern sidelobes (-14 dB for the hogtrough, -30 for the DABSEF antenna).

However, sidelobe multipath errors are less than peak mainbeam multipath errors even for the hogtrough. When this is considered together with the expected distribution of multipath azimuths and amplitudes, the usefulness of low difference pattern sidelobes for multipath error reduction is marginal.

4.4 ATCRBS Fruit

The requirement for low sum and difference pattern sidelobes will be a function of sensor coverage (terminal or en-route), terrain shielding, and ATCRBS fruit levels. Curves showing the relation between target aircraft range and potentially interfering ATCRBS fruit replies per second, as a function of antenna sidelobe levels, are shown in Fig. 4-5. The fruit model used has aircraft uniformly distributed in range, total rate of 36K fruit replies/second, and aircraft effective radiated power of +23 dBW.

Antennas for terminal area coverage (50 nmi) can have relatively high sidelobes (-25 dB rms), and still not have ATCRBS fruit replies affect monopulse direction finding/(DF) accuracy. Simulation results indicate that 16K potentially interfering fruit replies/second will add 0.07 degrees of DF error for aircraft interrogated off-boresight at the sum/difference pattern crossover point. The terminal site is generally aided by terrain shielding, which reduces coverage and potentially interfering ATCRBS fruit. As can be seen from the curves shown in Fig. 4-5, en-route sites with good coverage will require antennas with relatively low sidelobes to support accurate monopulse DF for aircraft targets at long range (to 200 nmi).

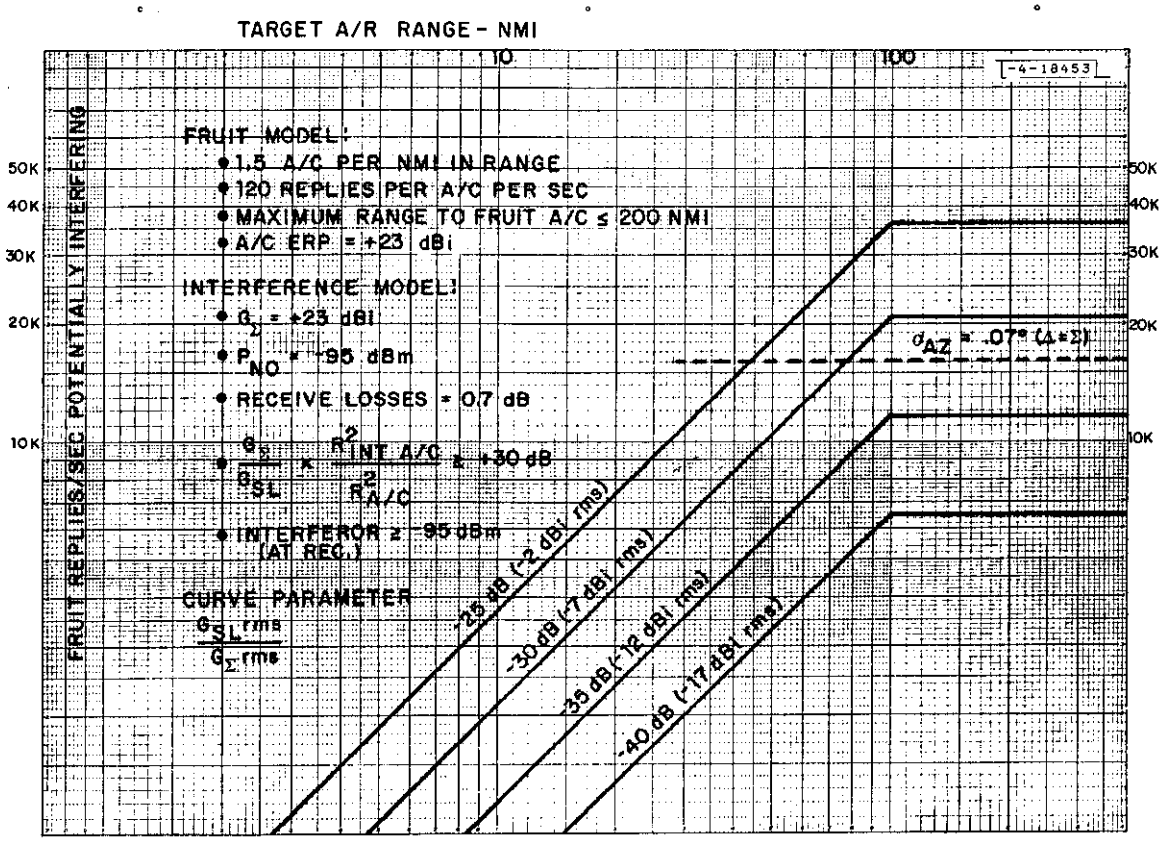

Fig. 4-5. Potential fruit rate vs aircraft range.

5.0 MONOPULSE PROCESSOR STABILITY AND SENSITIVITY

The performance of the monopulse processor described in Appendix A has been evaluated as a function of time, frequency, and amplitude using a fixed, surveyed, calibration transponder. (See Appendix A, Section 3.3)

5.1 Stability

The stability data was obtained from 66 calibrations taken during the first 6 months of 1975. Stability was evaluated at boresight and at $\pm 1^{\circ}$ off boresight. The results are shown in Figure 5-1. The errors show no long term drift and the standard deviations are $.045^{\circ}$, $.021^{\circ}$, $.034^{\circ}$, for -1°, 0°, and $+1^{\circ}$ offboresight respectively.

5.2 Amplitude Sensitivity

Amplitude sensitivity was determined by performing three calibrations at 1090 MHz while attenuating the received signal from the calibration transponder by 0 dB, -23 dB, and -39 dB. The results appear in Figure 5-2 and show that the bias errors due to amplitude are constant across the beam and less than 0.03°.

5.3 Frequency Sensitivity

The sensitivity of the monopulse processor to the received signal frequency was evaluated by performing 7 calibrations at various frequencies with the results shown in Figure 5-3. Note that at 1086, 1087, and 1094 MHz the errors exceed 0.1°. However, 1086 and 1094 MHz are outside the 1090± 3 MHz National Standard for ATCRBS transponders. Investigations at Lincoln Laboratory, [9] indicate that ATCRBS transponder frequencies are nearly normally distributed around 1090 MHz with a standard deviation of 1.75 MHz. In Section 3.6 the measured average azimuth estimate error per degree offboresight for a large sample of ATCRBS targets is shown. Since the dominant error mechanism appears to be transponder frequency, Figure 5-4 has been drawn to depict the result of weighting the frequency sensitivity data by the transponder frequency distribution. The expected average error in Figure 5-4 is 0.02° per degree offboresight. The ATCRBS azimuth measurement is generally taken to be the average of the estimates for replies that straddle boresight, thus, reducing the differential frequency contribution to the azimuth estimate errors to much less than 0.1°.

For DABS targets on the roll call, the offboresight azimuth at which the reply is received may lie anywhere within $\pm 1.5^{\circ}$ (from scan to scan), but with a tendency to lie nearer to -1.5° (the leading edge of the beam) due to the nature of the interrogation scheduling algorithm. Under the assumption of a right triangular distribution of interrogation offboresight angles (favoring the leading edge), then even a 1087 MHz target (having 0.2°/degree error slope) will only experience a scan-to-scan standard deviation of 0.07° due to this effect.

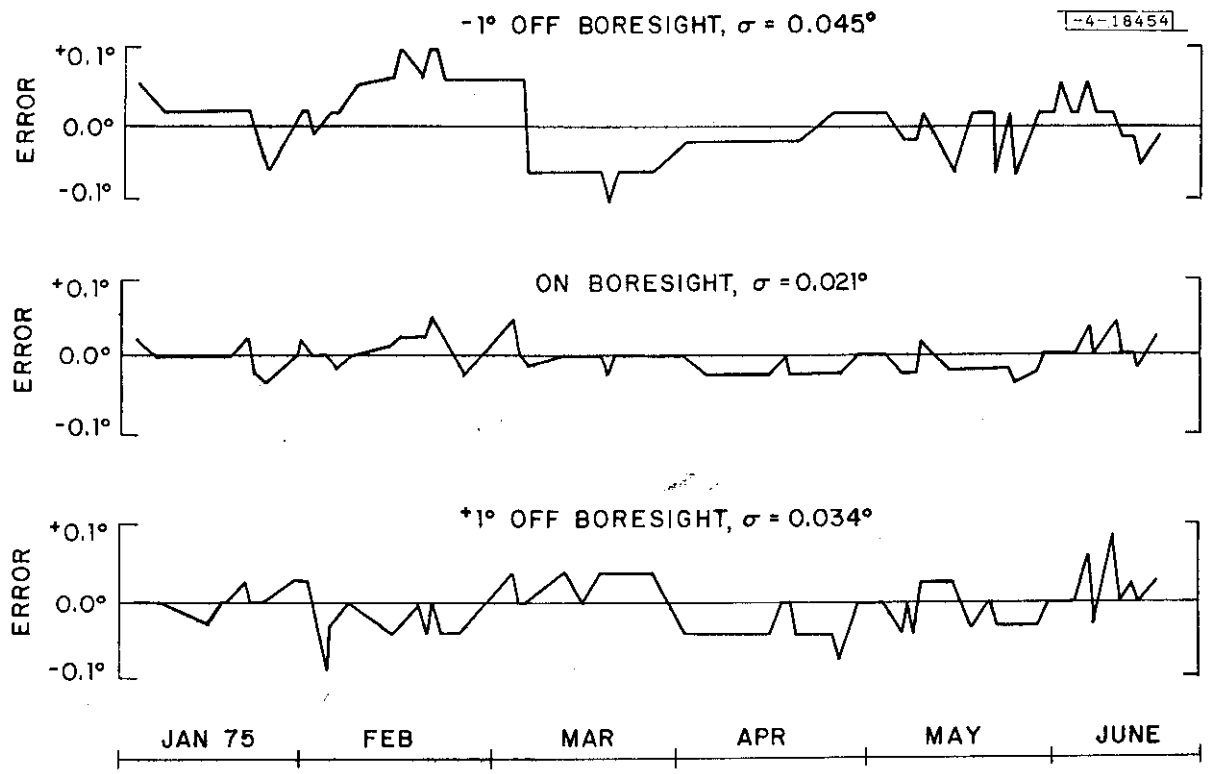

Fig. 5-1. Monopulse processor stability.

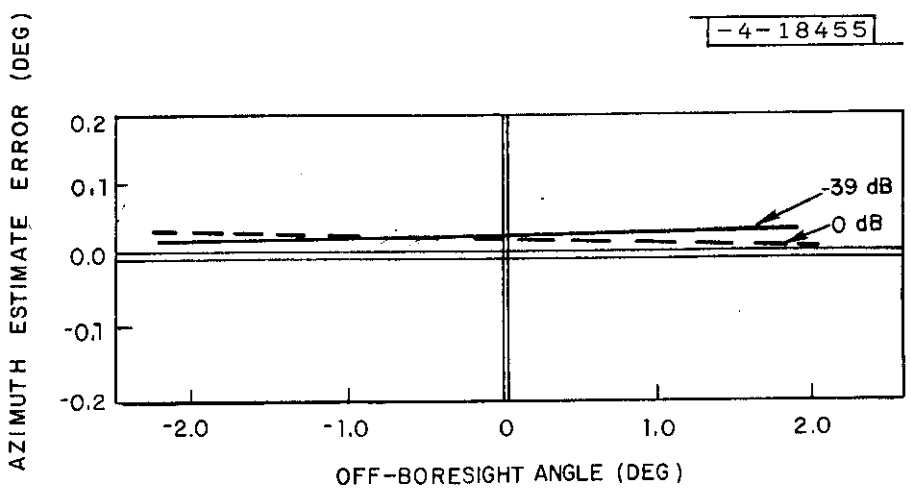

Fig. 5-2. Monopulse processor amplitude sensitivity.

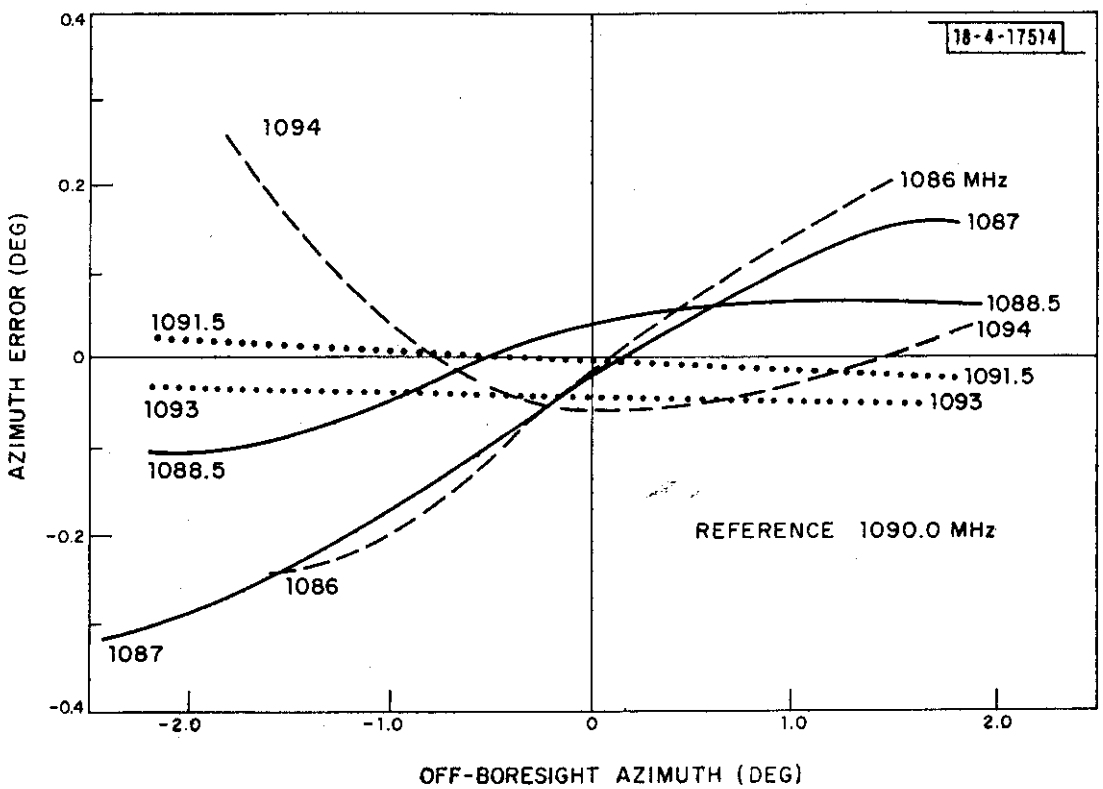

Fig. 5-3. Monopulse processor frequency sensitivity.

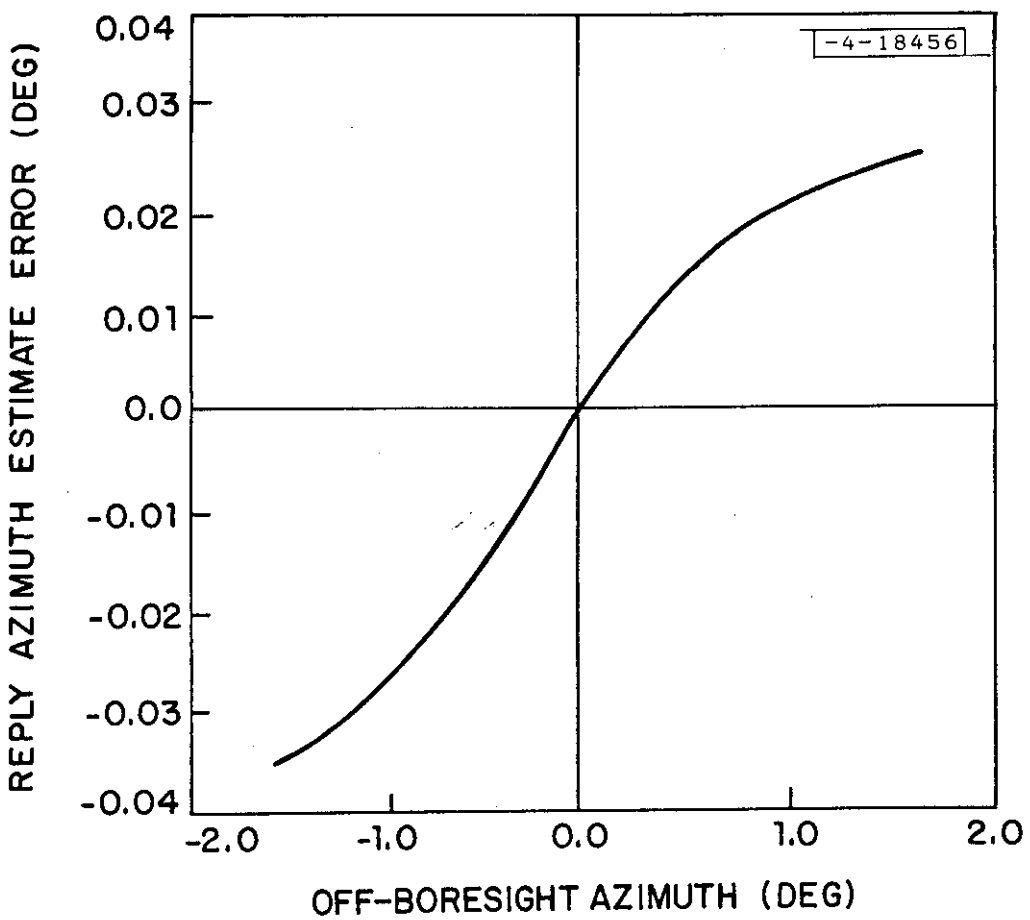

Fig. 5-4. Average frequency sensitivity.

6.0 AZIMUTH ACCURACY

The method for evaluating reply accuracy as a function of offboresight angle is based on two assumptions:

1. Aircraft motion during the beam dwell time is much smaller than the reply azimuth estimate errors.

2. An azimuth estimate made when the target is at boresight would have minimum error.

The validity of assumption 1 is guaranteed be restricting the analysis to targets at ranges greater than a few miles. Assumption 2. is justified by the frequency and amplitude sensitivities shown in Section 2.

Figure 6-1 graphically illustrates two typical monopulse characteristics where the y axis is the monopulse processor output (referred to as the real part), and the x axis is the corresponding offboresight angle in degrees. The two tables differ in slope and intercept. Consider line A-A as the monopulse characteristic of the calibration transponder (i.e., it is the monopulse calibration table) and line B-B as the characteristic of an ATCRBS target of opportunity under surveillance. This section will explain the azimuth estimation errors induced by differences in the two characteristics and describe the method developed for estimating these errors using reply data obtained during real time sensor operation. (The errors shown in these figures are exaggerated for clarity.)

Definitions

bs_k	The antenna boresight azimuth on sweep k.
θ_{act}	The actual target azimuth on the scan.
$\theta_{est\ k}$	The estimated azimuth of the reply on sweep k.
$\Delta\theta_{act\ k}$	The actual target off-boresight angle on sweep k.
rp_k	The monopulse value (the "real part") of the reply on sweep k.
$\Delta\theta_{corr\ k}$	The calibration table value corresponding to real part rp_k, i.e., $\Delta\theta_{corr\ k} = C_c(rp_k)$ where C_c is the calibration table.

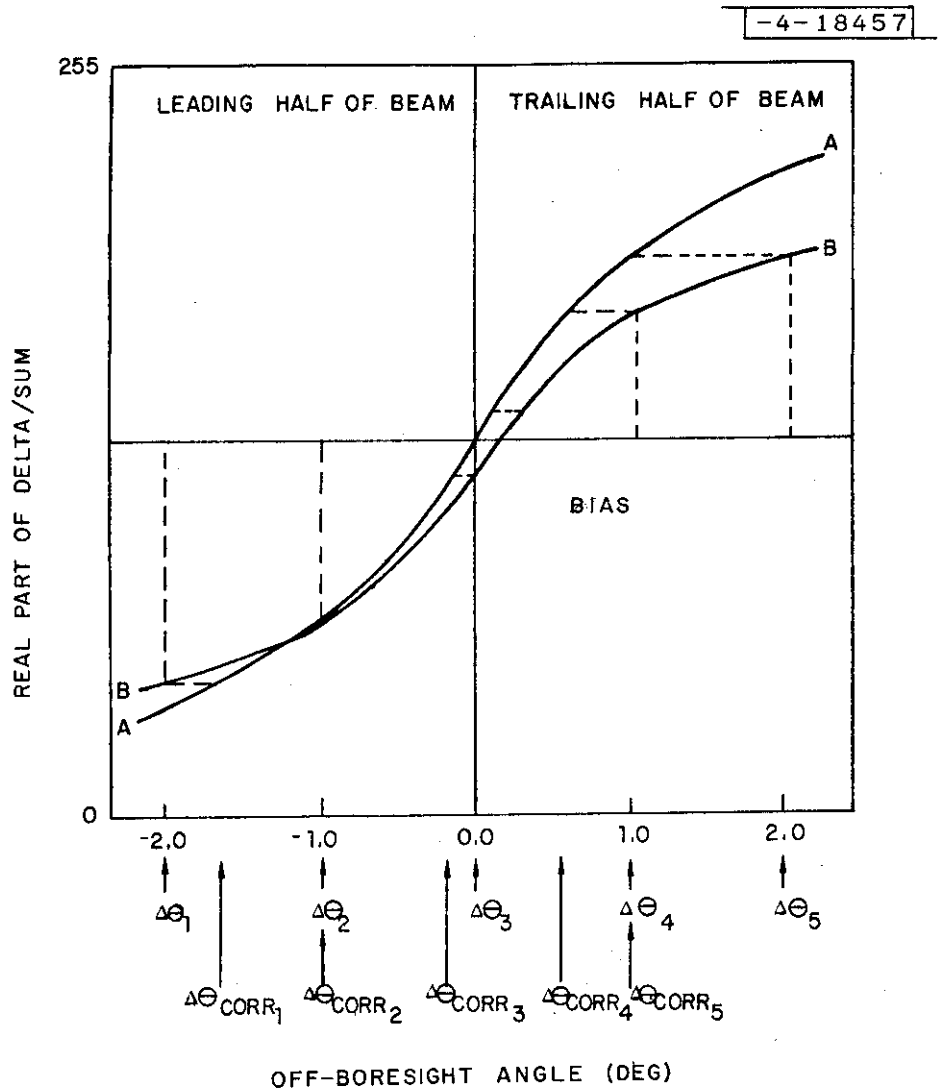

A–A	CHARACTERISTIC CALIBRATION TRANSPONDER
B–B	CHARACTERISTIC OF TARGET TRANSPONDER
$\Delta\Theta_i$	REAL OFF-BORESIGHT POSITION TARGET WHEN INTERROGATED
$\Delta\Theta_{CORR_i}$	INDICATED OFF-BORESIGHT CORRECTION

Fig. 6-1. Indicated off-boresight corrections.

Fig. 6.2 shows the resultant azimuth estimate, and individual reply errors, for the case where the target is at 10.0°, and replies are received at 1.0° intervals as the antenna scans from 8.0° to 12.0°. The intercept of the curve fit with the $\Delta\theta = 0$ Axis, is the reported aircraft azimuth, for this scan interval. A normalized plot of reply errors vs. the estimated reply position referred to boresite, is shown in Fig. 6-3. For the case shown, an exaggerated bias error term was used, and a plot of the true reply errors vs. true position of the replies referred to boresite is shown, for completeness. In practice this bias term is not measured, and is assumed small compared to individual errors. Real data from three scans are shown in Fig. 6-4, to indicate the resultant output of azimuth estimate error as a function of distance in degrees from boresite. A typical scatter plot of azimuth estimate error vs. angle referred to boresite, is shown in Fig. 6-5, for approximately 100 scans (500-600 replies). The slope of the error function for this aircraft near boresite is approximately $+0.04^{\circ}$/degree. A measured distribution of error slopes for approximately 140 aircraft targets-of-opportunity is shown in Fig. 6-6. For these targets, the median error slope was -0.018°/degree, and the distribution was approximately normal, with one standard deviation of 0.035°/degree.

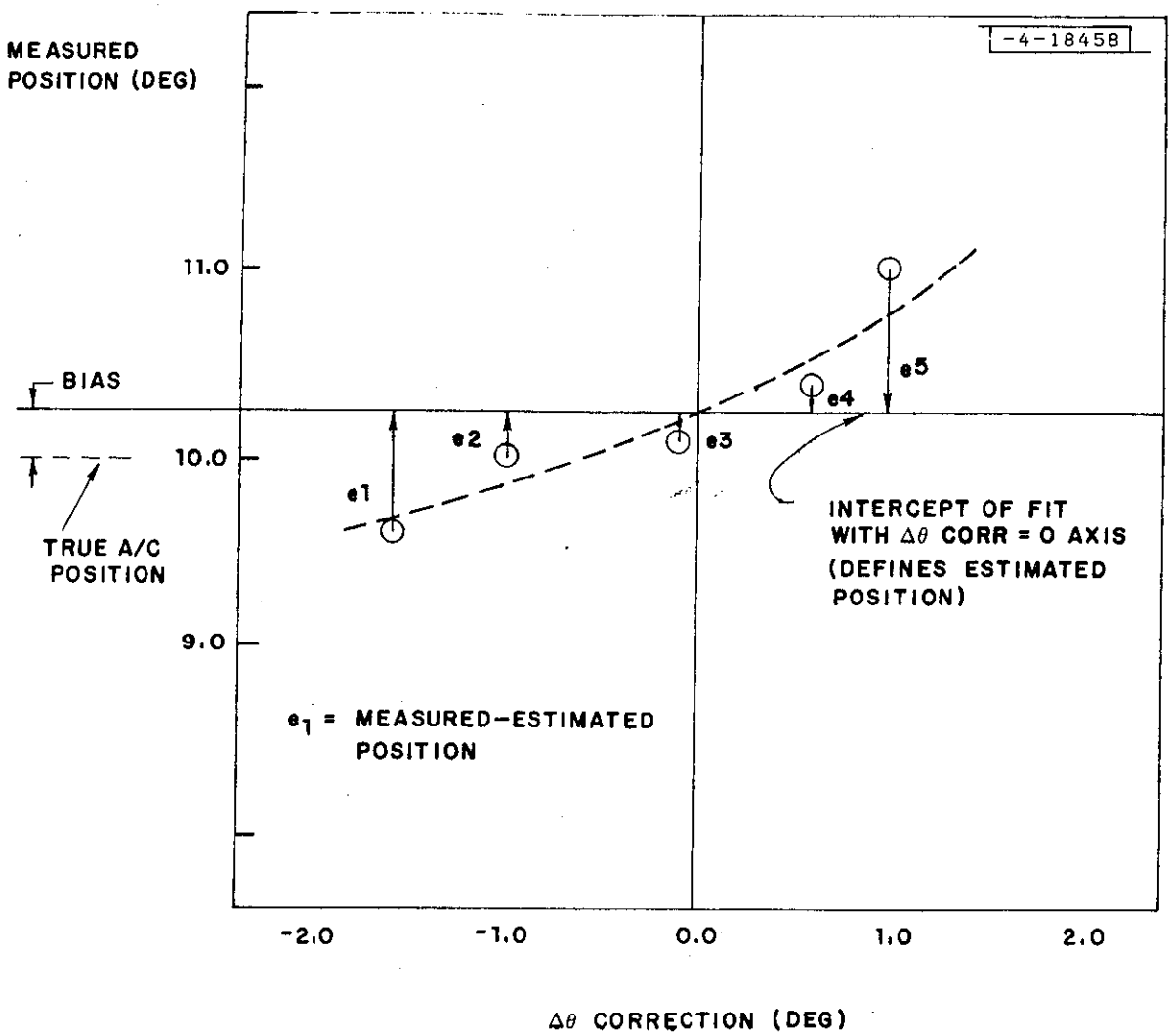

Fig. 6-2. Computation of estimated azimuth errors.

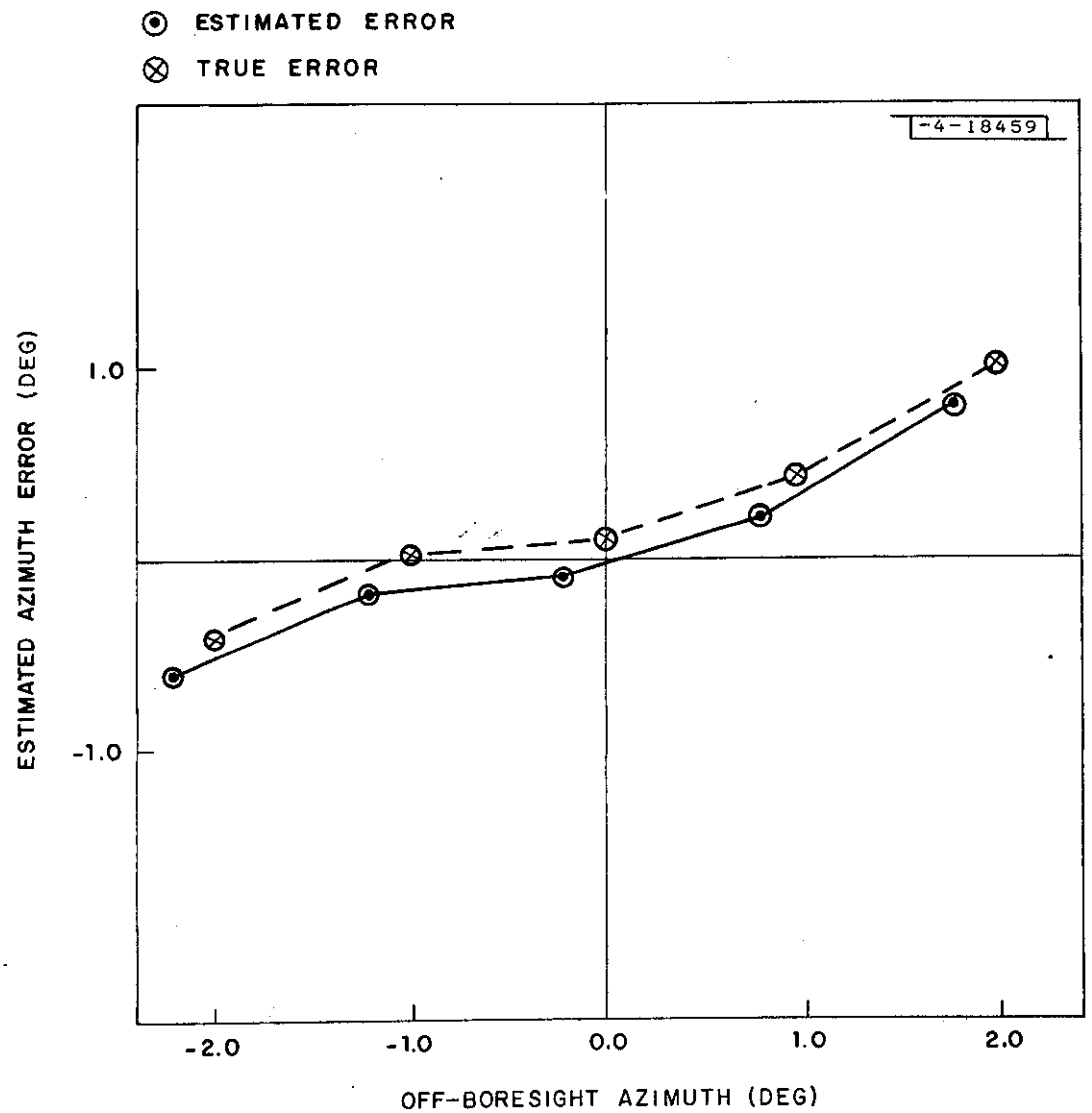

Fig. 6-3. Plot of computed errors and true errors.

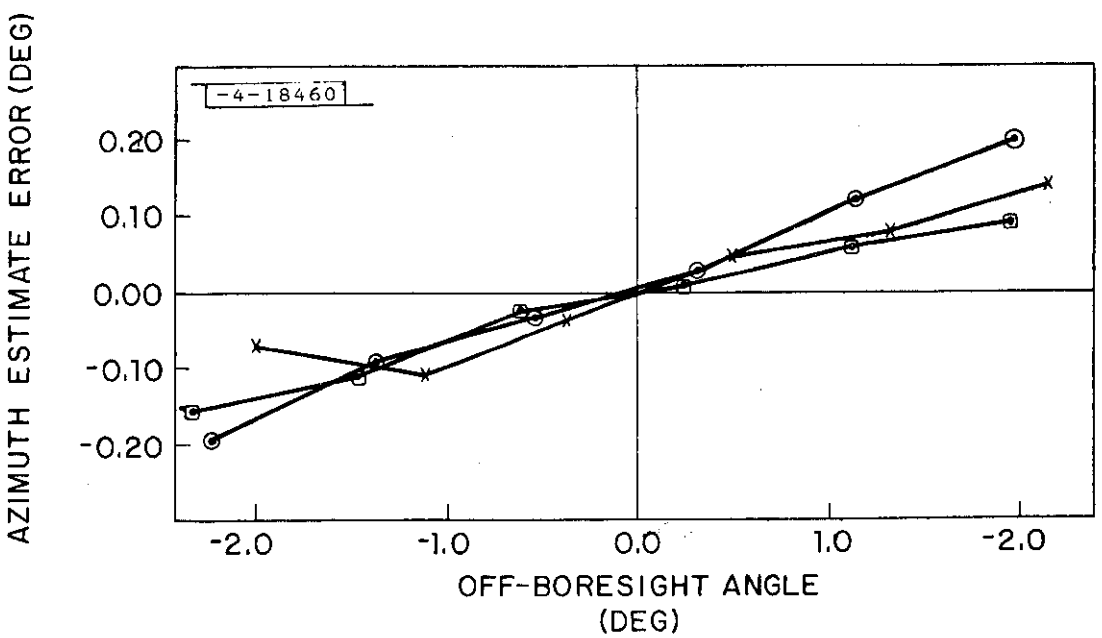

Fig. 6-4. Three scans of azimuth errors.

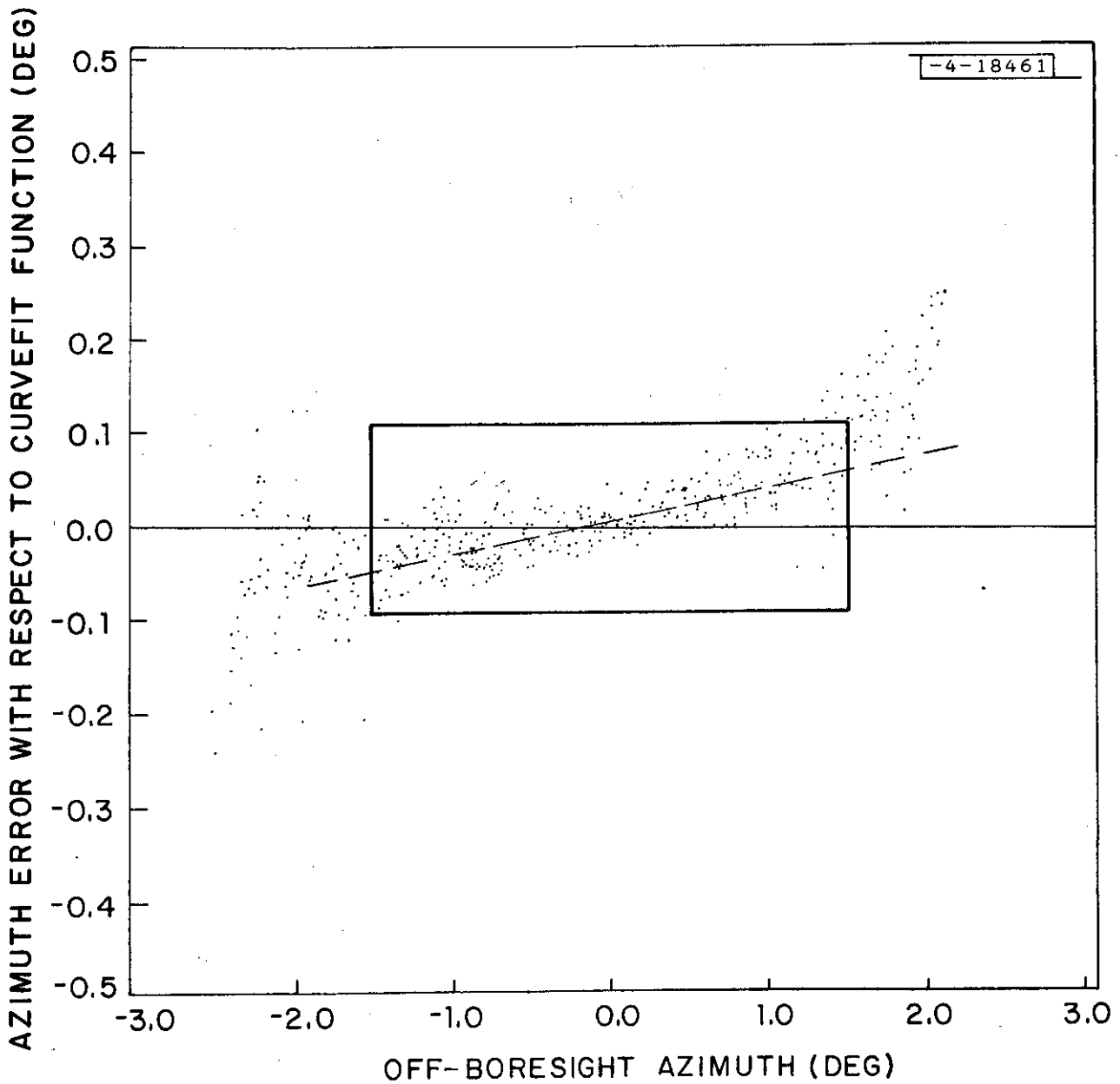

Fig. 6-5. Azimuth errors during 98 scans.

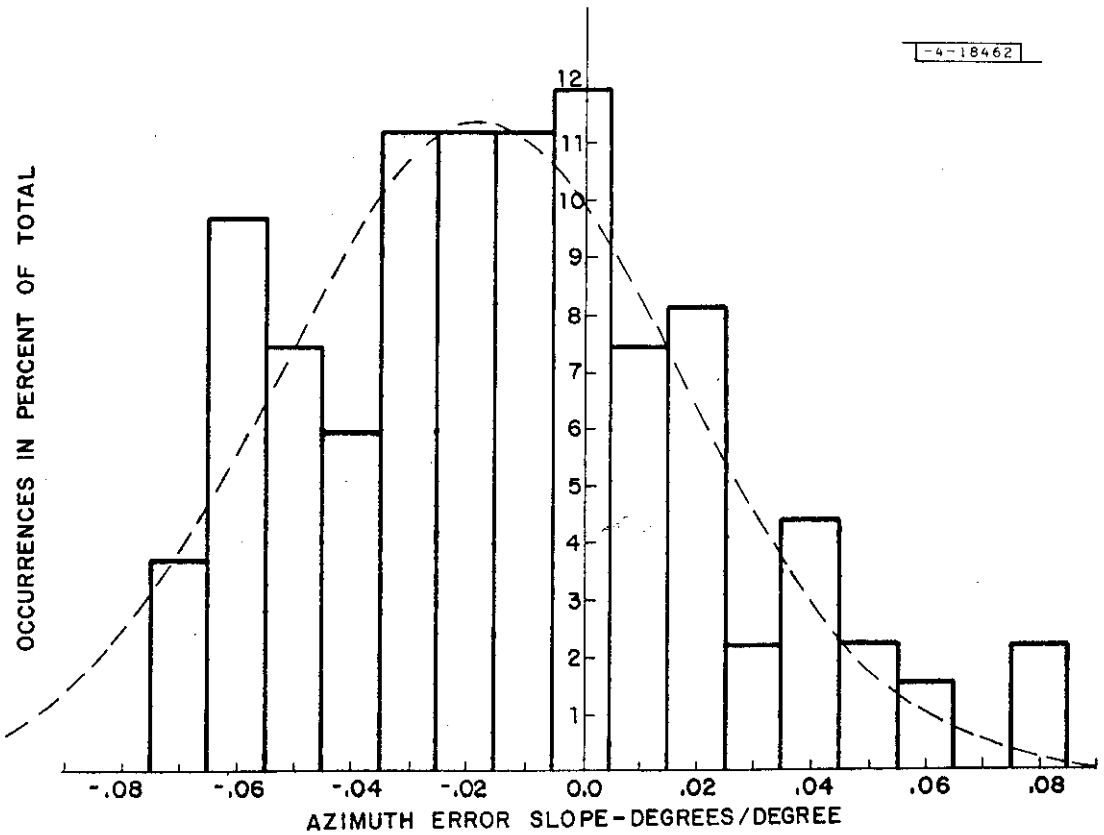

Fig. 6-6. Distribution of error slopes for 140 aircraft (measured).

7.0 POSITION ACCURACY

7.1 Method of Deducing Aircraft Actual Trajectory

Refer to Appendix B.

7.2 Experimental Results

7.2.1 Results for ATCRBS A/C

Statistics were gathered on 297 altitude reporting aircraft seen over 6 days of sensor operation. A total of 41,609 reports were collected. The overall standard deviation was .051°, and 26.4 feet as shown in Figure 7-1 and 7-2 respectively. Figures 7-3 to 7-5 show the variation in σ_θ with elevation and azimuth as well as the elevation report density function.

7.2.2 Results for DABS A/C

Four DABS transponders have flown under DABSEF Surveillance for many hours as part of the DABS/IPC (Intermittent Positive Control) testing program. Surveillance was usually maintained in both the all-call mode and the discrete mode. The several all-call replies received per A/C per scan were subjected to the accuracy vs offboresight angle analyses in the same way ATCRBS replies were. The scan-to-scan sliding window was applied to the position reports based on the single discrete reply per scan. The results for about 12000 scans of data taken over several days are shown below.

	DABS TRANSPONDER			
	#505	#EFE	#101	#551
All-call reply error slope (deg per deg off-boresight)	.019	.023	.030	.005
Target report azimuth accuracy (1 sigma in degrees)	.036	.060	.037	.030
Target report range accuracy (1 sigma in feet)	20	15	17	15

Figure 7-6 shows a typical Intermittent Positive Control (IPC) encounter between two DABS equipped aircraft. The target reports are shown as asterisks. The beginning and end of the line segment associated with each report represent the smooth position and one ahead (4 seconds) predicted position computed by the IPC x-y tracker (which assumes a 1σ azimuth accuracy of 0.1 degrees). Thus, the orientation and length represent tracker heading and speed. The high quality of the data can be seen by referring to the box of dimension d, corresponding to three times the 0.1 degree RMS requirement for DABS/IPC azimuth accuracy.

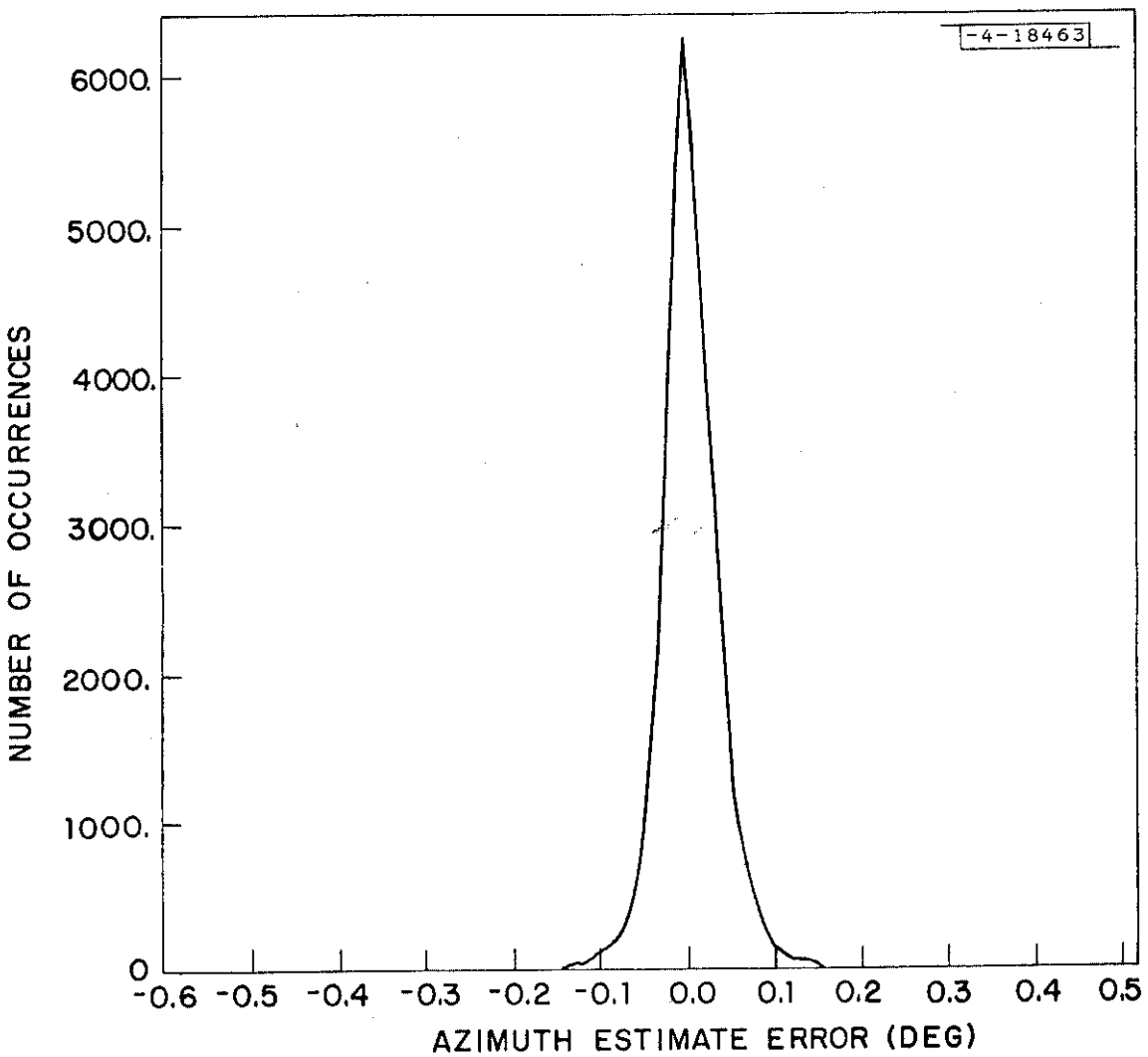

Fig. 7-1. Distribution of azimuth errors.

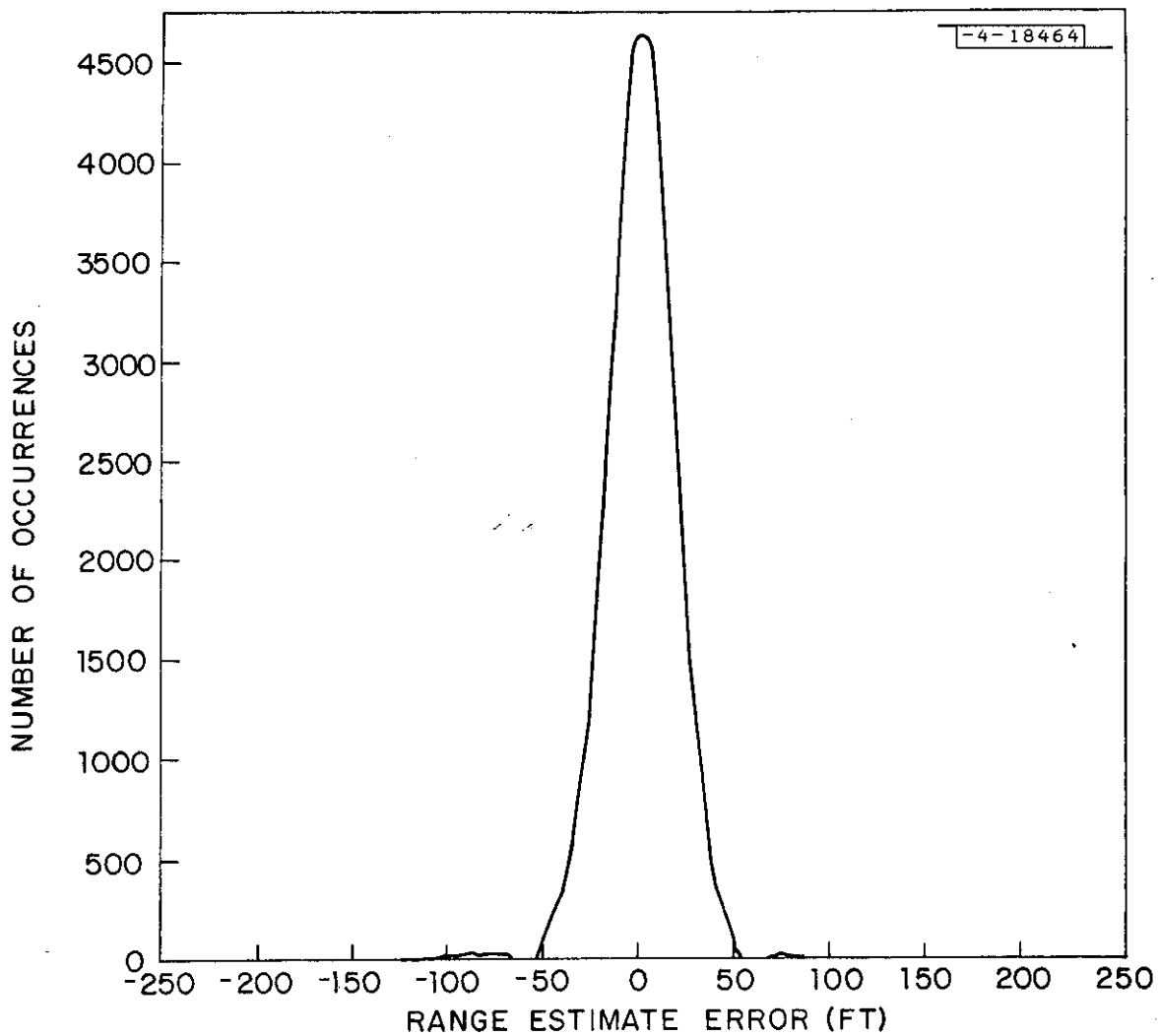

Fig. 7-2. Distribution of range errors.

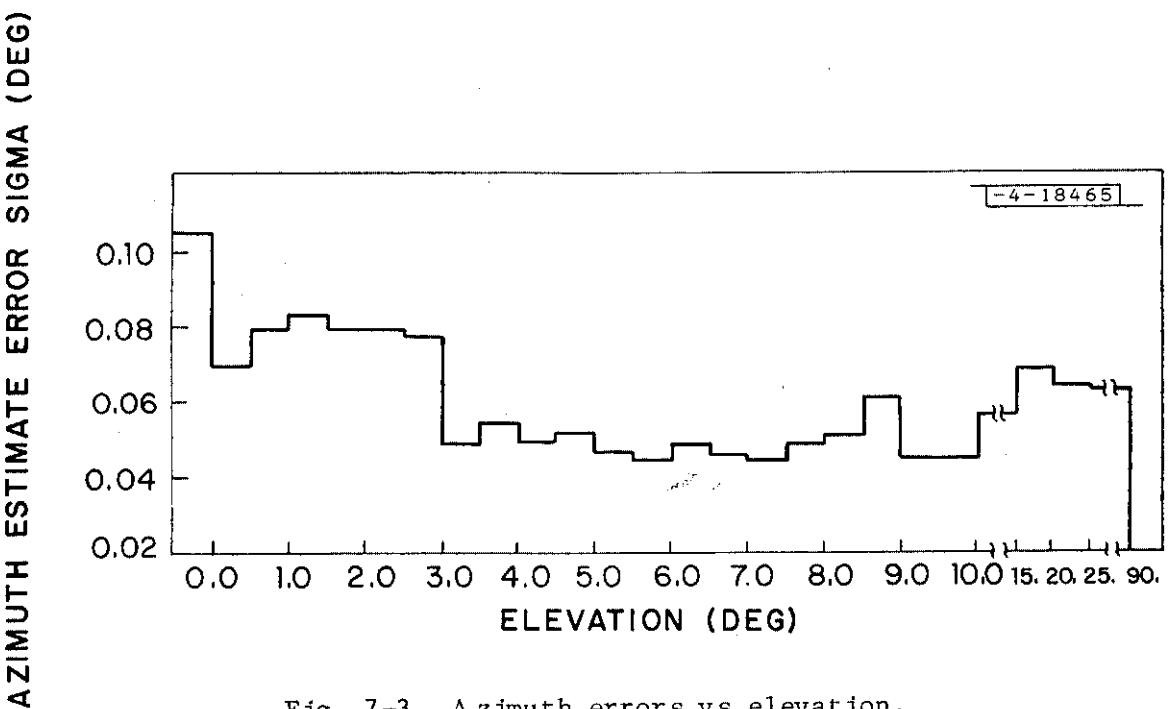

Fig. 7-3. Azimuth errors vs elevation.

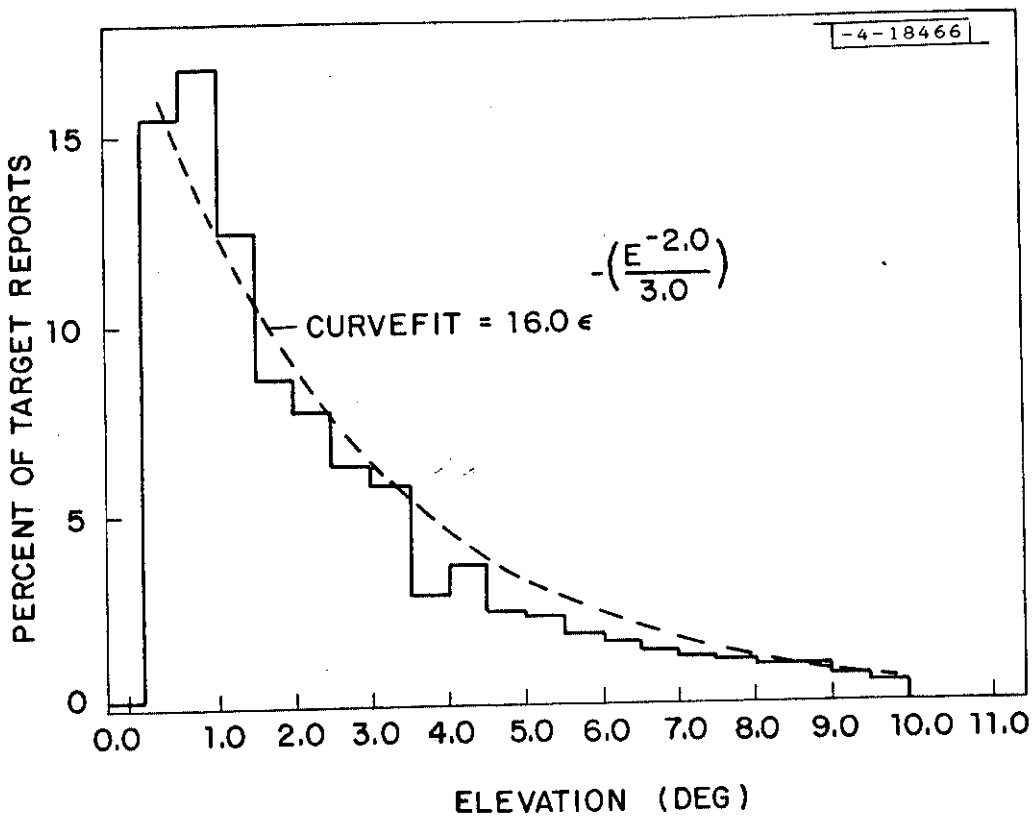

Fig. 7-4. Elevation distribution of target reports.

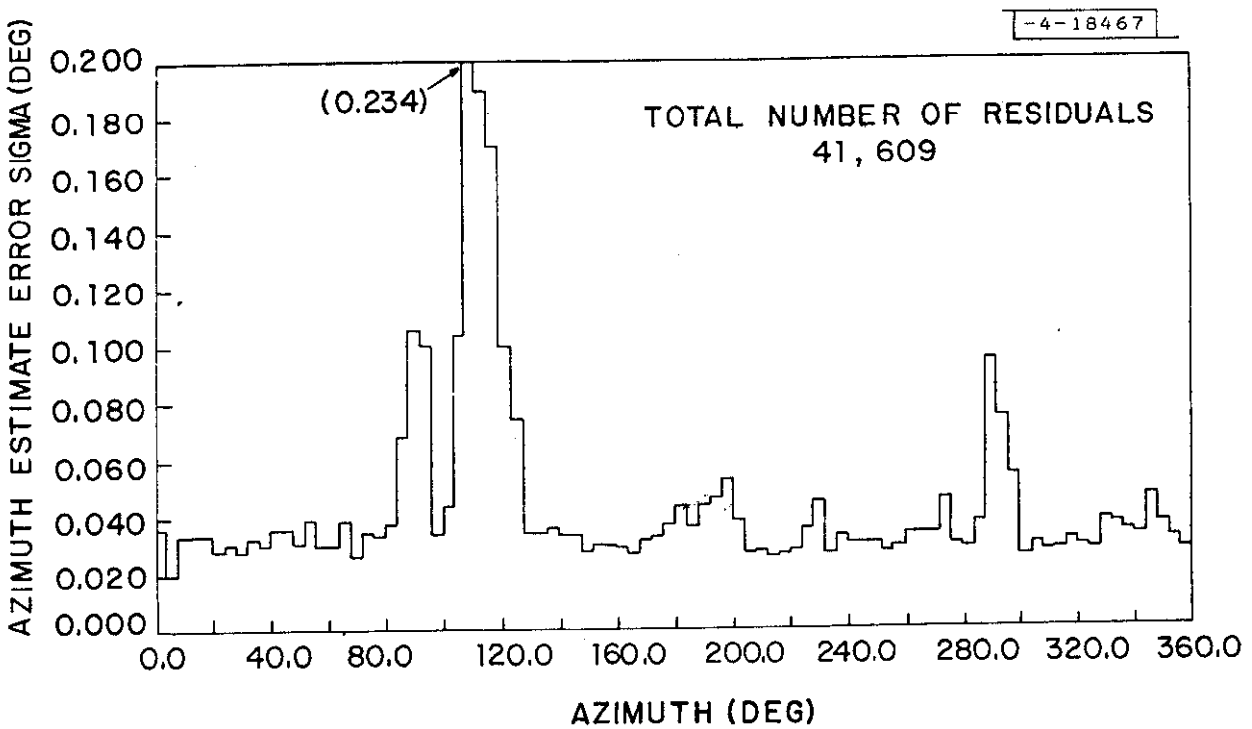

Fig. 7-5. Azimuth errors vs azimuth.

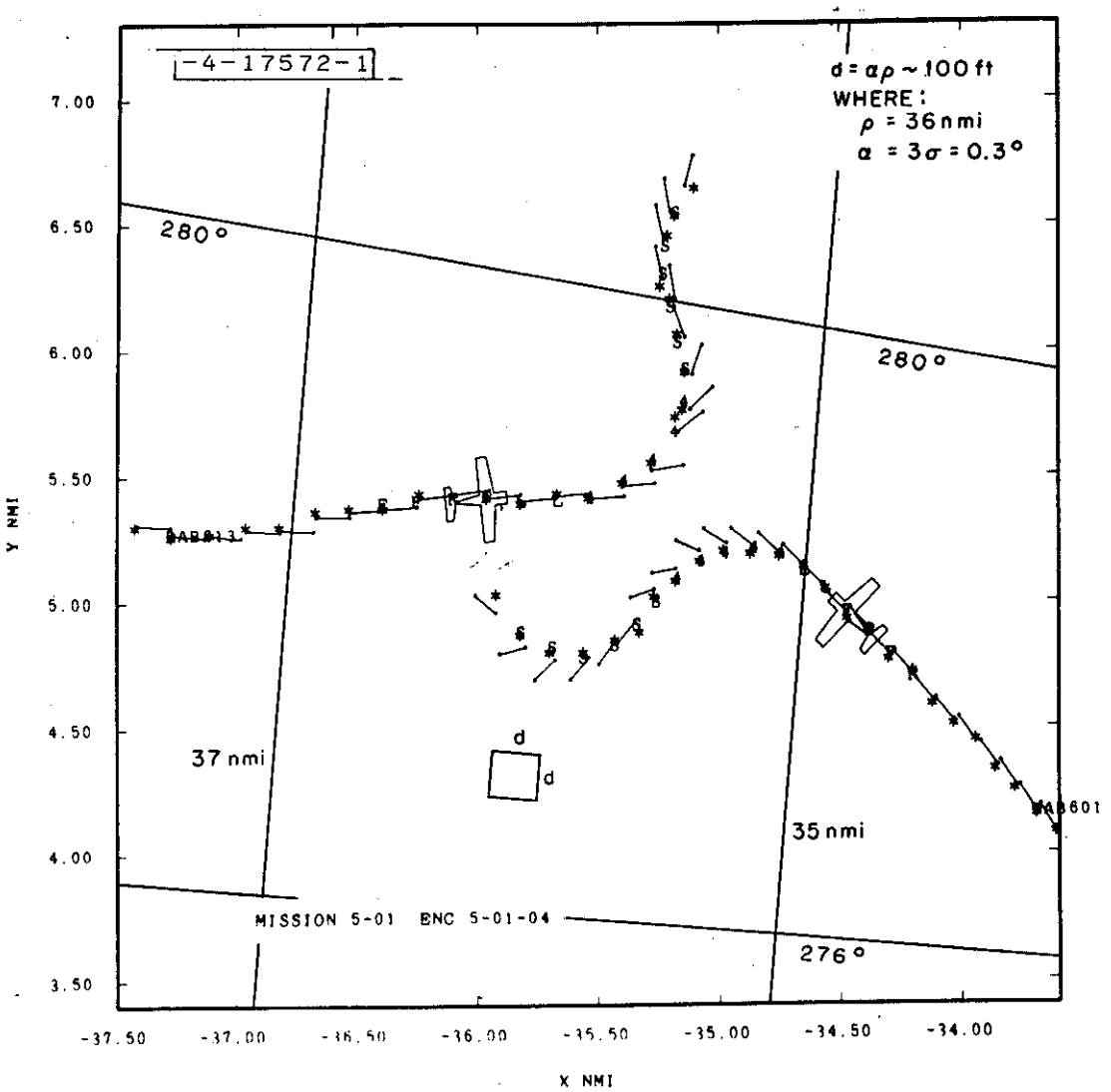

Fig. 7-6. Typical IPC encounter.

8.0 DIFFRACTION

A number of controlled experiments were conducted (Refs. 10 and 11) to demonstrate the validity of the theoretical model for azimuth estimation errors caused by diffraction around shadowing obstacles. For a particular shadowing obstacle (Hanscom Field smokestack, approximately 10 feet in width, and 1500 feet from the DABSEF array antenna) we have computed the expected azimuth estimation error for an aircraft at long range, and low elevation angle (below the top of the tower). The error as a function of the aircraft (target) to obstacle angular separation is shown in Fig. 8-1. The measured azimuth estimation error of a controlled aircraft flying behind the obstacle is shown in Fig. 8-1 as well. It can be seen that there is extremely good agreement between the expected and measured result. The small differences are attributed to the fact that there are random measurement errors (approximately 0.04, one sigma) which are convolved with the structured diffraction error. The theoretical model for obstacle shadowing error has been confirmed for difference geometries, using both controlled aircraft, and aircraft targets-of-opportunity.

The effect of obstacle shadowing on direction finding accuracy can be thought of as the result of distortion of the incident phase front introducing error in the estimation of direction of arrival of incident waves. Fig. 8-2 shows the theoretical azimuth estimation error vs. target-obstacle angular separation, for sliding window and monopulse estimators. The magnitude of diffraction errors for typical shadowing obstructions near airport beacon systems, is comparable to the ATCRBS quantization error, and may explain why these structured errors have not been observed in the past. The structured nature of errors induced by shadowing obstructions is apparent in the DABS data because of the resolution of the monopulse estimator. This structure can be seen from the data shown in Fig. 7-5, where three obstructions are clearly evident. One at approximately 90^{o}, is an FPS-18 radar antenna (700 feet), another at 110^{o}, is a large semicircular UHF array antenna (500 feet), and the third at 290^{o}, is the Hanscom Field smokestack (1500 feet) referred to above.

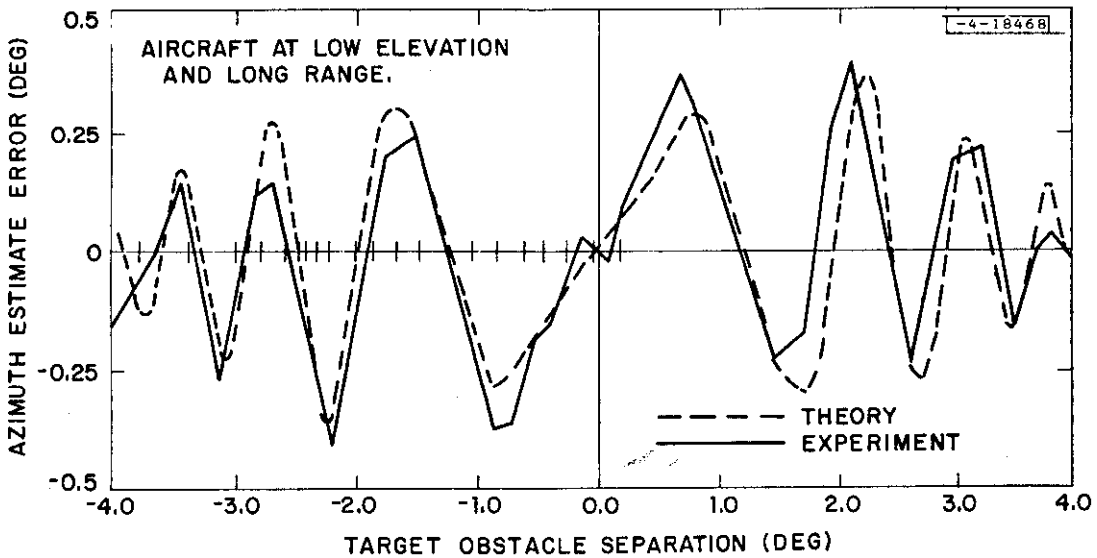

Fig. 8-1. Diffraction induced errors.

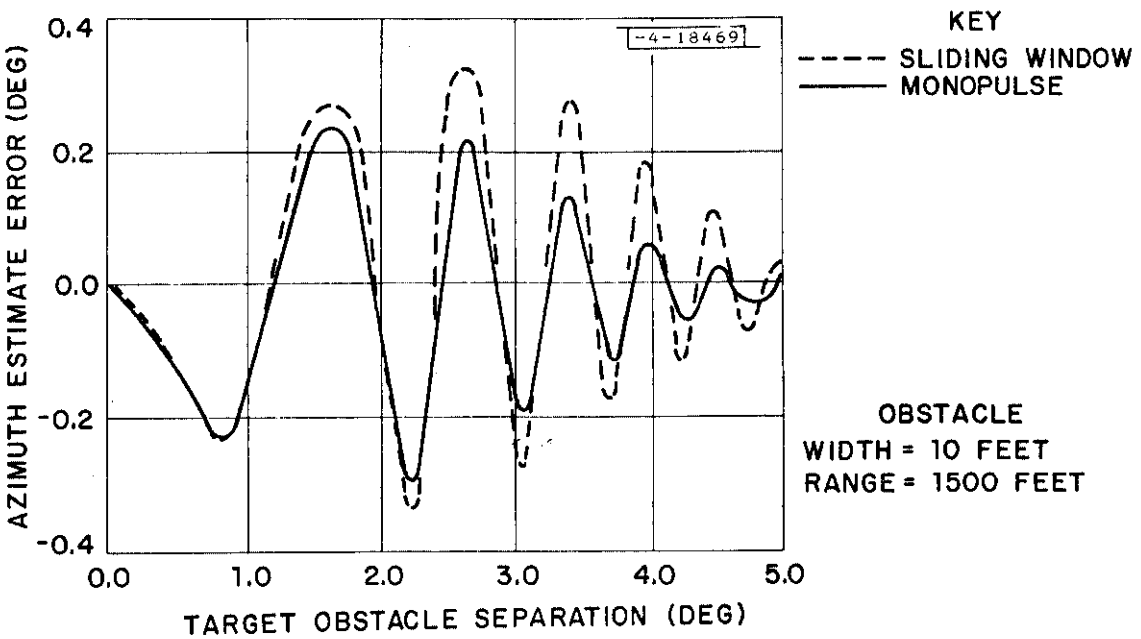

Fig. 8-2. Computed and experimental diffraction errors.

9.0 CONCLUSION

This report has described the need for a monopulse system to measure target azimuth using a single interrogation/reply per scan. The requirement for a new ATC beacon antenna with an additional difference beam port to provide the monopulse capability was discussed. Several methods of processing the sum (Σ) omni (Ω) and difference (Δ) antenna outputs to produce an output related to target offboresight were reviewed.

The choice of the half angle processor because of its unambigous output over a wide region of the mainbeam was explained. Various phenomena which limit accuracy or degrade performance were discussed. These included noise, interference from reflections, interference signals, and diffraction around obstructions. The effect of imperfect components in the processor were considered. The stability of the processor was described along with its sensitivity to signal frequency. The sensor calibration process and its effects on system performance was described.

Finally, data was presented for a large number of beacon targets-of-opportunity during actual sensor operation at DABSEF. The data showed reply azimuth estimate accuracy as a function of offboresight angle and target report accuracy on a scan to scan basis.

A monopulse direction finding capability has been developed, which supports the DABS requirement (0.1°, one σ) for single reply direction-of-arrival estimation, a capability which also supports ATCRBS direction finding at much reduced PRF (4-5 replies per scan).

APPENDIX A:

DESCRIPTION OF DABS EXPERIMENTAL

MONOPULSE SYSTEM

1.0 INTRODUCTION

This Appendix contains an overview of the DABS and ATCRBS modes of DABS (Section 2.0) and a description of the half-angle monopulse processor (Section 3.0). The material in Section 2.0 is intended to provide the overall context in which the monopulse processor operates, and the various subsystems are described only to a level of detail consistent with this purpose.

2.0 DABS SYSTEM DESCRIPTION

Section 2-1 will describe the ATCRBS mode of DABS from the antenna through reply correlation. (The final step, target-to-track correlation is omitted.) Section 2.2 will describe the DABS mode starting with the DABS reply processor, since the antenna, multi-channel receiver, and Video Pulse Quantizer can be considered common to both modes.

2.1 ATCRBS Mode of DABS

Figure A-1 shows a block diagram of the ATCRBS mode. Each of the sub-systems are described in the following sections.

2.1.1 DABSEF Antenna

The antenna is a 512 dipole-element planar array arranged as a rectangular grid with 32 columns of 16 elements each. The elements are printed circuit dipoles. Each vertical column of dipoles is housed within its own radome. The antenna support structure is a lightweight aluminum frame designed for low azimuth sidelobes. The antenna also provides separability of networks for elevation and azimuth distribution (and individual sum and difference networks). Table A-1 summarizes the significant antenna performance characteristics. These include:

Operating Frequency Bandwidth - Largely because of the wideband design approach adopted, the results show the antenna to have considerable operating bandwidth with sharp elevation pattern cut-off and low sidelobes over the full band.

Low Azimuth Pattern Sidelobes - Over the range of $+1^{\circ}$ to $+35^{\circ}$ in elevation, the maximum level of all azimuth sidelobes measured for both sum and difference patterns (0° to 360° in azimuth) was 26 dB.

Elevation Coverage Sector - Coverage over 35° with uniformity of level to within ±1 dB was achieved.

Monopulse Characteristics - Difference pattern with highly symmetrical characteristics and null depth of greater than 40 dB.

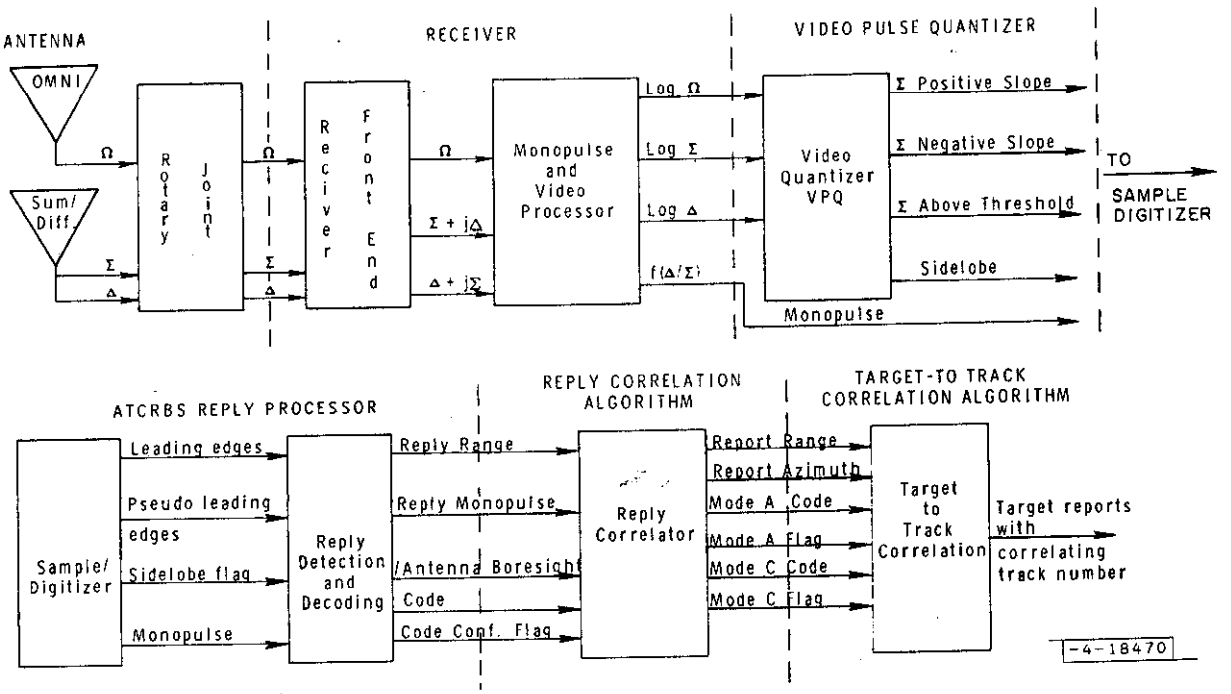

Fig. A-1. ATCRBS mode block diagram.

TABLE A-1 DABSEF ANTENNA CHARACTERISTICS

Array Antenna for DABS Experimental Facility

Main Array Antenna

Frequency of Operation	970 to 1150 MHz
Aperture Size	8' by 20'
Number of Array Elements	512 dipoles
Sum and Difference Patterns for Monopulse	
Azimuth Sum Beamwidth	3 ^{o}
Azimuth Difference Null Depth	40 dB max
Azimuth Pattern Sidelobes (5^{o} EL)	-30 dB max at 1090 MHz
Elevation pattern with sharp cutoff at horizon	
Elevation pattern slope at -6 dB point	3.1 dB/degree at 1090 MHz
Elevation Sector Coverage	Uniform within 2 dB over 35^{o}
Antenna Input VSWR	1.4:1
RF Power-handling Capability	5 kw peak 1 kw avg.
Gain - sum	22.5 dB
- difference	20.5 dB
Polarization	Vertical
Cross-Polarization	-40 dB
RF Losses	1.7 dB

Omni Antenna

Elevation Pattern	Matched to Array antenna
Azimuth Pattern	Uniform around 360^{o} to within 3 dB at +5^{o} elevation

Cross-polarization - Cross-polarization less than -40 dB.

Omni-Antenna Performance - Elevation pattern same as array pattern and azimuth coverage uniform to within ±1.7 dB.

Figures A-2 through A-4 show the azimuth sum and difference patterns, elevation pattern, and sum and difference near boresight. The three outputs, sum (Σ), difference (Δ), and omni (Ω), are processed by the multichannel receiver.

2.1.2 Multi-Channel Receiver

The receiving system consists of a front end and IF/video processor. The front end, located near the antenna, converts Σ and Δ to $\Sigma+j\Delta$ and $\Delta+j\Sigma$ (A and B respectively) limits A, B, and the omni (Ω), converts to IF, amplifies, and sends them to the IF/vodeo processor. The IF/video processor filters A, B, and Ω and forms the monopulse video and log $|\Sigma|$ video from A and B, and forms log $|\Omega|$ video. Finally the video quantizer operates on log $|\Sigma|$, log $|\Omega|$, and log $|\Delta|$ to yield:

a) $Q\Sigma A$ which indicates when log $|\Sigma|$ video exceeds a threshold

b) $Q\Sigma PS$ which indicates when log $|\Sigma|$ video has a positive slope

c) $Q\Sigma NS$ which indicates when log $|\Sigma|$ video has a negative slope

d) QSLS which indicates when log $|\Sigma|$ video exceeds log $|\Omega|$ or log $|\Delta|$ video by a certain amount. This signal represents the Receive Sidelobe Suppression (RSLS) function which restricts processing to the mainbeam.

Outputs (a) to (d) plus the monopulse video (described in Section 3.0) are input to the video pulse quantizer digitizer.

2.1.3 Video Pulse Quantizer/Digitizer (VPQ)

The VPQ samples $Q\Sigma A$, $Q\Sigma PS$, and $Q\Sigma NS$ at 8.276 MHz and logically operates on the samples so as to recognize the occurrence of pulse edges. The VPQ outputs a data stream, QLE, clocked at 8.276 MHz, that has a "1" whenever a pulse leading edge is detected and "0"s otherwise. Leading edges are declared whenever log $|\Sigma|$ video exceeds a threshold ($Q\Sigma A$ is "on") and the slope of log $|\Sigma|$ video transitions from high to low. This logic enables declaration of leading edges for overlapped pulses when the second pulse is sufficiently high in amplitude. Trailing edges are recognized in a similar fashion. They are used to reject short pulses and declare leading edges in certain pulse overlap conditions. The monopulse video is sampled and quantized to 8 bits shortly after each leading edge (except those in overlap conditions). The QSLS signal is also sampled after each leading edge resulting in the SLSF clocked data stream (also 8.276 MHz).

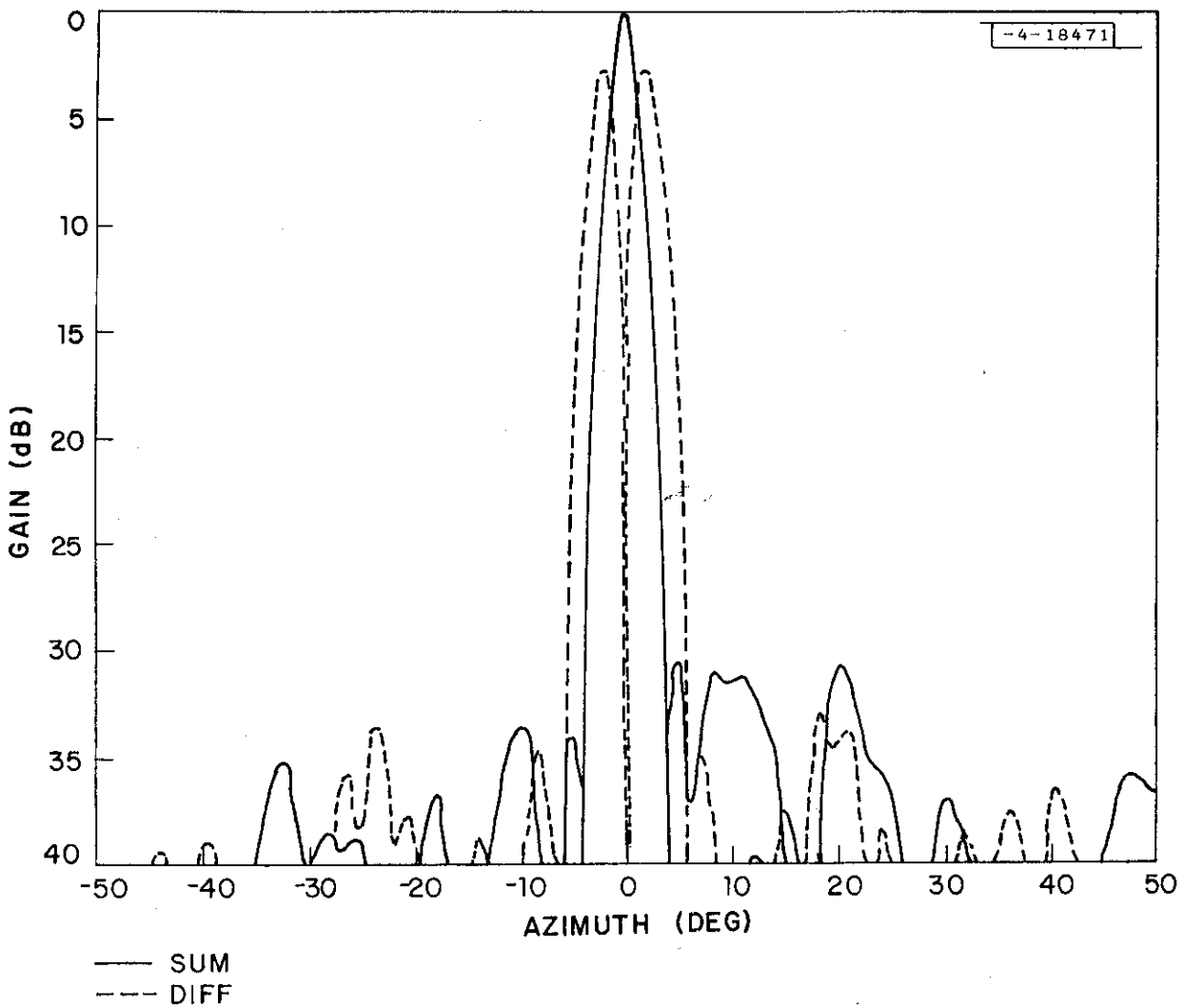

Fig. A-2. DABSEF antenna patterns vs azimuth.

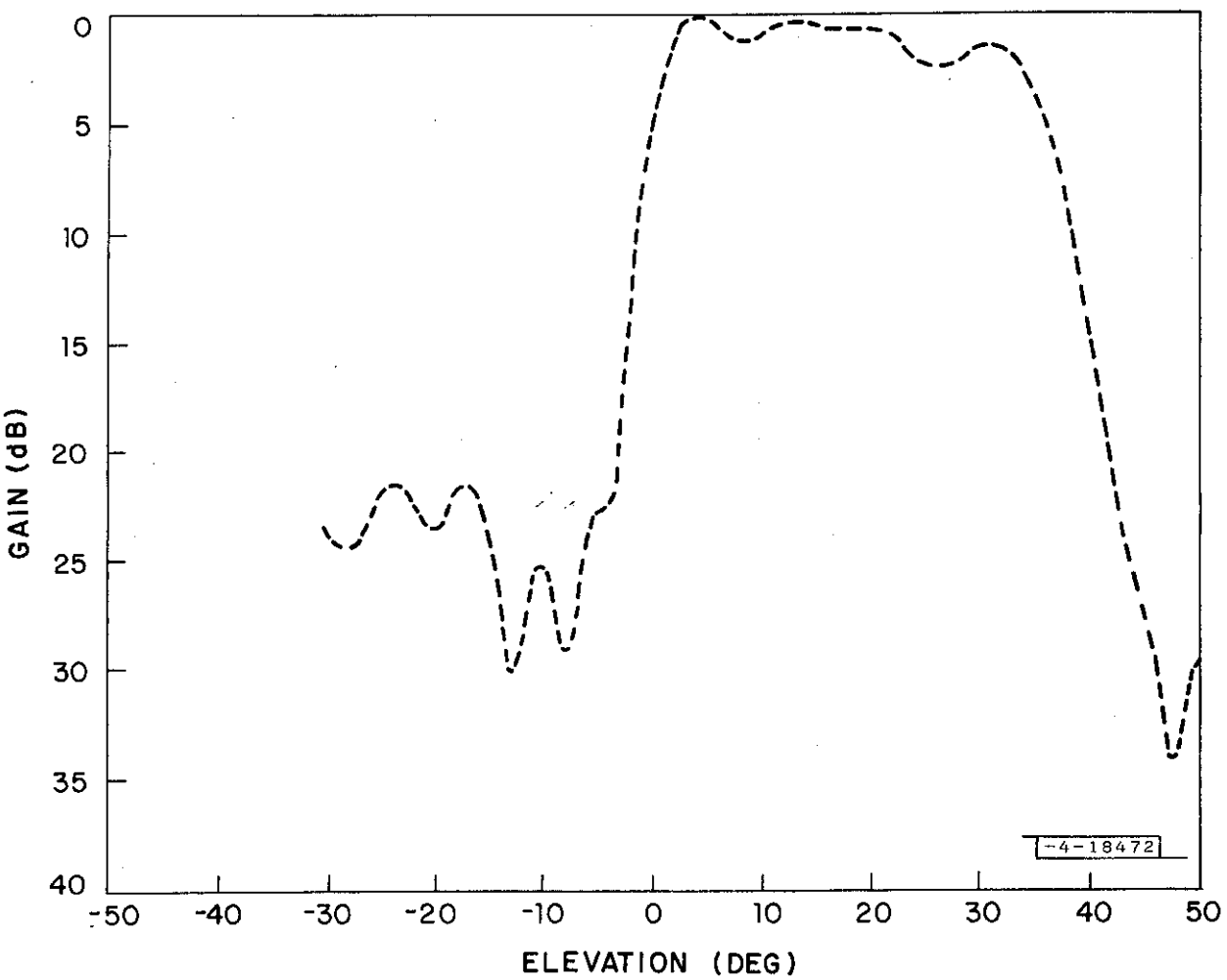

Fig. A-3. DABSEF antenna pattern vs elevation.

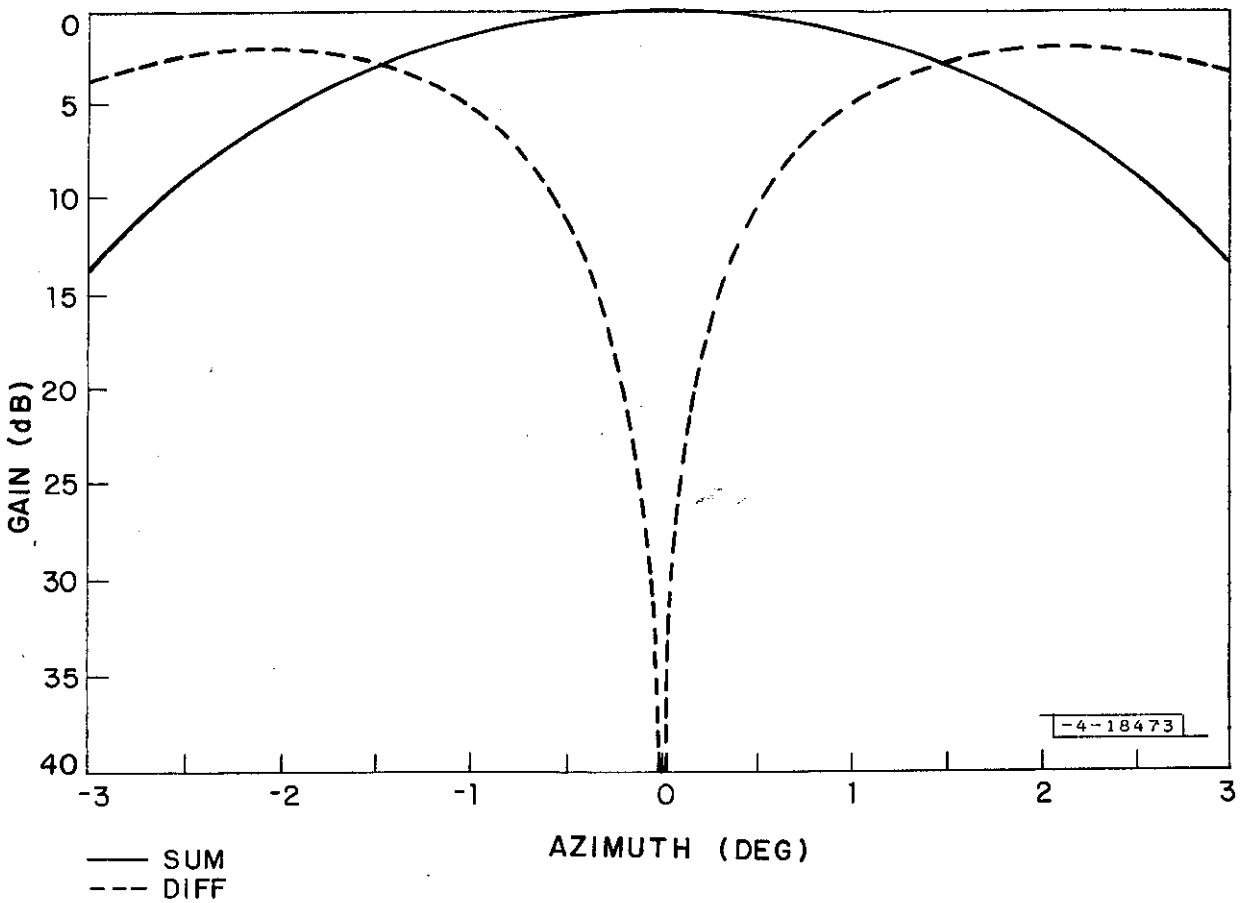

Fig. A-4. DABSEF antenna patterns near boresight.

2.1.4 Reply Processing

The DABSEF ATCRBS reply processor searches the ΣLE data stream for pulses separated by the F_1, F_2 spacing (requiring that at least one is main beam). The bracket detection logic is capable of resolving various types of interreply garbling and interference. When F_1,F_2 brackets are detected the associated code pulse positions in the ΣLE stream are examined. The presence or absence of a leading edge in the vicinity of those positions results in a "1" or "0" being declared. Due to noise, garbling, and other phenomena, it is possible for these declarations to be in error. Therefore, to aid in subsequent processing, each code bit has a corresponding confidence bit. The setting of these bits depends on the consistency of the monopulse values for the leading edges and the presence or absence of edges in the sample positions adjacent to that of the nominal code pulse positions. The monopulse value of each pulse is compared to the "average" of the preceding pulses. The average is initialized with the F_1 value (except during garbling when F_2 is used). It is updated by adding the current average to the new pulse's value and dividing by two, if the new pulse is sufficiently close to average. If not, the old average is retained and the code bit is declared a low confidence "1". When decoding and monopulse averaging is complete, the reply is sent to the reply correlation function with

a) mode indicator

b) range

c) monopulse average

d) antenna boresight at bracket detection time

e) code

f) code confidence

2.1.5 Reply Correlation

Replies from successive sweeps are correlated on the basis of range, azimuth, and code and combined into target reports. A reply that does not correlate with replies from previous sweeps is considered an initial target report having the range, azimuth, and code (Mode A or C) of the reply. The rules for updating target reports with correlating replies result in the report range and azimuth being the average of the two replies that straddle boresight or, if all replies are from the same side of boresight, the values for the reply closest to boresight. The report codes (A and C) and code confidence words are obtained by logical operations on the reply codes and code confidence/ bits.

2.1.6 Report Azimuth Determination

The averaging of sampled monopulse values during reply processing, combined with the reply averaging, reduce the noise variance in the ATCRBS target report.

In reply processing the "add and divide by two" process yields a sigma due to noise of

$$\sigma_{reply} = \sigma_{pulse} * \sqrt{\frac{1}{3}\left(1 + \frac{1}{2^{2n-3}}\right)}$$

This is a weak function of n, and since n can be as small as two (brackets only), σ will be taken as $\sigma_{pulse}/\sqrt{2}$. The averaging of the two reply azimuths that straddle boresight in reply correlation provides another factor $1/\sqrt{2}$, so

$$\sigma_{report} = \frac{\sigma_{pulse}}{2} \quad \text{(for noise effects)}$$

2.2 DABS Mode

2.2.1 Reply Processing

The DABS reply processor operates on the VPQ outputs to generate a 16 MHz data stream (SQΣD) indicating the presence of pulses above the DABS threshold. SQΣD is then input to the DABS preamble detector which searches for preamble pulse sequences. When a DABS reply preamble is detected a trigger pulse is generated which causes SQΣD, QSLS, and log $|\Sigma|$ to be sampled. The sampling rate is twice the information bit rate to enable decoding of the two Pulse Position Modulation "chips" that make up each information bit. The monopulse video is sampled in the same way and converted to 8 bit digitized values. Finnally, the log $|\Sigma|$ is sampled once per chip (short reply: 56 bits, 112 chips). The two log $|\Sigma|$ chip samples per information bit are then compared, and a data stream at the information bit rate is output indicating which of the two chips had a greater amplitude.

The message bit processor then logically operates on the log $|\Sigma|$, QLSL and the monopulse video chip samples plus the amplitude comparisons to declare the binary value of each information bit. As with ATCRBS, a confidence value accompanies each declaration. The message bits are then error detected and corrected.

2.2.2 Position Measurement Selection

DABS position measurements are made on the basis of only one reply per scan even if others were received. The general rult is to use the roll-call reply closest to boresight or, in the absence of roll-call replies, to use the all-call reply having the shortest range.

3.0 Monopulse Processor

3.1 Half Angle Implementation

The monopulse processor implemented at DABSEF is the half angle realization described in Section 2.3 of the Report. Two independent measurements of $\tan^{-1}(\Delta/\Sigma)$ are made and summed so that the processor output is $2 \tan^{-1} \Delta/\Sigma$ (for a triangular detector).

Since,

$$2 \tan^{-1} (\Delta/\Sigma) = [\arg (\Sigma + j\Delta) - \arg (\Sigma - j\Delta)] = \theta$$

the optimum Bell Labs result is achieved.

The measurements of $\tan^{-1} (\Delta/\Sigma)$ are obtained by phase detecting between $(\Sigma + j\Delta)$ and $j\Sigma$ in the one channel and between $-(\Delta + j\Sigma)$ and $-\Sigma$ in the other. This eliminates the ambiguities incurred when θ exceeds 90° (i.e., $\Delta = \Sigma$) in the Bell Labs approach. Utilizing both channels avoids any loss in signal to noise ratio, and reduces the effect of phase errors in the hybrid channels by one half.

3.2 Error Analysis

This section computes the azimuth estimation accuracy of the DABS half angle processor and the DABSEF antenna described in Section 2.3. We are concerned with a single DABS reply within the antenna half power beamwidth ($\pm 1.5^{\circ}$), and in an elevation angle to A/C regime limited to the coverage region 0° to 5°. In this region we assume that the monopulse pattern is constant.

The Δ/Σ ratio, of the DABSEF antenna, vs angle referred to boresight, is shown in Fig. A-5a. The derivative of this curve, in Δ/Σ units per azimuth degree, is shown in Fig. A-5b. These curves are used to convert processor errors in Δ/Σ units to azimuth errors in degrees vs angle referred to boresight.

The sources that contribute to errors in estimated angle of arrival consist of, but are not limited to, the following:

1. Differential pre-combiner gain/phase.

2. Differential channel phase error due to transponder frequency range (±3 MHz), and dynamic range of received signals (-20 dBm to -79 dBm).

3. Phase error due to sampling the pulsed transient, processor output signal, in a non-quiescent state.

4. Noise.

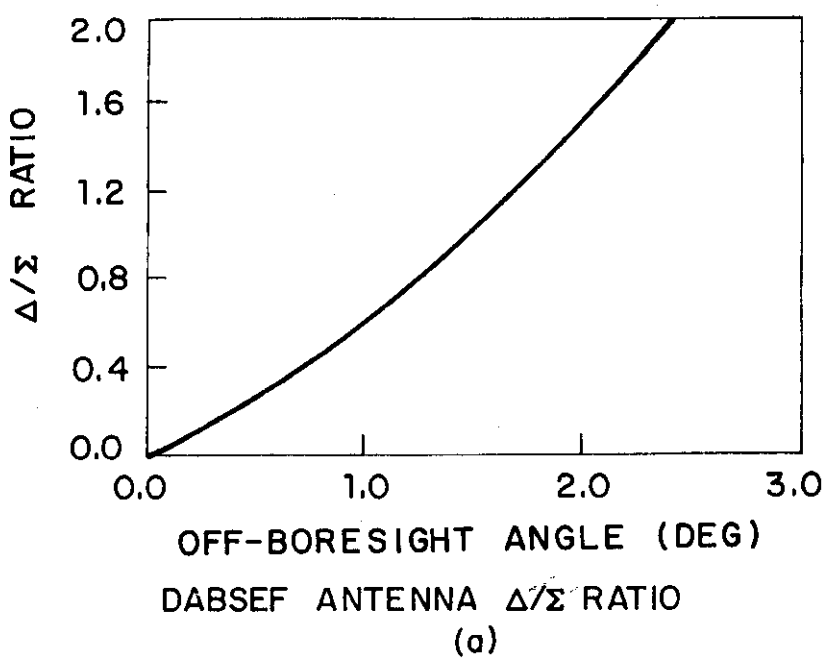

DABSEF ANTENNA Δ/Σ RATIO

(a)

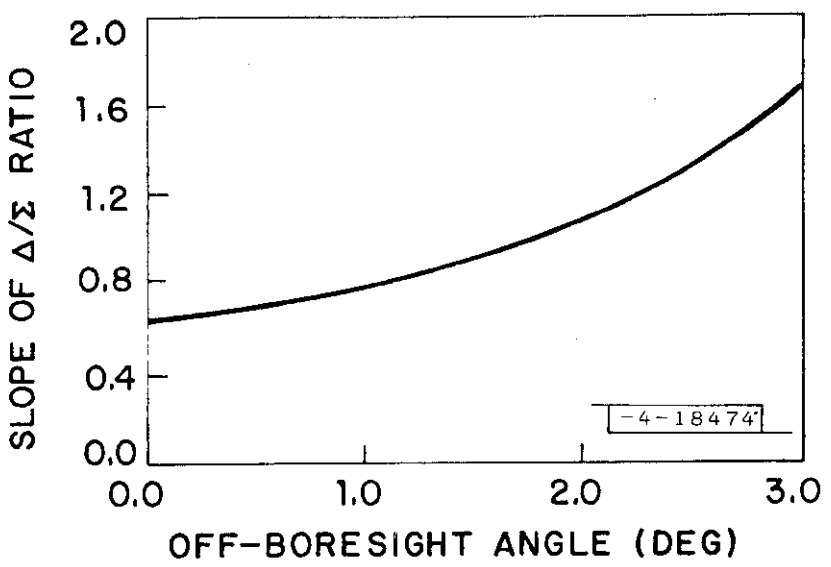

DABSEF ANTENNA SLOPE OF Δ/Σ RATIO

(b)

Fig. A-5. DABSEF normalized antenna pattern.

Other possible sources of estimation error relate to the antenna system, coupling of shaft encoders to the driven system, mechanical stability, quantization error in reading antenna position, and quantization error in recording the real part of the measured Δ/Σ ratio. These are considered to be small effects, and are not considered here. Another source of estimation error relates to the change in the monopulse channel levels vs A/C (target) elevation angle (approximately Cos EL dependent), but is not considered here.

In each case a standard deviation for the perturbing influence is assumed and transformed to the standard deviation in the Δ/Σ ratio by making use of the relationship between the processor output and the perturbation. Let:

e_{PRTRB} = Perturbing influence

$\bar{e}_{PRTRB}$ = mean of e_{PRTRB}

$\sigma_{e_{PRTRB}}$ = standard deviation of e_{PRTRB}

Δ/Σ_{IN} = a given Δ/Σ input ratio

Δ/Σ_{OUT} = processor output Δ/Σ ratio

$f(.,.)$ = the function $\Delta/\Sigma_{OUT} = f(\Delta/\Sigma_{IN}, e_{PRTRB})$

$\sigma_{\Delta/\Sigma_{OUT}}$ output standard deviation (a function of Δ/Σ_{IN} and $\bar{e}_{PRTRB}$, and $\sigma_{e_{PRTRB}}$).

Then:

$$\sigma_{\Delta/\Sigma_{OUT}} \cong \sigma_{e_{PRTRB}} f'(\Delta/\Sigma_{IN}, \bar{e}_{PRTRB})$$

$\sigma_{\Delta/\Sigma_{OUT}}$ is easily converted to off boresight angle estimation error for a given off boresight angle by utilizing the antenna Δ/Σ ratio versus off boresight characteristic.

Let:

θ = off boresight angle

$\Delta\theta$ = off boresight angle estimation error

$\sigma_{\Delta\theta}(\theta)$ = standard deviation of $\Delta\theta$ for a given θ

$g(.)$ = the function $\Delta/\Sigma_{IN} = g(\theta)$

Then:

$$\sigma_{\Delta\theta}(\theta) \tilde{=} \frac{1}{\frac{d(g(\theta))}{d\theta}} \sigma_{\Delta/\Sigma_{OUT}}(g(\theta))$$

or combining (1) and (2)

$$\sigma_{\Delta\theta}(\theta) \tilde{=} \frac{1}{\frac{dg(\theta)}{d\theta}} f'(g(r), \bar{e}_{PRTRB}) \sigma_{e_{PRTRB}}$$

Starting at the front end of the processor, the first possible source of error is differential gain/phase variations between the Δ and Σ channels, ahead of the $\pi/2$ combining hybrid.

Let:

β = ratio of Δ channel to Σ channel gains (β' in dB)

$\bar{\beta} = 1$ (0 dB)

$\sigma_{\beta'} = .25$ dB

Then

$$f(\Delta/\Sigma,\beta) = \beta\ \Delta/\Sigma$$

$$\sigma_{\Delta/\Sigma_{OUT}} = \sigma_{\beta}\ \Delta/\Sigma$$

Since:

$$\beta_{ratio} = 10^{(\beta'/20)}$$

Then:

$$\sigma_{\beta_{ratio}} = 10^{(\sigma_{\beta'}/20)} - 1$$

Therefore

$$\sigma_{\Delta/\Sigma} \tilde{=} \frac{\Delta}{\Sigma}\left(10^{(\sigma_{\beta'}/20)} - 1\right)$$

$$= (.0202)\ \Delta/\Sigma$$

A plot of this error function is shown in Fig. A-6a, where scales have been transformed to antenna units, using Figs. A-5a, A-5b.

Let ϕ = phase difference between the Δ and Σ channels

$\bar{\phi} = 0$

Then:

$$f(\Delta/\Sigma,\phi) = \frac{1}{2}\left[\tan \tan^{-1} \frac{\Delta \cos \phi}{\Sigma - \Delta \sin \phi} + \tan \tan^{-1} \frac{\Delta \cos \phi}{\Sigma + \Delta \sin \phi}\right]$$

The derivative evaluated at $\phi = 0$ is zero. Consequently the processor is insensitive to this source of error.

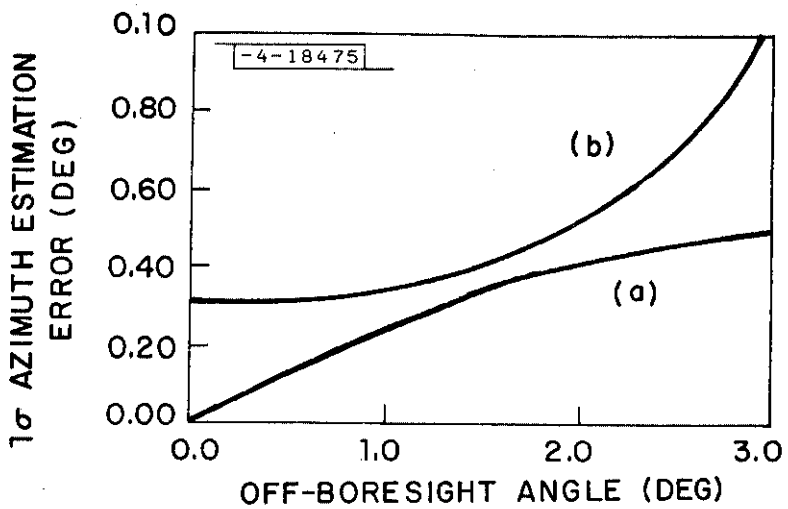

a. DUE TO: PRE-COMBINER DIFFERENTIAL GAIN

b. DUE TO: PRE-SELECT BAND-PASS FILTERS
MIXER PREAMPLIFIERS
I.F. BAND PASS FILTERS
PULSE TRANSIENT SAMPLING ERROR

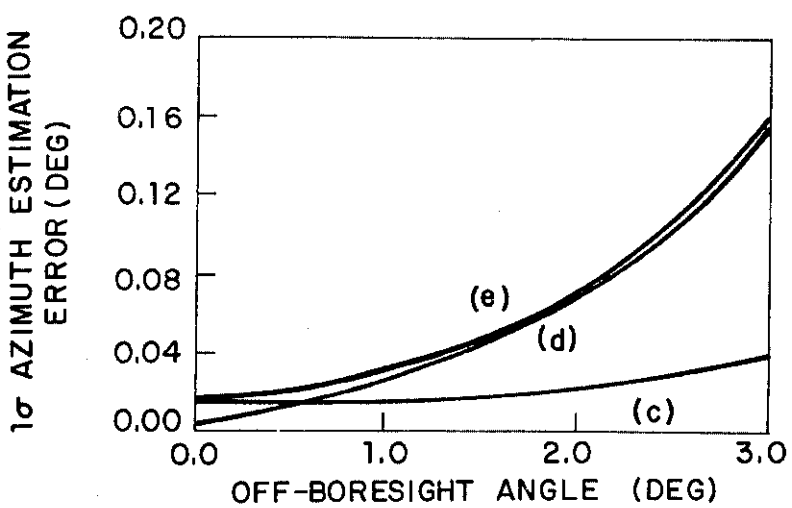

c. DUE TO: LIMITER PHASE TRACKING ERROR

d. DUE TO: LIMITER OUTPUT LEVEL VARIATION

e. DUE TO: c AND d

Fig. A-6. Monopulse processor error analysis.

System phase errors consist of errors which occur principally due to mismatched channel ϕ (ω) transfer functions, and those which are introduced by active elements as a result of change in $\phi(\omega)$ with signal level. The elements of the processor which are in the first category are: the front-end pre-select band pass filters, differential channel line length ($\Delta\tau$), the IF band pass filters, and the Δ/Σ sampling A/D converter (transient phase response varies with input frequency due principally to the IF band pass filters).

The output of the phase detectors would be exactly one half the angle between $\Sigma + j\Delta$ and $\Delta + j\Sigma$ for ideal triangular detectors. Thus, the detector output for a phase error ϕ is

$$\tan^{-1}(\Delta/\Sigma_{IN}) + \frac{\phi}{2}$$

The corresponding indicated Δ/Σ_{OUT} is then

$$\Delta/\Sigma_{OUT} = \tan\left(\tan^{1} \Delta/\Sigma_{IN} + \frac{\phi}{2}\right)$$

Differentiating and evaluating at $\bar{\phi} = 0$ yields

$$\Delta/\Sigma_{OUT} = \frac{\sigma\phi}{2}\left(1 + (\Delta/\Sigma)^2\right)$$

Peak-to-peak phase errors for the causes cited will be less than 8^{o}. It is assumed that the mean error is zero (at 1090 MHz), and that transponder frequencies will be normally distributed about 1090 MHz. A 1σ phase error of 2^{o} is chosen, a plot of the error function is shown in Fig. A-6b, where the scales have been transformed, as before. In practice, the effect of imperfect tracking of the IF band pass filters with signal frequency can be minimized by careful selection of the processor output sampling time referenced to the pulse leading edge.

The IF constant phase-limiters are the only elements in the processor which introduce phase error as a function of signal level. The limiters in the $(\Sigma + j\Delta)$ and the $(\Delta + j\Sigma)$ channels do not track in phase over the required 60 dB dynamic range. This is a minor effect, and peak-to-peak tracking phase error is expected to be less than 3^{o}. It is "assumed" that received signal levels will be normally distributed about a median (calibration) level, and the 1σ phase error is therefore taken to be 0.75^{o}. The error in the Δ/Σ ratio is then

$$\sigma_{\Delta/\Sigma}(\text{Limiter Phase}) = .0065\ (1 + |\Delta/\Sigma|^2) \qquad (5)$$

A plot of this error function is shown in Fig. A-6c.

The limiter output level will vary as a function of input level. It is expected that peak-to-peak variation will be less than 0.75 dB over the 60 dB input signal range. Again, assuming normally distributed signal levels about a median level, a 1σ output level variation of approximately (.75/4) dB has been chosen.

The detector output for a differential gain ratio of β between $\Sigma + j\Delta$ and $\Delta + j\Sigma$ channel is

$$\tan[\beta \tan^{-1} (\Delta/\Sigma)]$$

Differentiating, evaluating at $\bar{\beta} = 1$ and expressing $\sigma_{\beta_{ratio}}$ in terms of $\sigma_{\beta_{db}}$ yields

$$\sigma_{\Delta/\Sigma} = \tan^{-1} (\Delta/\Sigma) \cdot \frac{\pi}{180} \cdot [10^{(\gamma/20)} - 1] [1 + |\Delta/\Sigma|^2]$$

γ = 1σ differential output level in dB

= .75 dB/4 (estimate)

$$\sigma_{\Delta/\Sigma}(\text{Limiter Output Level}) = 3.81 \times 10^{-4} \tan^{-1} (\Delta/\Sigma) \cdot (1 + |\Delta/\Sigma|^2)$$

A plot of this error function is shown in Figure A-6d, and the combined error function (r.s.s.), is shown in Figure A-6e.

The last term which affects the estimate of Δ/Σ is additive, white, Gaussian noise. The 1σ error in Δ/Σ due to noise (SNR) per pulse is,

$$\sigma_{\Delta/\Sigma}(\text{Noise}) = \frac{1}{\sqrt{2\ \text{SNR}}} \quad (1 + |\Delta/\Sigma|^2) \quad * \quad \frac{\Sigma(0)}{\Sigma(\theta)}$$

where $\frac{\Sigma(0)}{\Sigma(\theta)}$ accounts for variations in SNR across the beam due to the sum beam pattern. Plots of this function are shown in Figure A-7a for +30 and +42 dB SNR with scales transformed as before. Curve No. 1 was combined with other error sources in a r.s.s. sense to obtain the curve shown in Figure A-7b. This represents the expected estimation error performance of the processor and DABSEF antenna for DABS replies at or above +42 dB referred to MUSL.

3.3 Monopulse Calibration

The DABS sensor is calibrated against a fixed transponder(s) at a known azimuth(s). The result is a look-up table which relates digitized monopulse video samples (γ) to offboresight angle. This section will describe the calibration process.

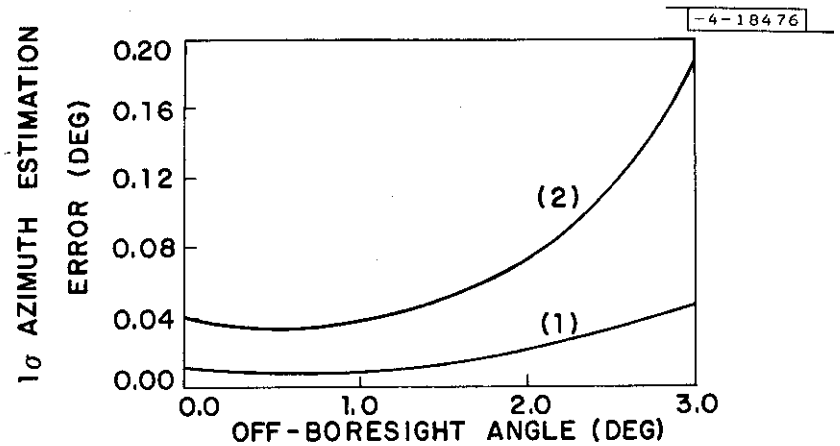

DUE TO: RECEIVED SIGNAL-TO-NOISE RATIO
1: SNR = +42 dB AT BORESIGHT
2 SNR = +30 dB AT BORESIGHT

(a)

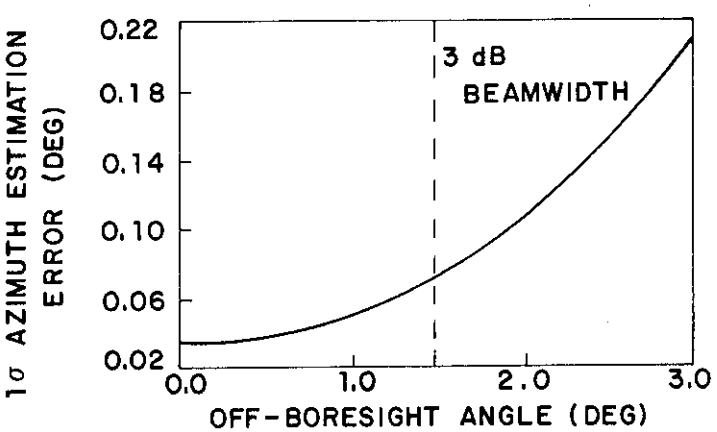

DUE TO: PRE-COMBINER DIFFERENTIAL CHANNEL GAIN
MIXER PREAMPS
BAND PASS FILTERS
PULSE TRANSIENT SAMPLING ERROR
LIMITERS
NOISE

(b)

Fig. A-7. Monopulse processor error analysis (Cont.).

Let:

θ_{true} = Azimuth of target (or calibration source during formation of look-up table) with respect to some reference, for example true north.

BS_{true} = azimuth of difference beam null with respect to north. (The difference beam null is an arbitrary but convenient definition of beam azimuth).

bs_{ind} = The output of the antenna shaft encoder

$\Delta\theta_{true}$ = The angle between the target and the null of the difference beam.

γ = digitized half-angle processor output

Then:

$$\theta_{true} = BS_{true} - \Delta\theta_{true} \tag{1}$$

Further let:

$$\Delta\theta_{true} = f(\gamma) \tag{2}$$

and define f(.) for an "aligned" system where alignment corresponds to a monopulse bipolar video output of zero (corresponding to $\gamma = 128$) when the target is at the difference beam null. The function f(.) is then the equivalent of Equation 2-6 of Section 2.3.

Now introduce two fixed offsets, one in the A/D correcter that digitizes the monopulse video and the other in the azimuth shaft encoder.

δ = A/D offset

$$\Delta BS = bs_{ind} - BS_{true} \tag{3}$$

Then

$$\gamma = f^{-1}(\Delta\theta_{true}) + \delta \tag{4}$$

so that combining (1), (3), and (4)

$$\theta_{true} = bs_{ind} - (f(\gamma-\delta) + \Delta BS) \tag{5}$$

where the term in parenthesis is obviously the monopulse look up table (a function of γ) which is interpreted as indicated off boresight angle $(\Delta\theta)_{ind}$

$$\theta_{true} = bs_{ind} - \Delta\theta_{ind} \tag{6}$$

$$\Delta\theta_{ind} = C(\gamma) = f\ (\gamma-\delta) + \Delta_{BS} \tag{7}$$

Finally, $f(\gamma-\delta)$ is the angle between the target and the difference beam null and ΔBS is the angle between the difference beam null and the processor/A/D system null.

The look-up table $C(\gamma)$ is formed using replies from a surveyed target; i.e., θ_{true} is known. Each reply (i) contains a value bs_i and γ_i, which are combined as shown below to obtain $C(\gamma)$.

$$C(\gamma) = \frac{\sum_i (bs_i - \theta_{true})\ g\ (\gamma_i - \gamma)}{\sum_i g(\gamma_i - \gamma)}$$

where $g(\gamma_i - \gamma) = 0 \quad \gamma_i \neq \gamma$

$$1 \quad \gamma_i = \gamma$$

Note that the offsets δ and ΔBS displace the look table along the γ and $\Delta\theta$ axes. However, as long as the offsets are unchanged from their values at calibration time, the azimuth estimates are unbiased.

If, however, the survey of the calibration source is in error a bias is introduced into all position measurements. This bias can affect ATC system configurations that use data from more than one sensor.

For any given target at any given time and position there exists a corresponding lookup table $C_T(\gamma)$ which relates γ to $\Delta\theta_{true}$. $C_T(\gamma)$ takes into account all target characteristics (such as transponder frequency and elevation) as well as the instantaneous characteristics of the antenna, receivers, half angle processor, etc. The consequence of using $C(\gamma)$, the stored lookup table, rather than $C_T(\gamma)$ is to create an error in the azimuth estimates

$$\varepsilon = \Delta\theta_{ind} - \Delta\theta_{true}$$

$$= C(C_T^{-1}\ (\Delta\theta_{true})) - \Delta\theta_{true}$$

APPENDIX B: METHOD OF DEDUCING AIRCRAFT ACTUAL TRAJECTORY

A fundamental objective of many data analysis programs is estimation of an actual aircraft trajectory, given a sequence of position measurements for that aircraft. The sliding window least squares curve fit is one technique for achieving such an estimate. The fundamental characteristic of the procedure is the use of a sliding window to obtain a position estimate corresponding to a target report. The window defines all data points contained in a fixed time period enclosing the target report for which an estimate is desired. In this application a second order least squares curve fit is applied to all applicable data points, and the "true" position is calculated from the curve fit equations. As the procedure advances to the next target report, the time window is also moved. This produces a sliding window which defines what data is to be used in the curve fit procedure.

To illustrate the sliding window procedure, assume an estimate of the target position is desired for scan N. Target report data (range, azimuth and time) for scans N-5 to N+5 are used in the fit, (assuming the time window is selected to correspond to 11 scans). A least squares curve fit is determined from the target reports, yielding equations for range and azimuth as a function of time:

$$\rho(\tau) = a_1 + a_2 (t - t_N) + a_3 (t - t_n)^2$$

$$\theta(\tau) = b_1 + b_2 (t - t_N)\ b_3 (t - t_n)^2$$

In the equations, t_N denotes the time associated with the target report for scan N, and the least squares estimate of the aircraft range and azimuth would be a_1 and b_1 for scan N. Velocity and acceleration components are also available if heading and ground speed estimates are desired.

In an actual implementation, it is not guaranteed that target reports exist for each scan. If the number of data points in the window is less than some minimum (typically 7), a fit is not attempted. In addition to missing target reports, insufficient data may also exist if target report measurements are flagged as "bad" data not to be used in the curve fit. However, if the measurements for a given scan are rejected and sufficient data is still available, a curve fit is still executed.

The bad point rejection scheme is applied independently to each curve fit (range and azimuth), so partial position estimates may exist for some scans. If the actual aircraft trajectory was the desired program output this would not be useful, but in this application a partial position estimate can still be used to calculate a measurement error in one of the two measurement coordinates.

The use of independent range and azimuth curve fits is designed to maximize the amount of measurement error information achievable from the input data. Independent curve fits in range and azimuth are also desirable in the sense that poor data in one coordinate does not corrupt the quality of the curve fit for the other coordinate. For a "typical" aircraft, the standard deviation of the range measurement error is 20 -25 feet, while the standard deviation of the azimuth measurement error is $.04^{o}$. At a range of 35 miles, the variance of the azimuth measurements would be about 150 feet, so it is clear that azimuth errors are the dominant factor in the surveillance errors. If an X - Y curve fit were used, azimuth errors would translate into the X and Y curve fits, and could produce apparent range error while simultaneously reducing the azimuth errors. The coupling that results from an X-Y curve fit was the primary factor in selecting the range-azimuth fit for the programs.

In contrast, it is noted that the second order equations in range and azimuth cannot model the idealized cases normally assumed in similar curve fit programs. If an aircraft were flying with constant acceleration on a perfectly linear track, ideal data applied to an X-Y curve fit would produce no error. The same data applied to a range-azimuth curve fit produces incorrect indications of errors in the measurements. Comparisons of the two tehchniques in simulations and with actual data indicate that the differences in the two techniques result in relatively small differences when averaged over many scans. In worst case geometries, the differences were typically less than 10 feet in range and $.02^{o}$ in azimuth for aircraft at ranges greater than 10 miles from the sensor operating at moderate speed (less than 200 knots) on basically linear trajectories.

In selecting a range-azimuth curve fit, it was concluded that the accuracy was sufficient for estimating the cumulative measurement errors. It also lends itself better to bad point rejection schemes since the entire measurement does not have to be rejected if the azimuth, for example, appears inconsistent.

Finally, a turn detection in X-Y is incorporated and used to filter out curve fit residuals for scans on which the aircraft is turning.

Each residual is incorporated into two data bases.

1. It is combined with other residuals from the aircraft. The output is the standard deviation of azimuth estimate error for that aircraft.

2. It is combined with the residuals for all other aircraft. The output is the standard deviation of all the residuals, and standard deviation plotted vs azimuth and vs elevation.

REFERENCES

1. Report of the Department of Transportation Air Traffic Control Advisory Committee, (December 1969).

2. J. C. Sureau, "A Summary of DABS Antenna Studies," Lincoln Laboratory, M.I.T., Project Report ATC-53 (3 February 1976).

3. J. C. Sureau, "Summary of Results of Antenna Design Cost Studies," Lincoln Laboratory, M.I.T., Project Report ATC-33 (25 April 1974).

4. E. M. Hofstetter and D. F. DeLong, Jr., "Detection and Parameter Estimation in an Amplitude Comparison Monopulse Radar," IEEE Transactions on Information Theory, IT-15, (1969) pp. 22-30.

5. S. Sharenson, "Angle Estimation Accuracy with a Monopulse Radar in the Search Mode," IRE Transactions on Aerospace and Navigational Electronics, pp. 175-179 (September 1962).

6. R. J. McAulay, "The Effects of Interference on Monopulse Performance," Lincoln Laboratory, M.I.T., Technical Note, TN 1973-30 (1 August 1973).

7. R. J. McAulay, V. Vitto, "A Simulation of the DABS Sensor for Evaluating Reply Processor Performance," Lincoln Laboratory, M.I.T., Project Report ATC-28, (July 1974).

8. T. P. McGarty, "Models of Multipath Propagation Effects in a Ground-to-Air Surveillance System," Lincoln Laboratory, M.I.T., Technical Note 1974-7 (25 February 1974).

9. G. Colby and E. Crocker, "Final Report Transponder Test Program," Lincoln Laboratory M.I.T., Project Report, ATC-9, (12 April 1972).

10. A. Spiridon, "Impact of Obstacle Shadows on Monopulse Azimuth Estimate," Lincoln Laboratory, M.I.T., Project Report ATC-50 (17 July 1975).

11. J.E. Evans, "A Ray Theory Model for Predicting Angular Errors Due to Shadowing for ATCRBS, DABS and MLS," Lincoln Laboratory, M.I.T. Project Report ATC-66 (to be published).